Eesti Maaülikool
Estonian University of Life Sciences

BIOSENSOR ARRAY FOR BOD MEASUREMENTS IN DIFFERENT TYPES OF WASTEWATER

BIOSENSOR-RIVI ERINEVATE REOVETE BIOKEEMILISE HAPNIKUTARBE UURIMISEKS

KÄTLIN PITMAN

A Thesis
for applying for the degree of Doctor of Philosophy
in Engineering Sciences

Väitekiri
filosoofiadoktori kraadi taotlemiseks
tehnikateaduse erialal

Tartu 2022

Eesti Maaülikooli doktoritööd

Doctoral Theses of the Estonian University of Life Sciences

Eesti Maaülikool
Estonian University of Life Sciences

BIOSENSOR ARRAY FOR BOD MEASUREMENTS IN DIFFERENT TYPES OF WASTEWATER

BIOSENSOR-RIVI ERINEVATE REOVETE BIOKEEMILISE HAPNIKUTARBE UURIMISEKS

KÄTLIN PITMAN

A Thesis
for applying for the degree of Doctor of Philosophy
in Engineering Sciences

Väitekiri
filosoofiadoktori kraadi taotlemiseks
tehnikateaduse erialal

Tartu 2022

Institute of Forestry and Engineering
Eesti Maaülikool, Estonian University of Life Sciences

According to verdict No 6-14/9-3 of June 10, 2022, the Doctoral Committee of the Engineering Sciences of the Estonian University of Life Sciences has accepted the thesis for the defence of the degree of Doctor of Philosophy in Engineering Sciences.

Opponent: **Assoc Prof, senior researcher, Kristīna Kokina, Dr.sc.ing.**
Faculty of Civil Engineering
Riga Technical University

Supervisors: **Researcher Merlin Raud, PhD**
Institute of Forestry and Engineering
Estonian University of Life Sciences

Assoc Prof Jaak Nerut, PhD
Institute of Chemistry
University of Tartu

Prof Timo Kikas, PhD
Institute of Forestry and Engineering
Estonian University of Life Sciences

Defence of the thesis:
Estonian University of Life Sciences, room B136, Kreutzwaldi 56/1, Tartu, on 29th August, 2022, at 12.00.

The English of this thesis was edited by Aabwell OÜ.

Publication of this thesis is supported by the Estonian University of Life Sciences. This study has been supported by Doctoral School of Energy and Geotechnology III (Estonian University of Life Sciences ASTRA project "Value-chain based bio-economy"), European Regional Development Fund and Archimedes Foundation.

ISSN 2382-7076
ISBN 978-9916-669-34-1 (trükis)
ISBN 978-9916-669-35-8 (pdf)

CONTENTS

LIST OF ORIGINAL PUBLICATIONS

This thesis is based on four articles. References to the publications in the thesis are given with their Roman numerals.

I. ETIS 1.1: **Pitman, K**.; Raud, M.; Kikas, T. (2015) Biochemical oxygen demand sensor arrays. *Agronomy Research*, 13 (2), 382−395.

II. ETIS 1.1: **Pitman, K**.; Raud, M.; Scotti, G.; Jokinen, V. P.; Franssila, S.; Nerut, J.; Lust, E.; Kikas, T. (2017) Electrochemical Characterization of the Microfabricated Electrochemical Sensor-Array System. *Electroanalysis*, 29, 249−258. 10.1002/elan.201600559.

III. ETIS 1.1: **Pitman, K**.; Nerut, J.; Lust, E.; Franssila, S.; Raud, M.; Kikas, T. (2017) Electrooxidation of Hexacyanoferrate(II) Anions and Electroreduction of Oxygen in the Microfabricated Electrochemical Sensor-Array System. *ECS Transactions*, 77 (11), 1771−1782. 10.1149/07711.1771ecst.

IV. ETIS 1.1: **Pitman, K**.; Nerut, J.; Raud, M.; Kikas, T. (2020) Characterisation of Electrochemical Sensor-array for Utilisation in Construction of BOD Bioelectronic Tongue. *Environmental and Climate Technologies* 24 (3), 39-54. 10.2478/rtuect-2020-0084.

The contribution of the author to the papers for publication

Paper	Study design	Data collection	Data analysis	Manuscript preparation
I	**A,** B, C	**A**, B	**A**, B	**A**, B, C
II	**A,** B, C	**A**, B, D, E, F, G	**A**, B, G	**A**, B, C, G, H
III	**A,** B, C, G	**A**, G	**A**, B, G	**A**, B, G, C, H
IV	**A,** B, C, G	**A**, G	**A**, B, C, G	**A**, B, C, G

A-Kätlin Pitman; B-Merlin Raud; C-Timo Kikas; D-Gianmario Scotti; E-Ville P. Jokinen, F-Sami Franssila; G-Jaak Nerut; H-Enn Lust.

LIST OF ABBREVIATIONS AND SYMBOLS

Abbreviations

ANN	artificial neural network
APHA	American Public Health Association
BOD	biochemical oxygen demand
CA	chronoamperometry
CV	cyclic voltammetry
DO	dissolved oxygen
NSR	normalised response
ORR	oxygen reduction reaction
PCA	principal component analysis
PLS	partial least squares
SPE	screen-printed electrode
SU-8	epoxy-based negative photoresist

Symbols

C	capacitance, F m^{-2}
D	diffusion coefficient of the reacting species, m^2 s^{-1}
E	electrode potential, V
I	electric current, A
I_0	electric current output in the 0.1M KCl solution, A
I_S	electric current output in the synthetic wastewater, A
j	current density, A m^{-2}
j_c	ORR current density (which is corrected with the background current density), A m^{-2}
p_{O2}	oxygen partial pressure, kPa
p_{tot}	total gas pressure, kPa
S	working electrode area, m^2
t	time, s
$v_{pumping}$	electrolyte solution pumping speed, cm^3 min^{-1}
$\%_{vol}(O_2)$	volume percentage of oxygen in the gas mixture, %
δ	diffusion layer thickness, m
v	potential sweep rate, V s^{-1}

INTRODUCTION

Every individual needs clean drinking water (Dutt et al., 2020). Water quality is very important because pure water resources are limited. Lakes, rivers, and oceans have been polluted mainly by waste which has been generated through human activity (Dutt et al., 2020). Water pollutants may be damaging both to human health and to the environment (Maduraiveeran and Jin, 2017). According to the World Health Organisation, environmental pollution costs around 8.9 million human lives annually around the world (Arduini et al., 2017).

In order to protect the environment, there is a need to examine water quality before that water is released from wastewater treatment plants. Water quality monitoring can be categorised into three types: the physical, chemical, and bacteriological testing of water (Hayat and Marty, 2014). One of the most important parameters to be tested in any wastewater is the biochemical oxygen demand (BOD). The BOD test determines the amount of organic compounds which are biodegradable in wastewater (Ponomareva et al., 2011). The traditional BOD test takes five (BOD_5) or seven (BOD_7) days. However, the process of controlling biological systems, wastewater treatment plants, industrial processes, and also natural water bodies, requires continuous information about water quality because only then is it possible to react immediately to results which may turn out to be other than optimal. Therefore the classical BOD measuring method is not suitable and a faster method is required for BOD determination. For this purpose different types of BOD biosensor have been proposed. BOD biosensors provide the opportunity to get the results in minutes instead of days.

There have been and continue to be many attempts to construct the appropriate sensors (Arlyapov et al., 2021; Guo et al., 2021) and sensor arrays (Bourgeois and Stuetz, 2002; Campos et al., 2012; Czolkos et al., 2016; Jouanneau et al., 2019; Onkal-Engin et al., 2005; Raud and Kikas, 2013; Sakaguchi et al., 2007; Tønning et al., 2005) to carry out BOD measurements. The research has shown that microbial sensors make it possible to gain more rapid results than with the conventional BOD method. However, most of the BOD biosensors are not usable in real life situations. The main drawbacks are their short operational life due to the instability of biological material, and their low accuracy.

The most common biological sensing element to be used in BOD biosensors is the bacterial membrane. The bacterial membranes can be made from pure bacterial cultures or can be mixture from different cultures or even consortia. One pure bacterial culture has a narrow substrate spectrum, but it is stable. The mixed bacterial cultures have a broader substrate spectrum, but their composition changes over time, and it causes signal instability.

The inconsistency of measurement results is due to differences in measurement methods and the construction principle used in the biosensors themselves. Only the easily digestible components in the sample are detected during the short measurement time of the BOD biosensor. In addition, those components which can be measured depend on the bacteria being used in the sensing element of the BOD biosensor.

One possibility when it comes to being able to approach these issues is to use different bacterial cultures with different substrate spectra in a sensor array in which different cultures are spatially separated from each other. The use of spatially separated, pure microbial cultures makes it possible to prevent contamination between different sensors in the array, while also ensuring a longer lifetime for the sensor. As different cultures in the sensor array are able to assimilate different compounds, better coverage will be achieved in terms of detecting organic pollutants in wastewaters.

The goal of this thesis was to construct a BOD biosensor array based on different bacterial cultures. Before starting any experimental work, a theoretical understanding was collected in terms of the biosensors and arrays, and this information was published in the article (**I**). To be able to construct the biosensor array, two different sensor array chips were tested (**II**, **III**, and **IV**). Based on the electrochemical experiments, a screen-printed sensor array-based chip was selected for the BOD biosensor array preparation and BOD measurement process (**IV**).

1. REVIEW OF THE LITERATURE (State of the art)

Sensors are devices that react to the change in environment and send a signal with information about specific parameters to a transducer (Lindquist, 2020; Wang and Wolfbeis, 2014).

Sensors can be classified into two main groups: physical (for measuring, for example, temperature or pressure), and chemical (designed to measure, for example, pH, oxygen, or glucose) (Kurbanoglu et al., 2020; Wang and Wolfbeis, 2014). Most sensors are based on transducers which make it possible to convert one type of signal into a measurable electrical signal, which can then be recorded and analysed. (Scott et al., 2007)

1.1. Biosensors

Biosensors form a certain subtype of sensor which consists of the biological sensing element, a physicochemical transducer, and the electronic system which handles signal processing (Bahadır and Sezgintürk, 2015; Sharma et al., 2020).

Biosensors convert the biological reactions which are influenced by the sample composition into a measurable signal (Ribeiro et al., 2020). Figure 1 illustrates the basic working principle of a biosensor. The biological recognition element interacts with the analyte in the sample medium to produce a biochemical response. The transducer converts this signal into a quantifiable signal. Depending upon the type of transducer, the changes may be chemical and physical (such as thermal, light emission, or direct electrical signal), and the type of signal determines the type of biosensor (Novodchuk et al., 2021). This signal is converted by the transducer into an electrical signal which can be measured, and is proportional to the analyte concentration in the sample (Sun et al., 2011).

Biosensors can be classified according to the transducer or by the biological recognition element being used (Thévenot et al., 2001). Many types of biological materials have been used in biosensor construction such as tissues, cells, microorganisms, organelles, enzymes, antibodies, deoxyribonucleic acid (DNA), receptors, or nucleic acids (Ha et al., 2015; Su et al., 2011; Xu and Ying, 2011), but also viruses, protozoa, fungi, algae, and microfauna (Lindquist, 2020).

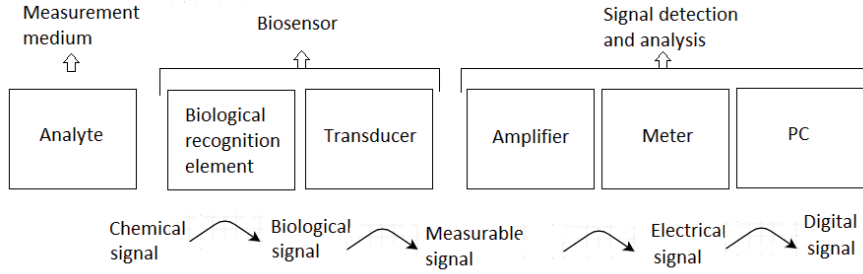

Figure 1. A schematic of a biosensor (the arrows show the signal and its movement), along with a representation of the signal flow in the biosensor system.

Enzymes and antibodies are widely used in biosensors since they are specific and selective to the selected analyte (Xu and Ying, 2011). Enzymes make it possible to ensure a rapid response, high stability, and also biocompatibility. However, the cost of enzymes can be very high (Biswas et al., 2017). On the other hand, microorganisms do not need the costly purification procedure and are able to interact with a wide range of analytes (Xu and Ying, 2011). Microorganisms are also usually more resistant to the inhibitory substances and more tolerant to pH and extreme temperature than enzymes and proteins (Nakamura, 2018; Xu and Ying, 2011). Microorganisms are more versatile because they contain multiple enzymes which make possible the detection of a broader range of analytes (Xu and Ying, 2011). The main drawback in microorganism-based biosensors is the slower response times and the lack of specificity when compared to enzyme-based sensors (D'Souza, 2001).

Different types of transducers have been used in the construction of biosensors. The main transducing systems are classed as electrochemical (involving amperometric, potentiometric, conductometric, voltammetric, and impedance) (Biswas et al., 2017; Khoshbin et al., 2018; Li et al., 2017; Martynko and Kirsanov, 2020), optical (involving fluorescence, bioluminescence, or colorimetrical) (Su et al., 2011), thermal (Castillo et al., 2004; Rodriguez-Mozaz et al., 2005), and acoustic. (Bahadır and Sezgintürk, 2015; Ejeian et al., 2018)

Electrochemical sensors monitor changes in electrochemical effects using amperometry (Su et al., 2011; Biswas et al., 2017), potentiometry (Su et al., 2011), conductometry (Su et al., 2011; Biswas et al., 2017), voltammetry or impedance methods (Biswas et al., 2017).

Optical biosensors, however, measure the optical properties and characteristics of transducer when the analyte interacts with the biological recognition element (Ribeiro et al., 2020). Optical biosensors can be small and are not affected by electrical noise (Lei et al., 2006). Thermal biosensors are based on the measurement of heat which is produced during biochemical reaction (Zheng et al., 2005).

Piezoelectric or microbalance biosensors are based on the measurement of change in the resonance frequency which is caused by the mass of the crystal and the immobilised biological material. Depending on the adsorption of analytes onto the surface of the piezoelectric sensor, the electrical signal changes and the difference in mass can be assessed (Rawal et al., 2020).

Generally, the most often-used transducers are electrochemical and optical transducers (Su et al., 2011). Amperometry is the preferred method because it is more rapid and has a higher sensitivity than any other method (Biswas et al., 2017). The amperometric method is robust, easy-to-use, and allows the use of small sensors.

Different types of biosensors have been widely used as promising tools in the quantitative detection of target analytes, or in early-warning systems, depending on the precise requirements for the analytical system in question (Qi et al., 2021). Many applications for biosensors have been reported, such as in terms of the measurement of BOD, phenols, heavy metals (Biswas et al., 2017; Khoshbin et al., 2018; Maduraiveeran and Jin, 2017), pesticides (Zhao et al., 2020), surfactants, plasticisers, hormones, antibiotics, pharmaceuticals, and toxicity (Ejeian et al., 2018; Gupta et al., 2019), but also in food quality analysis (Lv et al., 2018; Ye et al., 2019), and the monitoring of the environmental and industrial processes (Bhalla et al., 2016; Sharma et al., 2020; Ye et al., 2019).

Potential commercial biosensors are on the market for use in medical, food, agricultural, the military, the veterinary and environmental applications (Bahadır and Sezgintürk, 2015). The most well-known types of biosensors are those which are related to the process of blood glucose monitoring (Dai et al., 2019; Martynko and Kirsanov, 2020), and pregnancy detection kits (Sharma et al., 2020). The market value of biosensors was at about USD 12.4 billion in 2013 (Sharma et al., 2020).

1.1.1. Biosensor for BOD

Biochemical oxygen demand – The American Public Health Association (APHA) Standard Methods Committee accepted the BOD_5 test in 1936 (Bahadır and Sezgintürk, 2015). The BOD analysis is an empirical test which is used to determine the relative oxygen requirement of wastewater, effluents, and polluted water (APHA, 1985). This can be correlated with the concentration of biodegradable organic pollutants in the measured sample (Ahmed and Shah, 2017; Jouanneau et al., 2019). The test measures the amount of molecular oxygen being used during a specified incubation period for the biochemical degradation of organic material, and the oxygen being used to oxidise inorganic material such as sulphides, ferrous iron, and reduced forms of nitrogen (APHA, 1985).

The BOD analysis includes sample dilution and placing it into an airtight bottle in a dark place at 20 °C for the entire incubation period. The amount of dissolved oxygen is measured before and after incubation, and the BOD is calculated based on concentration of dissolved oxygen before and after the incubation period. (APHA, 1985; Commault et al., 2016; Kashem et al., 2015) During the incubation period, the biodegradable organic compounds are consumed by microorganisms and are thereby transformed into microbial biomass, carbon dioxide, and water. This process can be described with the following equation (Jouanneau et al., 2014):

$$X_0 + S_{org} + O_2 \xrightarrow{N,\ P,\ MN} X_f + T_p + CO_2 + H_2O, \quad (1)$$

where X_0 is the initial biomass, S_{org} is the organic carbon sources, N is the nitrogen source, P is the phosphorus source, MN is the mineral nutrients, X_f is the final biomass, and T_p is the transformation products of biodegradation (Jouanneau et al., 2014).

The conventional method for BOD determination is somewhat time consuming. This method requires five (BOD_5) or seven (BOD_7) days to be able to produce the results, and sometimes even as long as twenty-one days (I). However, for the management of wastewater treatment systems, more rapid BOD estimation and feedback are required (Guo et al., 2021).

BOD biosensors – More rapid results can be obtained using BOD biosensors. Karube reported on the first BOD biosensor in 1977, which consisted of a Clark electrode and a form of yeast, *T. cutaneum* (Karube et al., 1977; Lei and Yi, 2010; Ponomareva et al., 2011). Nisshin Denki (Electric) Co Ltd produced the first commercial BOD biosensor in 1983. (Chee, 2013; Ejeian et al, 2018)

Since then many types of biosensors have been developed and reported, with these being based on different biological recognition elements (**I**) and transducers (Raud et al., 2010). Most of the more commonplace BOD biosensor are based on various microorganisms (such as *Bacillus subtilis*, *Escherichia coli*, *Klebsiella*, *Pseudomonas fluorescens*, etc. (**I**)) and various electrochemical transducers.

A widely-used approach to the development of an amperometric BOD biosensor is the use of an oxygen electrode (Zaitseva et al., 2017) such as, for example, the Clark-type dissolved oxygen electrode. This electrode is an amperometric sensor, one which consists of a Pt working electrode, along with an Ag/AgCl counter/reference electrode in a 3 M KCl electrolyte solution, both of which are covered with a gas-permeable membrane (Pouvreau et al., 2008). At the correct voltage, oxygen is reduced at the working electrode and the generated current is proportional to the oxygen concentration (Mišlov et al., 2015). Dissolved oxygen reduces at the electrode according to the following reaction (Liu et al., 2014):

Cathodic reaction: $O_2 + 2H_2O + 2e^- = H_2O_2 + 2OH^-$. (2)

In this study, biofilm-type BOD microbial biosensors were used, where membranes which contained whole cells of microorganisms acted as biological recognition elements. The schematic for a biofilm-type biosensor in which microorganisms and a Clark-type dissolved oxygen electrode are used is shown in Fig. 2. This type of biosensor is based on the measurement of the oxygen consumption by microorganisms, which can then be correlated with the amount of the analysed substrate (Zaitseva et al., 2017). The membranes which contain the microorganisms are placed in close contact with a transducer (Fig. 2), which measures the bacterial respiration rate (Liu and Mattiasson, 2002). (Ejeian et al., 2018) When the biosensor is placed in a clean measurement solution, a small bacterial respiration rate can be measured as most of the dissolved

oxygen is diffused through the membrane and is measured with the electrode. When a sample which contains organic substrate is added to the measurement solution, the bacterial respiration rate increases as the bacteria starts to assimilate the organics. As some of the oxygen is consumed by the bacteria, less oxygen diffuses through the membrane and is measured by the electrode. (Arlyapov et al., 2012; Li et al., 2017) The decrease in measured dissolved oxygen concentration is proportional to the BOD of measurement solution, and this can be used for the final BOD calculation. (Raud and Kikas 2013)

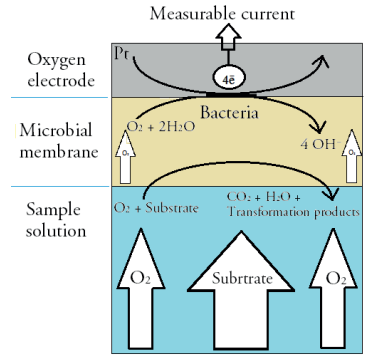

Figure 2. Microbial biosensor in a sample solution.

The biomaterial for the biological recognition element should oxidise a broad range of organic compounds so that the sensor-BOD value would correlate with the BOD value which is measured by means of the standard method (Zaitseva et al., 2017). Different, pure microbial cultures have been used in BOD biosensor construction, such as various yeasts (Arlyapov et al., 2012), microbial consortia, and activated sludge microorganisms (Chee, 2013; Pasco et al., 2011; Xu and Ying, 2011). Generally, the single strain sensor has good stability and a long lifetime, but a rather narrow substrate spectrum when it comes to being able to analyse complex samples (Liu et al., 2011). This makes it possible to gain a good sensor stability over time, but the substrate range is rather limited by the metabolic stabilities of the selected strain (Jouanneau et al., 2019). On the other hand, the mixed cultures are able to oxidise a broad range of substrates. However, they are unstable over a longer period of time since the composition of the culture changes over that time (Arlyapov et al., 2020; Commault et al., 2016). Better results have been achieved when using complex industrial samples if semi-specific microorganisms are used, as these are capable of assimilating those refractory compounds

which are found in industrial samples (Kibena et al., 2013; Raud et al., 2012; Raud and Kikas 2013).

In order to use the BOD biosensor for analytical purposes, the biosensor needs to be calibrated. The accuracy of results depends on the calibration solution and its composition (Chee, 2013; Ngoc et al., 2020). For the best results, the calibration solution should resemble the samples which are intended to be analysed. A standard solution made of glucose and glutamic acid (GGA) (Pasco et al., 2011) has been widely used for BOD biosensor calibration. However, the two components in this solution are a good nutrient source for the microorganisms and, therefore, this solution may not be quite so suitable for analysing samples which contain more complex and less biodegradable compounds. Less biodegradable compounds in samples are not assimilated during the short measurement time of the biosensor, leading to an underestimation of the BOD value (Ngoc et al., 2020). Better results have been gained when Organisation for Economic Cooperation and Development (OECD) synthetic wastewater has been used. The composition of this solution is more complex and, therefore, it has more similarities with genuine wastewater than does the glucose and glutamic acid (GGA) solution (Liu and Mattiasson, 2002). To be able to improve the accuracy of the results, artificial samples which contain selected refractory compounds mimicking the composition of actual effluents can also be applied when it comes to carrying out calibration. In addition, modified standard solutions which are based on glucose and glutamic acid have successfully been used (Ngoc et al., 2020).

For biosensors, two main measurement approaches and methods are available. The flow system approach is advantageous for the rapid and repeated analysis of multiple samples compared to the batch approach (Oota et al., 2010). The flow-injection analysis provides an opportunity to automate the analysis process. The automatic system is also free of some manual errors which can otherwise creep in. (Bratov et al., 2010) The flow-injection analysis makes it possible to develop automatic measurement systems, which in turn makes it possible to ensure automatic sampling with sample preparation (concentration, extraction, masking, etc.) (Bratov et al., 2010).

Those measurement methods which are used for bacterial respiration rate include the steady-state method (end-point, dynamic, or equilibrium),

and the kinetic method (the initial slope method) (Ponomareva et al., 2011). The steady state method uses the signal difference between the two steady states for the BOD estimation. On the other hand, the initial slope method applies a change in the initial rate of the sensor response, and this can be correlated with the BOD value (Oota et al., 2010). It takes between 8-40 minutes (and usually about 25 minutes) to get results with the steady-state method, while it takes only 15-30 seconds with the initial slope method (Ponomareva et al., 2011).

The most important characteristics of any BOD biosensor are linearity, sensitivity, and the time required for one assay. Biosensor parameters are determined by the type of biological recognition element being used, along with the parameters involved (Gupta et al., 2019), and also by the measurement approach which is being taken. In this study, sensitivity and linear range were selected as the main quality criteria.

Sensitivity and linear range can be determined during calibration when plotting sensor signal response against an analyte concentration (Thévenot et al., 2001). The linear range is defined as the amplitude of substrate concentration which is proportional to the BOD sensor signal (Chan et al., 2000; Rastogi et al., 2003). Sensitivity is determined by the slope of the calibration curve (Chan et al., 2000; Niyomdecha et al., 2017). The sensitivity and linear range are in an inverse relationship: the higher the linear range, the smaller the sensitivity, and *vice versa*. This biosensor is suitable for the measurement of samples which have larger BOD values. The sensitivity and linear range depend on the measurement method being used, and also on the cell density being used, in the biological recognition element. With increasing cell density, the sensitivity of the BOD sensor increases but the linear range decreases (Kim and Kwon, 1999). The linearity of the sensor is wider when using the initial rate method when compared to using the steady-state calibration method (Ponomareva et al., 2011).

Selectivity is the ability of the biological recognition element to detect and measure the different compounds in the sample (Bhalla et al., 2016). Selectivity depends on both the transducer and the biological recognition element (Thévenot et al., 2001). When it comes to BOD biosensors the preference is to use microbes with low specificity and high oxidation activity for a wide range of organic compounds (Oota et al., 2010). Selectivity can be increased by screening microbial strains

which have broad substrate specificities (Arlyapov et al., 2013), or by choosing appropriate microorganisms for specific wastewaters with complicated compositions (Oota et al., 2010).

As said before, one way in which a broader substrate window can be gained is to use semi-specific microorganisms. The second option in terms of gaining results which are more precise is to use mixed cultures of microorganisms. This makes it possible to widen the substrate spectra which can be detected by the biosensor when compared to the use of biosensors which are based on pure cultures (Kharkova et al., 2019). When using several known microbial strains, two strategies can be proposed: one involving a mixture of known microbial strains and the other involving the use of several microbial strains individually, which makes it possible to enlarge the substrate spectra of the biosensor and to ensure the level of reproducibility (Jouanneau et al., 2019).

1.2. Biosensor arrays

The construction of and the principle behind sensor arrays are both inspired by the neurophysiology of gustation (the taste) and olfaction (the smell) (Ciosek and Wroblewski, 2007). These senses provide basic information about the chemical composition of the environment (Cave et al., 2019), while the brain's neuron system can analyse the information and react according to the experience (Ma et al., 2021).

The idea of artificially reproducing a natural smell and taste sensing system dates back to 1943 (Vlasov et al., 2005). The artificial olfactory system for gas and smell analysis based on an artificial sensor system was first constructed in the 1960s (Vlasov et al., 2008). Sensor arrays are similar to traditional olfactory sensing systems as they apply chemometric methods and artificial intelligence to achieve the same goals regarding the discrimination, identification, or quantification of samples (Podrażka et al., 2018).

According to the definition by the International Union of Pure and Applied Chemistry (IUPAC), 'an electronic tongue is a multisensorsystem, which consists of a number of low-selective sensors and uses advanced mathematical procedures for signal processing based on' pattern recognition and/or multivariate data analysis (del Valle, 2010). The same principle applies to electronic noses. However, electronic tongues are

meant for use in liquid analysis, while the electronic noses are designed for in gas analysis (Vlasov et al., 2008).

Within the array there may be a variable number of sensors, but not more than forty (Vlasov et al., 2005). The number of sensors depends on the solvable assignment and research options (**I**). The optimum number of sensors in the array depends on the measurement system, the analytical task at hand, and the availability of sensor materials with the appropriate different properties. This number may vary from four to forty, but the optimum is between six and ten (**I**). A too low number of sensors will make it impossible to incorporate all of the available information which is contained within the chemical signal. At the same time a too high number of elements will 'dilute' the information.

Instead of employing highly selective sensors, the sensors which are used in sensor arrays have low selectivity and are cross-sensitive. The cross-sensitivity regards the ability of a sensor to respond reproducibly to a number of different analytes in the solution (Podrażka et al., 2018), and to produce a stable response in a sample analysis. In addition, different sensors should produce different results in sample analysis so that, when an array of sensors is used, a fingerprint-like response to a sample is gained for further analysis (Vlasov et al., 2005). When compared to a single sensor, which provides only one output, a sensor array makes it possible to gain a data vector, which may provide additional chemical information, when being subjected to a multivariate data analysis (Bratov et al., 2010).

Various transduction principles have been employed in sensor arrays. The most frequently-used sensing parameters are mass, optical signal, or electrochemical signal (Banerjee et al., 2016; Rodríguez-Méndez et al., 2016; Shi et al., 2018). Amongst these, the most widely-used sensors (potentiometric, amperometric, voltammetric, or impedance sensors) are based on different electrochemical methods (Rodríguez-Méndez et al., 2016). It is also possible to apply a data fusion strategy, in which responses from sensors which are based on different transduction principles are combined (Cetó et al., 2016).

The sensors in any sensor array can be modified by the different materials, or by biological materials, when preparing biosensor arrays. The receptor in any bioelectronic tongue is generally of a biological

origin, such as those which employ the use of enzymes, peptides, antigens, antibodies, cells, or tissues (Tan and Xu, 2020; Wasilewski et al., 2019). Different enzymes, such as oxidoreductases and hydrolases, are the widely-used as biorecognition elements in biosensor arrays (**I**). The bioelectronic tongues rely on the same basic principles as do electronic noses and tongues. However, these are made up of several biosensors. The cross-sensitivity is provided by bioreceptors, which often cross-react with different compounds (Cetó et al., 2016).

Sensor arrays are being used in a wide range of applications, with higher accuracy and better quality (Shi et al., 2018), such as in terms of wastewater and organic pollutant indices, including Microtoxs, algaetest, chemical oxygen demand (COD), BOD, total organic carbon (TOC) (Cetó et al., 2016), food quality measurements, health sectors, and so on (Blanco et al., 2015; Ge et al., 2012)

1.2.1. Sensor array data analysis

The sensor-array measurements produce a large amount of multidimensional data as an output, which is difficult to analyse using traditional methods. To extract information about the system which is being analysed from this data application of multivariate analysis methods, preference is usually given to a chemometrics tool and artificial intelligence (Sousa et al., 2021; Wesoły and Ciosek-Skibińska, 2018). Various methods and approaches have been applied on analysis of sensor array data when it comes to the extraction of qualitative or quantitative information, such as pattern recognition, and the classification or calibration of sensor arrays, and the quantification of analytes (Głowacz et al., 2021).

The main goal of classification and pattern recognition is to ensure data reduction, data structure analysis, data modelling using regression, and classification models (Scampicchio et al., 2008). The most widely-used methods for data analysis are artificial neural networks (ANN), principle component analysis (PCA), and partial least squares (PLS) (Bratov et al., 2010).

PCA is widely-used linear qualitative analysis method which is employed in preliminary investigations, along with the visualisation of data, and data dimensionality reduction (Sousa et al., 2021). This method makes it

possible to ensure the reduction of the dimensionality of data without the loss of any important information (Głowacz et al., 2021; Wesoły and Ciosek-Skibińska, 2018).

Multivariate regression methods are used for multicomponent calibration using sensor arrays (Bratov et al., 2010; Wesoły and Ciosek-Skibińska, 2018). To be able to apply this method and to gain good results, a proper strategy is essential and the optimisation of experimental plan is necessary, especially where it involves the choice of calibration solutions, the calibration model to be selected, and a reduction of the number of calibration solutions (Bratov et al., 2010). The most commonly-used multivariate calibration method is the PLS method, which employs two data sets for the purpose of sample analysis, one for calibration and one for validation or analysis (Wesoły and Ciosek-Skibińska, 2018).

In the case of non-linear data, an artificial neural network (ANN) has been widely-used (**I**). ANN is based on massively parallel computing architecture, which imitates the behaviour of biological brain functions. ANN is trained with the input data so that the model is able to identify the connections between input and output data. Weight factors and interconnections are established between different model layers, which are later used for interpretation of new data (Xiao-wei et al., 2018).

1.2.2. BOD sensor arrays

BOD sensor arrays which are reported are based on the use of metal electrodes (Campos et al., 2012), or conducting polymer sensors (Bourgeois and Stuetz, 2002; Onkal-Engin et al., 2005), or enzyme sensors (Czolkos et al., 2016; Tønning et al., 2005), and also sensors which employ different immobilised microorganisms (Jouanneau et al., 2019; Raud and Kikas 2013; Sakaguchi et al., 2007).

The metal electrode array makes use of the ability of single metal sensors to react differently to different compounds in the solution. For example, Campos and co-workers (Campos et al., 2012) used a metal electrode array which consisted of Au, Pt, Rh, Ir, Ag, Ni, Co, and Cu electrodes, along with a PLS analysis to measure BOD both in influent and effluent samples which had been collected from the Submerged Anaerobic Membrane Bioreactor pilot plant. The results revealed good regression between the signal and the BOD values (r^2 is 0.975 and 0.828

respectively from the influent and effluent waters samples). The metal tongue was usable for a period of at least five months without requiring any maintenance other than a simple polishing before measurements was conducted. (Campos et al., 2012) However, the metal electrode arrays has some limitations, such as low selectivity and known measurement interferences (such as, for example, heavy metals) (Janata and Bezegh, 1988).

Several conducting polymers are used to make sensor arrays. The conducting polymer sensors are referred to by the composition of their sensing part. These conducting polymer-based sensor arrays are more selective than are metal electrode arrays. Bourgeois and Stuetz tested a sensor array, which consisted of eight conducting polymer sensors, which were used to measure the resistance of wastewater in order to provide an estimate of water quality. The PCA plot of collected data from wastewater sample measurements makes it possible to pick out wastewater samples which have been spiked with diesel. The sensor array had a good selectivity and high stability for at least six months. (Bourgeois and Stuetz, 2002)

In another study, the electronic nose consisted of twelve different sensors which had been modified with conducting polymer, made by Neotronics Scientific Ltd, Essex, UK. The electronic nose was calibrated every week with 1,2-propandiol solution. The ANN was used to analyse the data, which made it possible to predict the BOD values with over 90% accuracy. However, a new model may be required after one month due to changes in the electronic nose efficiency in relation to changes in the composition of the sewage. (Onkal-Engin et al., 2005) Furthermore, if the electronic nose is used to determine the BOD value, the non-volatile organic compounds in the sample may remain undetected.

Enzyme-based sensor arrays have very high selectivity (Lourenco et al., 2016), but they have a narrow substrate spectrum (**I**). Therefore these arrays are very good for analysing the target analyte, but when it comes to sensing BOD it is necessary to measure different compounds. The different enzymes can be combined in the array to measure the BOD. For example, Czolkos and contributors compared two types of amperometric enzyme biosensor array systems in wastewater. The reference solution was the standard mixture of 10 μM catechol and 0.5 mM acetylthiocholine chloride which were added to the buffer. The

data was subsequently analysed with PCA and PLS regression. The correlation between traditional BOD and sensor-BOD for arrays type 1 and 2 were 0.69 and 0.74 respectively. (Czolkos et al., 2016)

Tønning et al. used screen-printed sensors which had been modified by tyrosinase, horseradish peroxidase, acetyl cholinesterase, and butyryl cholinesterase to be able to measure different wastewater samples. The sensors were calibrated with a phosphate buffer which had been spiked with 0.553 mM acetylcholine chloride, 16.6 μM catechol, and 55.5 μM H_2O_2. The drift was measured. The PCA was used to differentiate between the samples. The samples were successfully differentiated according to treatment quality. (Tønning et al., 2005)

It is possible to get broader substrate spectrum when it comes to microorganisms than it is with pure enzymes, because the cells have several enzymes and different enzymes cascades, which are working at the same time (Gupta et al., 2019). Several papers have been published in which reported sensor arrays had been modified with microorganisms. Jouanneau and co-workers used a total of eight different bacterial strains in the array in order to analyse the BOD. The test was carried out in 96-well microplates, and they were able to measure the fluorescence signal, which was characteristic of the strain's biological activity. The BOD_5 values for the 104 genuine samples were measured and a good correlation was gained ($r^2 = 0.85$) with the reference. (Jouanneau et al., 2019)

Sakaguchi et al. used bioluminescence, which was measured with *Photobacterium phosphoreum* IFO 13896, a digital camera, and a mobile-type personal computer. The biosensor array was calibrated with a glucose–glutamic acid solution (BOD_5 = 220 ppm). This system was capable of measuring concentrations from 1 ppm to 16 ppm. The calibration curve was linear in this range. The biosensor array measured the values and the conventional BOD method values agreed with them within about 10%. (Sakaguchi et al., 2007)

In addition, various synthetic industrial wastewaters were measured with a bioelectronic tongue which consisted of dissolved oxygen electrodes which had been modified with different semi-specific microorganisms. PCA was used to distinguish between the different samples, and PLS regression revealed the correlation between the BOD_7 and sensor-BOD.

The sensor-BOD differed from BOD_7 by less than 5.6% in all samples. (Raud and Kikas, 2013)

1.3. Methods for (bio)sensor array fabrication

There are various methods which can be used to construct the sensor arrays. However most of those which are used involve screen-printing and microfabrication technologies. Miniaturised sensor array chips have their advantages, such as low manufacturing costs, and only small amount of sample is required for analysis to be carried out, along with the decreased reaction time. Different types of test can also be carried out simultaneously on the same device. (Derkus, 2016)

1.3.1. Screen-printed electrodes (SPEs)

Screen-printing is a stencil-printing method, one in which a patterned stencil is used as the core component to produce the designed pattern (Chu et al., 2017). The ink or printable materials are dropped to the open areas through the patterned stencil mesh (Chu et al., 2017; Li et al., 2012). The ink is pushed through the holes in the stencil, resulting in the desired pattern being created (Chu et al., 2017; Tran et al., 2018). Multiple layers can be printed using different materials. However, before printing the second layer, the first printed layer has to be dried off fully by means of applying a thermal treatment. (Li et al., 2012)

Screen-printing is simple, reproducible, and various inks and substrates can be used (Li et al., 2012; Xiao-wei et al., 2018; Tran et al., 2018). The electrode substrate may involve the use of ceramics, paper, plastic (polyester), and even a compact disc (CD) or digital versatile disc (DVD), and flexible substrates (Arduini et al., 2017; Kudr et al., 2017; Moro et al., 2019; Serrano et al., 2013). Mostly SPEs are made using silver, gold, and carbon ink (Li et al., 2012; Serrano et al., 2013; Tran et al., 2018). However, as gold is expensive, the other materials are used such as, manganese oxide, or bismuth oxide (Li et al., 2012; Serrano et al., 2013).

SPEs are disposable (Li et al., 2017), give rapid responses and are versatile (Li et al., 2012; Xiao-wei et al., 2018). Manufacturing SPEs is a cheap and robust process, and the bonus here is that they can be produced on a large-scale basis (Li et al., 2017; Moya et al., 2017; Nasiria and Khosravani, 2020; Serrano et al., 2013). Screen-printing technology

comes with lower resolution than does process which involve inkjet printers, microfabrication, or roll-2-roll techniques (Arduini et al., 2017). The wax-screen-printed channels has 100 μm in printing width (Liu et al., 2015). The gravure offset printing method provides conductor lines and spaces down to 20 μm (Pudas et al., 2004).

Screen-printing technology has been used in making solar cells (Ganesan et al., 2019), sensors and biosensors, organic light-emitting devices, thin film transistors (Tran et al., 2018), and paper-based analytical devices (Baharfar et al., 2020; Taleat et al., 2014).

1.3.2. Microfabrication technologies

Microfabrication technology comes from the integrated circuits and semiconductor industry and it focuses on the miniaturisation of engineering systems (Baracu and Gugoasa, 2021). Microfabrication is a universal term which is used to describe the devices, which are usually made by using silicon wafers but which may include glass, plastics, or other substrates. The objects of microfabrication process are on the micro scale, at least in one dimension, sometimes the size of the width of a human hair (Ikumapayi et al., 2021). The processes are carefully controlled and are carried out in special sanitised cleanrooms due to the small size of the features being involved .(Franssila, 2006; Ikumapayi et al., 2021)

There are many processes and techniques available, all of which can be used in the preparation of electrochemical sensors. Depending upon the sensor configuration, the main methods which can be used have been outlined (Collard et al., 2013; Baracu and Gugoasa, 2021; Franssila, 2006; Jiawen et al., 2020; Kokkinos and Economou, 2020):

- Deposition: a thin layer of material is deposited onto a substrate, usually using the chemical vapour deposition approach or the physical vapour deposition approach.
- Patterning: desired patterns can be formulated via the use of light-sensitive photo-resists using photolithography.
- Etching: using etching or the lift-off processes, some layers can be selectively removed and a pattern can thereby be transferred from the photoresist layer onto the conductive film or substrate.

- Bonding: two or more substrates can be bonded together to form a uniform microfabricated device.
- Insulation: insulating material can be deposited on top of the patterned conductive film (Kokkinos and Economou, 2020).

Various materials can be used in the fabrication of sensors and sensor arrays. The substrate materials which are used in microfabrication processes include glass, ceramics, or polymer organic materials, or even silicon wafers. (Franssila, 2006; Ikumapayi et al., 2021; Xu et al., 2021) Silicon is strong, flexible, smooth, flat, cheap, and is available in a wide variety of sizes, shapes, and resistivities (Franssila, 2006). Microelectrode arrays can be patterned from gold, silver, tungsten, platinum, indium tin oxide, and carbon (Blair and Corrigan, 2019; Xu et al., 2021). The high-temperature gas sensors can be made from oxides of gallium, zirconium, or hafnium (Vasiliev et al., 2016). Besides the aforementioned materials, alloys are also widely-used in these processes (Franssila, 2006).

Microfabrication is expensive technology when it comes to small-scale production and prototyping since it requires a cleanroom environment. However, in larger scales, microfabrication technologies make it possible to ensure batch-fabrication, which makes possible the production of inexpensive sensors and, therefore, disposable maintenance-free sensors. (Blair and Corrigan, 2019; Ejeian et al., 2019; Lee et al., 2007; Suzuki, 2000) In addition, miniaturised sensor arrays can be combined with a flow-through system to gain a fully automatic measurement system in which rapid results can be obtained (Suzuki, 2000).

1.3.3. Other methods

Besides screen-printing, there are other printing methods available when it comes to producing sensors, such as gravure printing, inkjet printing, spray-printing, slot-die printing, offset printing, flexo printing, and other emerging forms of printing technology (Moya et al., 2017; Neves et al., 2018; Oliveira et al., 2018; Tran et al., 2018). Printing technology is based on the process of depositing several layers on the insulating supports (Arduini et al., 2017).

When it comes to gravure printing, the ink is transferred directly onto the substrate by means of the graved cylinder (Tran et al., 2018). Inkjet printing involves a non-contact technique (Moya et al., 2017), in which

the accurately-positioned ink droplets are sprayed onto the substrate in the desired pattern to be able to achieve the final required printing output (Tran et al., 2018). The conducting materials which are used in inkjet printing involve silver, gold, carbon, and conducting polymers (Moya et al., 2017). It is possible to print onto a flexible substrate (such as PEN), polyethylene terephthalate (PET), polyimide, paper, glass, silicon, and 3D structures (Moya et al., 2017).

Additive manufacturing (also known as 3D printing) can be used to prepare biosensors (Muňoz and Pumera, 2020). In 3D printing, the material is transferred point-by-point and layer-by-layer. As a result 3D pieces are formed (Hwa et al., 2017; Sochol et al., 2018). The 3D printing technique uses several thermoplastic materials (such as acrylonitrile butadiene styrene (ABS), polylactic acid (PLA), and polyethylene terephthalate (PET)) (Sochol et al., 2018). The 3D printing technology can be implemented even in case of wearable (bio)sensors (Kalkal et al., 2021).

In addition to this, there are other more specific methods available when it comes to being able to produce (bio)sensor arrays. However, such methods have not been described here (Arduini et al., 2017; Fathi et al., 2021; Kudr et al., 2017; Lee et al., 2007; Moya et al., 2017; Neves et al., 2018; Wang et al., 2021).

2. AIMS OF THE STUDY

There exists a need for a precise, reliable, and easy-to-use biosensor array for wastewater characterisation in wastewater treatment plants. The main aim of this doctoral thesis is to design and construct a biosensor array in order to be able to rapidly measure the BOD.

In order to achieve the required goal, the following tasks were established:

1. Study the current state of the BOD sensor arrays (**I**).
2. Study the usability of the microfabricated and screen-printed sensor array as a BOD sensor array (**II**, **III**, and **IV**).
3. Test the performance of the BOD sensor array in standard solutions and in a genuine sample (**IV**).

The hypotheses tested in this study are as follows:

1. It is possible to measure oxygen concentration with a microfabricated sensor array.
2. A microfabricated sensor array is suitable for BOD measurements.
3. It is possible to measure oxygen concentration with a DropSens550 screen-printed electrochemical array.
4. The DropSens550 screen-printed electrochemical array could be used as a BOD-sensor array.
5. The BOD value of the actual wastewater can be measured with the modified DropSens550 screen-printed electrochemical array.

3. MATERIALS AND METHODS

3.1. Microfabricated sensor array

A microfabricated sensor array is shown in Fig. 3. A microfabricated sensor array from the silicon and the borosilicate wafers was made by using microfabrication technology. The two parts of the sensor array were bonded together with an epoxy-based negative photoresist (SU-8). This sensor array had six sets of Pt electrodes. The working electrode had dimensions of 700 × 400 μm. The counter electrode surrounded the working electrode from three sides in a U-shape, being 200 μm wide and 2600 μm long. The exact procedure regarding how the microfabricated sensor array was made is published in paper **II**.

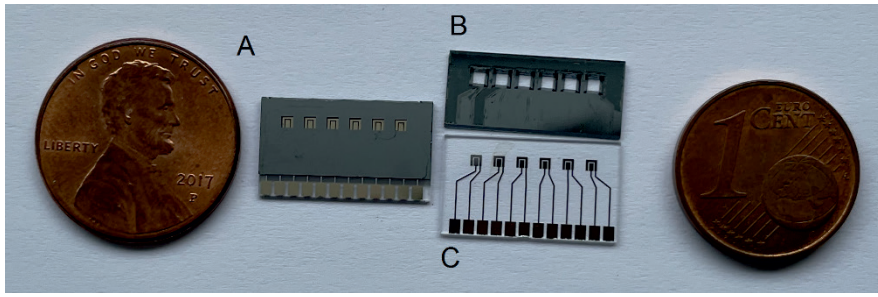

Figure 3. Microfabricated sensor array microchip: **A**) top view of the sensor array microchip; **B**) the silicon wafers with openings; **C**) the borosilicate wafers with Pt electrodes.

3.2. Screen-printed array

The DropSens550 (Metrohm DropSens, Spain) screen-printed electrochemical array (Fig. 4A) had 8 sets of 3 electrodes. The working electrode (a circle of 2.5 mm in diameter) and the counter electrode (around the working electrode, Fig. 4B) were made from Pt. The reference electrode was a silver band electrode. The total dimensions of the array were 3.8 × 2.0 × 0.1 cm (length × width × height).

The electrode's diameter was measured (Fig. 4B). This was carried out with three different sets of electrodes. The Stereomicroscope Zeiss Discovery.V12 and the programme Zen lite 2011 were both used. The working electrode was a disk with a diameter of 2.5 mm, while the

counter electrode was a ring with an inner diameter of 4.0 mm and an outer diameter of 5.2 mm (average of three measurements).

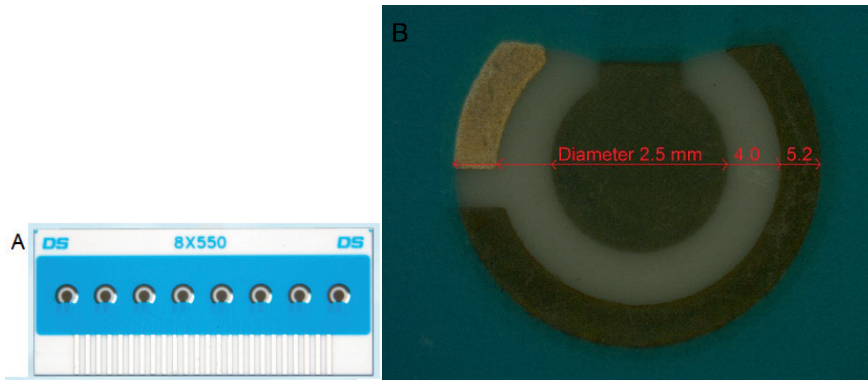

Figure 4. DropSens550: **A**) a screen-printed electrochemical array; and **B**) a single electrochemical cell.

3.3. Electrochemical measurements with microfabricated sensor array

The cyclic voltammetry (CV) and electrochemical impedance measurements were carried out with the potentiostat Reference 600 (Gamry Instruments Inc.). A three-electrode setup was used (Bard and Faulkner, 2001). The working electrode was Pt in the microfabricated sensor array. The fritted glass membrane separated the working electrode from the counter electrode, which was a large Pt wire mesh. The reference electrode was Ag|AgCl| aqueous saturated KCl.

The behaviour of the microfabricated sensor array was tested in two electrolytes: 1.0 M the potassium chloride solution (Cas 7447-40-7, assay 100.0%, Lach-Ner (Czech Republic)), and the 0.5 M H_2SO_4 solution (≥ 95%, Fluka Analytical, TraceSELECT®, for trace analysis), both of which have good conductivity. In these experiments, argon gas (99.9999%, AGA) was used to bubble through the solution for 15 minutes before the experiments in order to remove oxygen from the solution.

The oxygen reduction reaction (ORR) at different partial pressures was also studied in the 0.5 M H_2SO_4 solution. The partial pressure of oxygen (99.999%, AGA) in the solution varied from 0 to 98 kPa. Five different mixtures of argon and oxygen were used. Before the measurements were taken, the solution was saturated with the gas mixture for a total

of fifteen minutes. All of the electrochemical measurements were conducted at room temperature. The gas mixtures were prepared using the Brokhorst® mass flow controllers (EL-FLOW Select®) (**III**).

The glassware was cleaned using hot concentrated H_2SO_4 with a small addition of hydrogen peroxide (EMSURE, ISO 30 wt%). The cell was put together, filled with concentrated H_2SO_4, and was left to cool down. Next, all the glassware was washed a total of ten times using demineralised water and was then rinsed three times using Milli-Q^+ (18.2 MΩ cm) water.

The mechanical cleaning of the microfabricated sensor array could not be undertaken because the electrodes in the wells could not be reached with the polishing paper. Therefore the use of a chemical cleaning process became necessary. The first step in the purification process of the sensor array was the use of a ultrasound treatment (using a Bandelin electronic RK 52H, 60 W, 35 kHz) in an acetone solution (> 95%, APC Chemicals) for a total of ten minutes. This task was carried out once for every chip. If this procedure were to be repeated several times, the chip disintegrated because the SU-8 which binds together the two parts of the chip, detached.

The platinum electrodes were generally cleaned before each electrochemical measurement. Therefore, prior to each test, the chip was treated with hot concentrated sulphuric acid (at 50 °C) with a slight amount of hydrogen peroxide added on the previous evening. The chip was washed in the morning with Milli-Q^+ water and then boiled in Milli-Q^+ water between three to five times.

The characterisation of the microfabricated sensor array was performed after its activation. The results shown are averaged over at least three experiments and the error bars in graphic show the standard deviations of the averaged value.

3.4. Electrochemical measurements with DropSens550 screen-printed electrochemical array

The potentiostat PalmSens (Palm Instruments BV) and Reference 600 (Gamry Instruments Inc.) were used for CV and chronoamperometry (CA) measurements with a DropSens550 screen-printed electrochemical

array. The CV data were measured at different potential sweep rates (ν), from 10 to 1000 mV s^{-1}. The CA data were measured at −0.5 V vs Ag|AgCl|0.1 M KCl for 120 s with 1 s interval. During the pre-step, the electrode potential was held at +0.5 V vs Ag|AgCl|0.1 M KCl for 30 s to achieve a reproducible surface state prior to each measurement. For each experiment, a three-electrode arrangement was used (Fig. 4). The working electrode was an inner Pt circle electrode, while the counter electrode was a Pt band electrode around the working electrode, and the reference electrode was a silver band electrode. The electrodes were covered with agarose membranes. The latter were prepared from 180 mg agarose and 8.4 cm^3 distilled water and net discs (Scrynel, PE 500 HD, with a diameter of ¼ inch).

The electrochemical parameters of the DropSens550 screen-printed electrochemical array were measured by inserting the sensors into a solution which had been saturated with oxygen (99.999%, AGA) or nitrogen (99.999%, AGA), or a mixture of the two. The saturation time was always 30 minutes. The partial pressure of oxygen in the mixture of gases was varied, from 0 kPa up to 98 kPa, with a total of fourteen compositions. The total pressure of the gas was 101 kPa. The Brokhorst® mass flow controllers (EL-FLOW Select®) were used to prepare the gas mixtures (**IV**).

The custom-made sandwich-type flow-through cell (Fig. 5) consisted of two sides which had been tightened using butterfly screws. The DropSens 550 screen-printed electrochemical array, the membranes, the black distance piece, and the orange silicone sealing were placed between the two sides. The orange silicone sealing was used to create a channel to the solution. The black distance piece was needed to hold the membranes in place (**IV**).

In the first part of the experiments (Section 4.2), the electrolyte was pumped using a Master Dual Pump, model AL 1000, and a 20 cm^3 syringe was used. The electrolyte pumping speed ($v_{pumping}$) was changed from 0 to 3 cm^3 min^{-1}. In the second part of the experiments (Section 4.3), the solution was pumped through the measuring cell using a pump from FIAlab Instruments Inc. (USA).

It was found that it was not necessary to activate the DropSens550 screen-printed electrochemical array separately. The current was

averaged over the wells 3–7. It was found that for side wells the current density $|j|$ was higher because of the additional mixing of the solution i.e. presence of solution vortexes near the entrance and exit of the cell. The measurements were performed with different DropSens550 screen-printed electrochemical arrays. Error bars indicate the standard deviation of the averaged current density.

3.5. Microbial material

A *Pseudomonas putida* Pc15 strain was provided by the *Collection of Environmental and Laboratory Microbial Strains* (CELMS), Institute of Molecular and Cell Biology, University of Tartu, Estonia, (Estonian Electronic Microbial database, 2021), as imposed by the depositor, Eeva Heinaru (**IV**).

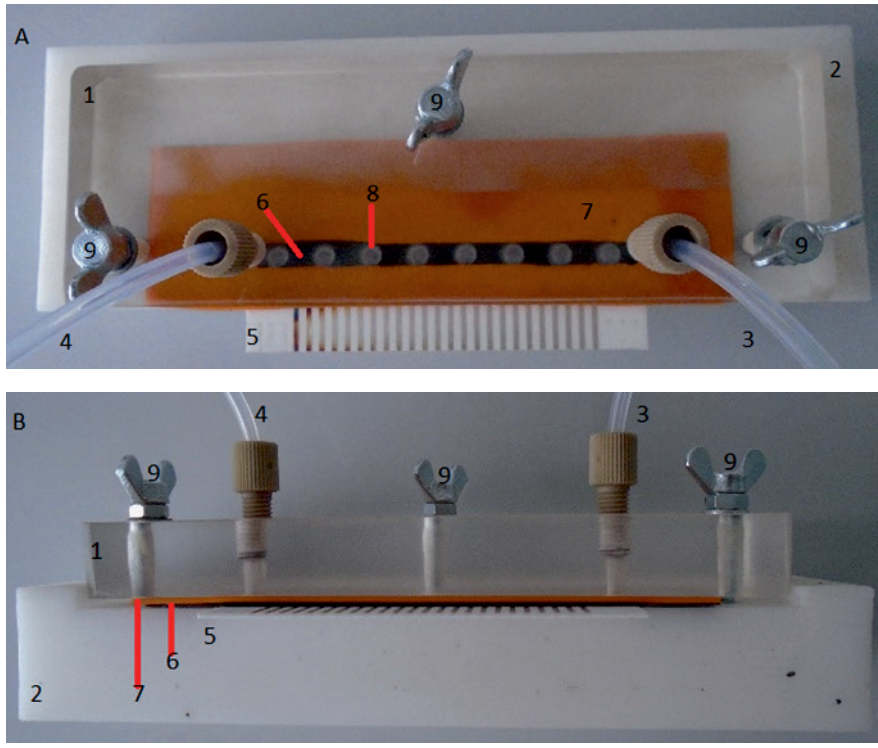

Figure 5. Custom-made flow-through cell: **A**) top view; and **B**) side view. The flow-through cell consists of: 1) cell top part; 2) the lower part of the cell; 3) the inflow tube; 4) the outflow tube; 5) the DropSens 550 screen-printed electrochemical array; 6) the black distance piece; 7) the orange silicone sealing; 8) the membrane; and 9) the screw (**IV**).

3.6. Cultivation of microorganisms

A Luria-Bertan (LB) liquid medium (10 g L^{-1} tryptone (Fischer Scientific (Belgium)), 5 g L^{-1} yeast extract (Fischer Scientific (Belgium)), and 5g L^{-1} NaCl (Lach-Ner (Czech Republic))) was used for the cultivation of bacteria. The cultivation was carried out under aerobic conditions in a rotating shaker (Heidolph, Germany) at 350 rpm and at 30 °C.

A total of 2 cm^3 of LB medium was inoculated with a *Pseudomonas putida* Pc15 strain. After sixteen hours of incubation, the inoculum was added to 250 cm^3 of culture medium which had been incubated in a rotating shaker at 350 rpm and at 30 °C. Cultivation time was five hours until the late exponential growth phase was achieved, after which the cells were collected for immobilisation.

3.7. Immobilisation of microorganisms

To immobilise the microorganism, the culture medium was centrifuged (using a Thermo Scientific, Heraeus Megafuge 40 Centrifuge) at 4000 rpm for a total of fifteen minutes and at a temperature of 25 °C. The supernatant was decanted and the cells were washed three times with a phosphate buffer solution (K_2HPO_4, 7 g L^{-1} (Cas 7758-11-4, Lach-Ner (Czech Republic)) and KH_2PO_4 7 g L^{-1} (Cas 7778770, Lach-Ner (Czech Republic)), pH 6.85), before being centrifuged again.

Entrapment in agarose gel matric was used for immobilisation, and plastic net discs were used as a support (Scrynel, PE 500 HD, ¼ inch diameter). 0.18 g agarose (Type I-A Low EEO) was mixed with a 7.5 cm^3 phosphate buffer and heated to 70 °C until the complete melting of the agarose was achieved. The mixture was cooled to 45 °C and 900 µl of previously prepared cell paste was added. The agarose and cell suspension were mixed thoroughly and dispersed on the net discs. The membranes were placed between two glass plates, and then pressure was applied in order to gain an even thickness of membranes. The membranes were set at 4 °C in a solution of OECD synthetic wastewater (peptone 1.6 g L^{-1} (LOT 177485; Cas 73049-73-7, Fischer Scientific (US)), beef extract 1.1 g L^{-1} (LOT-59P038 Biolife (Italy)), urea 0.3 g L^{-1} (Cas 57-13-6), NaCl 0.07 g L^{-1} (Cas 7647-14-5, Lach-Ner (Czech Republic)), $CaCl_2 \cdot H_2O$ 0.04 g L^{-1} (Cas 10035-04-8), and $MgSO_4 \cdot 7H_2O$ 0.02 g L^{-1} (Cas 10034-99-8)) diluted with a phosphate buffet to gain a BOD_5 of 5 mg L^{-1}.

3.8. Experimental setup for the BOD biosensor array

One hour before the measurements were carried out, the membranes were placed in a 0.1 M KCl solution at room temperature to allow the bacteria to adjust to the temperature. 0.1 M KCl solution, aerated with a pump (Resum, Pro Silent a 100, China), was used as a measurement solution.

The experimental setup was similar to that of Section 3.4. The membranes were set up so that the first hole (in the black distance piece) was left empty, while the second and third holes were modified by agarose membranes, and the rest of the five holes were modified with membranes which contain immobilised bacteria. The agarose membranes which contained the bacterial culture were numbered separately from one to ten.

The 0.1 M KCl solution was pumped through the measuring cell (equipment from FIAlab Instruments Inc., USA) for a total of 10 min at a pumping speed of 2 cm^3 min^{-1}. CA was used and electrochemical measurements were conducted with the PalmSens potentiostat. During the pre-step, the potential was held at +0.5 V vs Ag|AgCl|0.1 M KCl for 30 s. After the pre-step, the potential was changed to −0.3 V vs Ag|AgCl|0.1 M KCl for 120 s.

In order to calibrate and measure unknown samples, the samples were aerated and pumped through the biosensor cell for 10 min. After that, CA was carried out.

The membranes were calibrated with modified OECD synthetic wastewater (peptone 1.6 g L^{-1} (LOT 177485; Cas 73049-73-7, Fischer Scientific (US)), urea 0.3 g L^{-1} (Cas 57-13-6), beef extract 1.1 g L^{-1} (LOT-59P038) Biolife (Italy)) in 0.1 M KCl solution). When compared to the recipe from OECD, in this study NaCl, $MgSO_4$, and $CaCl_2$ were not used because they may have interfered with the electrochemical measurement.

The performance of the biosensor array was tested with genuine industrial wastewater. Liquid waste from the lignocellulosic bioethanol production process was selected in order to test the BOD array. The sample was obtained from the residue of a bio-ethanol production process - the pre-treatment of birch wood by nitrogen explosive decompression

method at 200 °C. This sample contains various compounds, which are the product of the hydrolysis of hemicellulose and cellulose. The composition of this sample is well-suited for the biosensor measurement since the sample contains a good many rapidly degradable compounds. The genuine industrial wastewater was measured with the biosensor array and the conventional APHA method (APHA, 1985) Section 507 for BOD_5 in order to provide a comparison with the results.

Several independent measurements were carried out with the BOD biosensor array and the error bars indicate the standard deviation of averaged results.

3.9. Data analysis

Data processing work was carried out using Microsoft Excel 2013 software.

Current density (j) was calculated from the measured current (I in A) using the following equation:

$$j = \frac{I}{S}, \qquad (\mathrm{A\ m^{-2}}) \quad (3)$$

where S (in m^2) is the working electrode area.

To characterize ORR, the corrected current density (j_c in A m^{-2}) was calculated by subtracting the current density measured in the Ar-saturated solution from the current density measured in the oxygen-saturated solution.

The capacitance (C) was calculated using the following formula:

$$C = \frac{j}{v}, \qquad (\mathrm{F\ m^{-2}}) \quad (4)$$

where j is the current density and v is the potential sweep rate (in V s^{-1}).

The mean of electric current was normalised using the following equation:

$$\mathrm{NSR} = \frac{I_0 - I_S}{I_0}, \qquad \text{(none)}(5)$$

where I_0 is output (in A) in the 0.1 M KCl solution, I_S the output (in A) in a solution which contains synthetic wastewater, and NSR is a normalised response (**IV**).

4. RESULTS AND DISCUSSION

4.1. Electrochemical experiments with a microfabricated sensor array

4.1.1. Preliminary experiments

The Pt electrodes are known to produce a characteristic curve in an acid solution (Bard and Faulkner, 2001; Shinozaki et al., 2015). Based on the shape of cyclic voltammogram it is possible to access the state of the Pt electrode and the purity of the electrolyte. During the production step, the microfabricated sensor array electrodes (Section 3.1) were also coated with an SU-8 layer. Due to this they did not produce a characteristic curve in the CV measurements. Therefore it was necessary to clean the sensor array prior to the tests. If a characteristic curve is acquired in a sulphuric acid solution, this indicates that contact with the electrode is established and that the Pt electrode behaves as expected.

Cleaning steps with the acetone and concentrated sulphuric acid were unavoidable. The detailed cleaning process regarding the microfabricated sensor array electrodes is characterised in the experimental section (Section 3.3). After cleaning had taken place, the CV measurement with the sensor array exhibited a characteristic curve (Fig. 6). The electrode's potential was swept from −0.18 V to 1.20 V vs Ag|AgCl|sat. KCl, and this was performed between fifty to a hundred times (the potential sweep rate was 500 mV s^{-1}). During this process, the platinum electrode surface was cleaned (in Fig. 6, one spike is divided into two spikes in the hydrogen adsorption/desorption region, from −0.18 V to 0.20 V vs Ag|AgCl|sat. KCl both in the cathodic scan and in the anodic scan). The shape of the cyclic voltammogram for the uncleaned electrode did not resemble the correct curve for platinum.

During the activation process, the current density $|j|$ increased in the hydrogen adsorption/desorption region (from −0.18 V to 0.20 V vs Ag|AgCl|sat. KCl), and in the oxygen adsorption/desorption region (from 0.40 V to 1.20 V vs Ag|AgCl|sat. KCl). The final curve shape is the same as for polycrystalline Pt (Gottesfeld, 1987; Shinozaki et al., 2015). This indicates that the electrode is operational. The tests were

continued only if the contact had been reached and a characteristic curve had been established in the sulphuric acid solution. The activation process was performed before every microfabricated sensor array measurements (4.1.2 and 4.1.3).

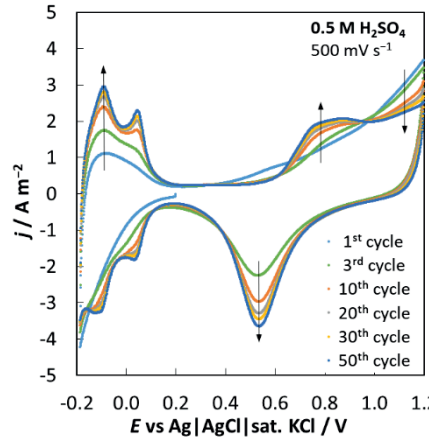

Figure 6. The sample cyclic voltammograms for the Pt working electrode of the microfabricated sensor array in the 0.5 M H_2SO_4 solution saturated with argon (fifty cycles). The arrows indicate the development of the characteristic shape during cycling (**III**).

4.1.2. The electrochemical characterisation of a microfabricated sensor array

The electrodes in the sensor array chip were characterised in a 0.5 M sulphuric acid solution, as this is a standard system for which Pt electrochemical behaviour is well-known, and in a 1 M KCl solution, as measurements were planned to be carried out in the future using this electrolyte. The resulting cyclic voltammetry curves for both solutions are shown in Fig. 7.

The results of the measurements in the 1 M KCl solution are discussed below. The current density for anodic and cathodic scans is proportional to the potential sweep rate (Fig. 7A, inset), which means that the capacitive process mainly takes place on the boundary of Pt and the 1 M KCl solution. The current density increases at a more negative potential than −0.05 V vs Ag|AgCl|sat. KCl, which may be due to hydrogen evolution (Fig. 7A). An increase in the current density (Fig. 7A) is also seen at potentials more positive than 0.60 V vs Ag|AgCl|sat. KCl, which may be due to the formation of the oxide layer on the Pt surface.

Therefore a measurement range selected for future experiments was between −0.05 V and 0.60 V vs Ag|AgCl|sat. KCl.

The CV data for the sulphuric acid solution are given in Fig. 7B. The resulting curve shape corresponds to polycrystalline Pt (Gottesfeld, 1987; Shinozaki et al., 2015). Hydrogen adsorption and desorption regions are well visible at potentials below 0.15 V vs Ag|AgCl|sat. KCl. At potentials more positive than (anodic sweep) 0.60 V vs Ag|AgCl|sat. KCl, a layer of oxide is produced on the Pt surface, which is reduced during a cathodic scan. There exists an electrical double layer region between the latter two areas. The capacitance (Formula 4) is almost independent of the potential sweep rate, except for the lower potential sweep rates at potentials which are more negative than −0.10 V vs Ag|AgCl|sat. KCl. The increase in capacitance is due to the evolution of hydrogen from the Pt electrode in an acidic solution.

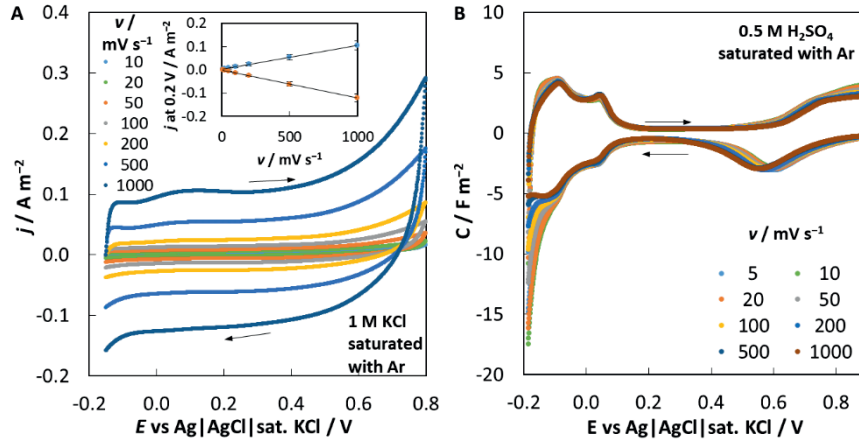

Figure 7. The cyclic voltammograms for the Pt working electrode at different potential sweep rates in: **A**) the 1 M KCl solution; and **B**) the 0.5 M H_2SO_4 solution (saturated with argon) (**III**).

Fig. 7 indicates that the sensor array electrodes are working, so it was possible to proceed with sensor array characterisation in the solutions containing oxygen at various concentrations.

4.1.3. The electroreduction of oxygen

As BOD is measured via the oxygen content in the solution, it was necessary to determine whether Pt electrodes on the chip were responding

to oxygen. The methodology used for these measurements is given in Section 3.3. The sensitivity of the chip electrodes to the oxygen content in the H_2SO_4 solution is characterised in Fig. 8.

The oxygen reduction process on the Pt electrode is irreversible and takes place predominantly through the four-electron pathway in an acid solution (Song and Zhang, 2008):

$$O_2 + 4H^+ + 4e^- = 2H_2O. \quad (6)$$

As oxygen reduction on the Pt electrode is irreversible, there is no anodic peak in the backward-moving scan. The difference between anodic and cathodic scans is very small (Fig. 8B), i.e. there is no hysteresis. A plateau is reached near 0 V vs Ag|AgCl|sat. KCl. At potentials more negative than −0.1 V vs Ag|AgCl|sat. KCl, the formation of hydrogen peroxide is again possible on the electrode through the two-electron pathway, and the current density $|j|$ decreases (Song and Zhang, 2008):

$$O_2 + 2H^+ + 2e^- = H_2O_2 . \quad (7)$$

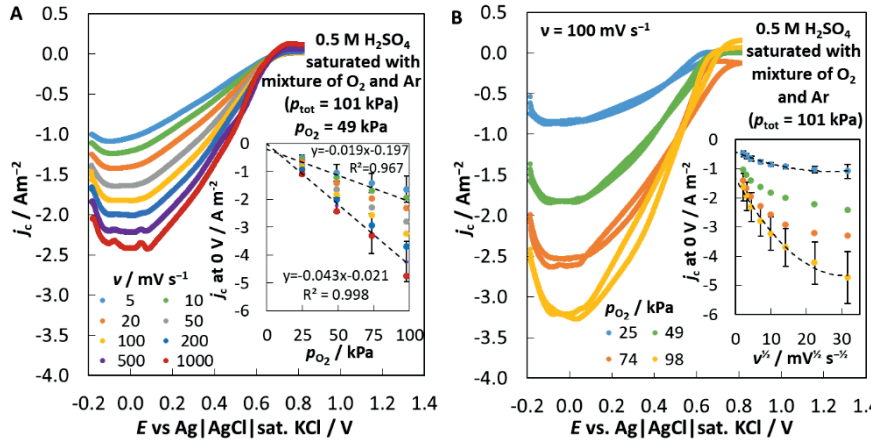

Figure 8. The electroreduction of oxygen with a microfabricated sensor array in the 0.5 M H_2SO_4 solution saturated with a mixture of argon and oxygen (p_{tot} = 101 kPa): **A**) oxygen partial pressure was kept constant and the potential sweep rate was varied (cathodic scan); and **B**) the potential sweep rate was kept constant and the partial pressure of the oxygen was varied (**III**).

Fig. 8B and the inset of Fig. 8A clearly show that the current density is different at different partial pressures of oxygen. The current density

$|j|$ increases as the partial pressure of oxygen increases, so the Pt electrode's current density depends upon the oxygen content and this allows the sensor array to be used for its desired purpose. The limiting current density is proportional to the partial pressure of oxygen at all studied sweep rates used (Fig. 8A, inset). In this figure, the initial ordinate is very close to zero.

A simplified formula can be used to characterise the diffusion layer thickness δ (Bard and Faulkner, 2001; Štulík et al., 2000):

$$\delta = \sqrt{\pi D t}\,, \qquad \text{(m)(8)}$$

where t is time (in s) and D is the diffusion coefficient of the reacting species (in $m^2\ s^{-1}$). In the case of oxygen reduction, the thickness of the diffusion layer is comparable to the size of the electrodes. At higher sweep rates, the radial diffusion becomes more significant than linear diffusion. Therefore, the shape of j_c vs v curves deviates from linearity (Fig. 8B, inset).

Electrochemical measurements have shown that the microfabricated sensor array could be used as a BOD sensor. However, the bacteria must be immobilised in a non-removable way inside the chip for a given sensor. This is somewhat problematic, as the electrodes of the given sensor array required cleaning with hot concentrated sulphuric acid before each measurement (and at a temperature of 50 °C). The immobilised microorganisms would not survive a cleaning of the electrodes with sulphuric acid or an ultrasonic bath treatment, and the bacteria should have been re-immobilised for each measurement. Therefore it would have been impossible to use the sensor multiple times if such routine cleaning of the electrodes is necessary.

4.2. The electrochemical characterisation of the DropSens550 screen-printed array

As the analysis in the Section 4.1 showed that it was impossible to apply the first sensor array to be tested fully, it was decided to try the DropSens550 sensor array instead. This was first examined in terms of how the different cell assembly methods (shown in Fig. 5) affect the received signal (Section 4.2.1.1). The effect of solution pumping rate was examined (Section 4.2.1.2). The following study investigated whether

this sensor array could be used to measure different oxygen levels in a solution (Section 4.2.2). The methodology used for the electrochemical measurements in this section is given in Section 3.4.

4.2.1. Preliminary experiments

Comparison of cyclic voltammetry response for different cell designs – Three different setups regarding the flow-through cell were tested during the course of this work:

- The flow-through cell with a channel alone.
- The flow-through cell with a distance piece and channel.
- The flow-through cell with a distance piece with membranes inserted into it, and a channel.

The CV results are given in Fig. 9. The current densities $|j|$ are smaller with the distance piece than they are without the distance piece (Fig. 9). The distance piece with wider holes (of a diameter of 5 mm) had higher current density values $|j|$ than did the distance piece with smaller holes (of a diameter of 3 mm). Reproducibility was better with the distance piece when it had the wider holes than with the distance piece with the smaller holes due to the fact that, in the case of the smaller holes, the free mixing of the solution is hindered. Therefore the following experiments were carried out with the distance piece which had the larger holes (of a diameter of 5 mm).

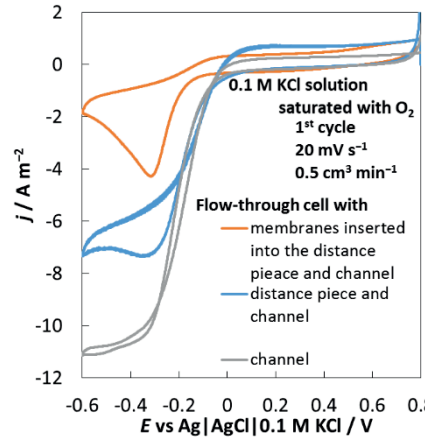

Figure 9. The sample cyclic voltammograms in the 0.1 M KCl solution saturated with oxygen for different cell designs.

After adding additional cell pieces (involving both a distance piece and membranes), the ORR current density $|j|$ decreases more as the mixing of the solution near the electrode uniforms the oxygen concentration only up to the membrane and a thick diffusion layer is formed inside the membrane itself. In addition, the diffusion regime probably changes from stationary to nonstationary. However, the flow-through cell with membranes inserted into the distance piece and with the channel had to be used as, in the next step, it was planned to modify the membranes with microorganisms.

Dependence of response on pumping speed of solution – It became necessary to check whether the pumping speed was affecting the measurement results, and how this could reveal itself. The flow-through cell which is shown in Fig. 5 was used to measure the current density (Fig. 10) at different pumping speeds in an oxygen-saturated 0.1 M KCl solution, while the electrode potential sweep rate was 20 mV s^{-1}. The results of wells from three to seven have been averaged. It was noted that the current density of the outer wells (wells 1, 2, and 8) tended to be higher, probably due to the additional mixing of the solution which seems to have taken place near the entrance and outlet of the cell. At all pumping speeds, the diffusion-limited current density plateau was formed (Fig. 10A). A small spike on the curve could be seen if the pumping speed was set at 0.1 cm^3 min^{-1}. This is probably caused by a non-stationary diffusion effect, which means that the pumping speed is insufficient when it comes to forming a uniform diffusion layer. If the pumping speed were to be set to a higher rate, then the current density values $|j|$ also tend to be higher (Fig. 10A, inset). The limited current density for the anodic and cathodic sweep is similar. If the pumping speed is higher than 0.9 cm^3 min^{-1}, the diffusion-limited current density becomes constant (Fig. 10A, inset).

To see whether the system has a memory effect, the cyclic voltammograms were measured in ascending order (from 0 to 0.9 cm^3 min^{-1}), and then in descending order of pumping speed (from 0.9 to 0 cm^3 min^{-1}). There is no hysteresis between these two series (Fig. 10A, inset). This confirms that ORR in this system takes place under stationary conditions and there is no notable memory effect.

The impact of the pumping speed on cyclic voltammograms (Fig. 10B) and chronoamperometric response (Fig. 11) was investigated when

membranes were placed on the electrodes in an oxygen-saturated solution. The CA measurements were taken after the CV measurements had been taken. The solution pumping speed was varied between 0 and 3.0 cm^3 min^{-1}.

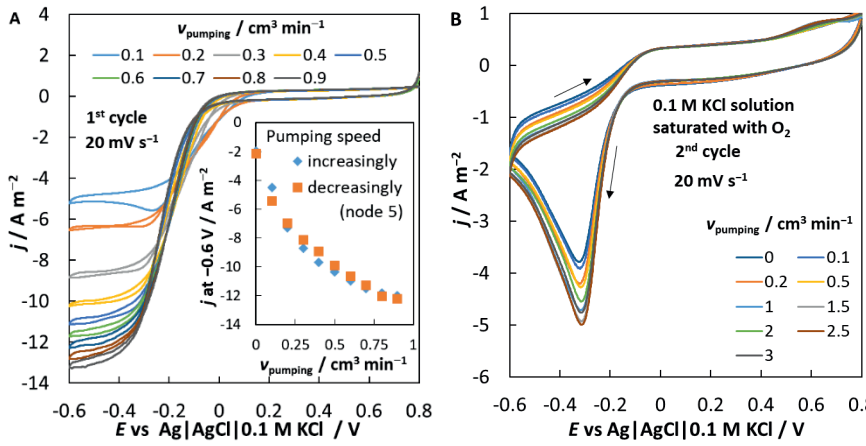

Figure 10. The dependence of cyclic voltammograms on the pumping speed in a 0.1 M KCl solution saturated with oxygen for different cell designs: **A**) the flow-through cell alone with a channel; and **B**) with additional agarose membranes (**IV**).

When comparing the cyclic voltammograms in parts A and B of Fig. 10, it became apparent that the shape of the measured curves is different, and the absolute value of the current density $|j|$ is greater without membranes than it is with membranes. This is due to the different cell assembly, as was expected (Fig. 9). The dependence of cyclic voltammograms on the pumping speed is rather moderate because the solution outside the membranes is mixed well enough to have a constant response even at low pumping speeds.

The hysteresis between the cathodic and anodic scans is pronounced, with this being caused by non-stationary diffusion (Fig. 10B), i.e. during the anodic sweep the concentration gradient was substantially lower. The potential sweep rate was probably too high to be able to achieve stationary behaviour. The ORR on the Pt electrode was irreversible; there was no anodic peak during the reverse scan. The pumping speed was not high enough to achieve a mass transport limited current plateau at cathodic potentials.

The CA results are shown in Fig. 11A. After the electrode potential is shifted from +0.5 V to −0.5 V vs Ag|AgCl|0.1 M KCl, the current

density $|j|$ increases due to ORR. After an initial increase, the current density $|j|$ begins to decrease due to the decrease of the concentration gradient, which in turn is due to the increase in the thickness of the diffusion layer. If the diffusion layer approaches the outer boundary of the membrane then a constant response is achieved. The current density $|j|$ increases with the pumping speed as in the case of the CV measurements.

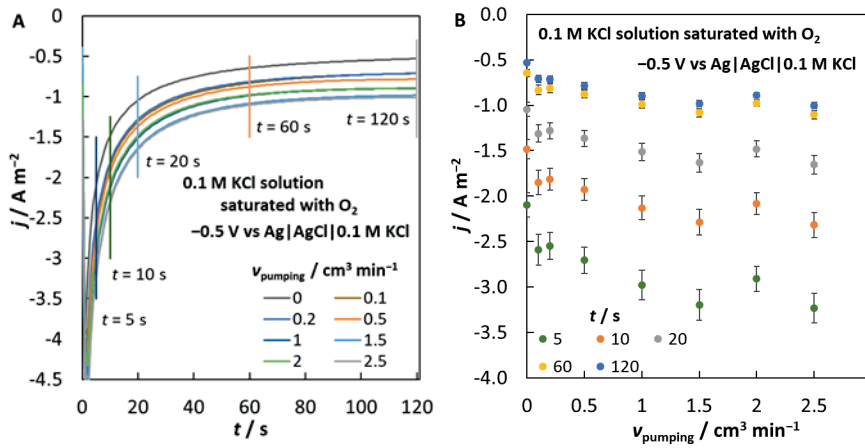

Figure 11. A) The dependence of the cronoamperometric (CA) curves on the pumping speed for a 0.1 M KCl solution saturated with oxygen. **B**) Dependencies of the current density on the pumping speed at different measurement times. The CA measurements were carried out at −0.5 V vs Ag|AgCl|0.1 M KCl after completion of the cyclic voltammetry measurements. The flow-through cell with membranes was used (**IV**).

If the pumping speed was higher than 1.5 $cm^3\ min^{-1}$, then the measurement signal $|j|$ did not increase remarkably and a constant value was achieved (Fig. 11B). The ORR rate is determined by the concentration gradient in the membrane. At higher pumping speeds it no longer changes because the solution outside the membrane has been mixed well enough, i.e. c_{O2} = const. From the above discussion, it can be concluded that a higher pumping speed (> 1.5 $cm^3\ min^{-1}$) does not provide a better result and would tend to lead to the measuring solution being wasted. Therefore a pumping speed of 2 $cm^3\ min^{-1}$ was selected for use in further tests when employing a flow-through cell with membranes.

The CA measurements for the flow-through cell with membranes were also taken before the CV measurements were done. However, the consistency of the second round of CA measurements, i.e. after the CV measurements were taken, always turned out to be better than that of

the first. This could be explained in two ways: a) the CV measurement has a cleaning effect on the electrodes; and b) it takes time to achieve a reproducible oxygen diffusion gradient in the membrane (the CV measurement took about ten minutes). If the cleaning effect of the CV measurement is an area of concern, then it is vital to carry out a CV measurement before the CA measurement is carried out, otherwise the CA measurement will not show the correct dependence of current density on the pumping speed.

Due to the use of membranes in the measurement process, it is unlikely that a stable response will be achieved in the flow-through cell if it contains membranes, compared to the flow-through cell without membranes. However, the membranes do have to be used.

4.2.2. Testing the DropSens550 screen-printed electrochemical array as an oxygen sensor

The ORR was studied on the electrodes of the DropSens550 screen-printed electrochemical array with membranes in an 0.1 M KCl electrolyte with various oxygen concentrations (see the method shown in Section 3.4). The CV and CA measurements were carried out. The CA measurements were carried out before and after the CV measurements. The results of the CV measurements are given in Fig. 12. The first and second scans were very similar. Such similarity was accomplished because the fluid was pumped continuously during the scans and the current no longer decreased during the second scan, i.e., the potential sweep rate was slow enough to reach a pseudo-stationary state. The time spent in the potential region in which ORR did not take place was probably long enough to saturate the membrane with oxygen.

A few additional remarks should be added here, such as: a) the current density differed from zero in the potential region from 0 V to 0.6 V vs Ag|AgCl|0.1 M KCl, and was symmetrical around the potential axis. This was caused by the charging and discharging of the electrical double layer (see Section 4.1.2.); b) at even more anodic potentials (E > 0.6 V vs Ag|AgCl|0.1 M KCl), the increase in current density was probably caused by the formation of an oxide layer on the surface of the Pt electrode; and c) there was an ORR peak on the cyclic voltammograms if the oxygen concentration in the electrolyte was zero. This was probably caused by the residual oxygen in the agarose membrane.

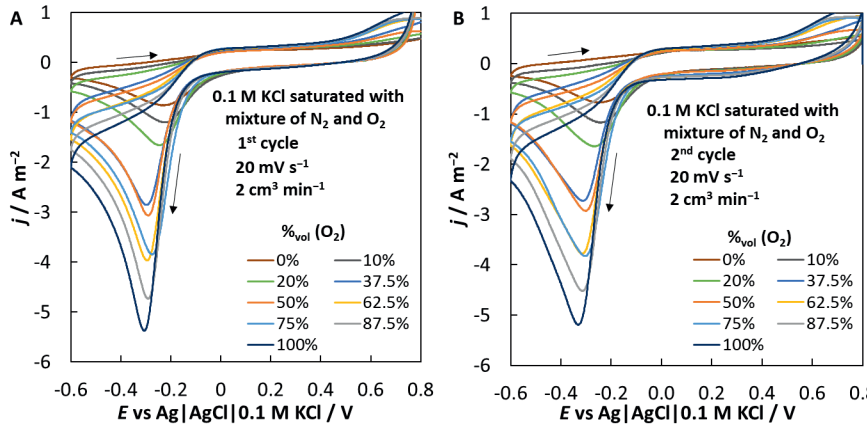

Figure 12. The cyclic voltammograms in the 0.1 M KCl solution saturated with a mixture of nitrogen and oxygen (p_{tot} = 101 kPa) at different partial pressures of oxygen: **A**) first cycle; and **B**) second cycle. The flow-through cell with membranes was used (**IV**).

The results of the CA measurements are shown in Figs. 13 and 14. The electrode potential for measurements was −0.5 V vs Ag|AgCl|0.1 M KCl as, according to the CV measurements, the ORR is mass-transfer limited at this potential. The potential was initially held at 0.5 V vs Ag|AgCl|0.1 M KCl, where no ORR take place. This ensures a more homogeneous oxygen concentration in the membrane. After the potential jump, the current density $|j|$ increases sharply as the charging of the electrical double layer takes place (Fig. 13). Simultaneously, ORR starts at the electrode. After this, the current density decreases as the oxygen is consumed from the diffusion layer and the oxygen concentration gradient decreases. Current density stabilises after approximately 120 s, as the solution is continuously pumped over the electrodes and a pseudo-stationary state is reached, i.e. the oxygen concentration gradient is constant. The general shape of the CA curves before and after the CV measurements are carried out can be seen to remain the same.

The current density depends on the oxygen concentration. The calibration curves have been constructed at different times from the beginning of the CA measurement (Fig. 14). These dependencies are linear at all time points. The standard deviation (for all eight sets of electrodes) of the current density is lower for the data points, which are collected after a longer electrolysis time because a more reproducible concentration gradient is achieved. The ordinate for these lines is different from zero. If the CA measurement is carried out after the CV measurement has

been carried out, the repeatability and linearity of the CA response is better. Apparently, cycling helps to stabilise the oxygen concentration gradient.

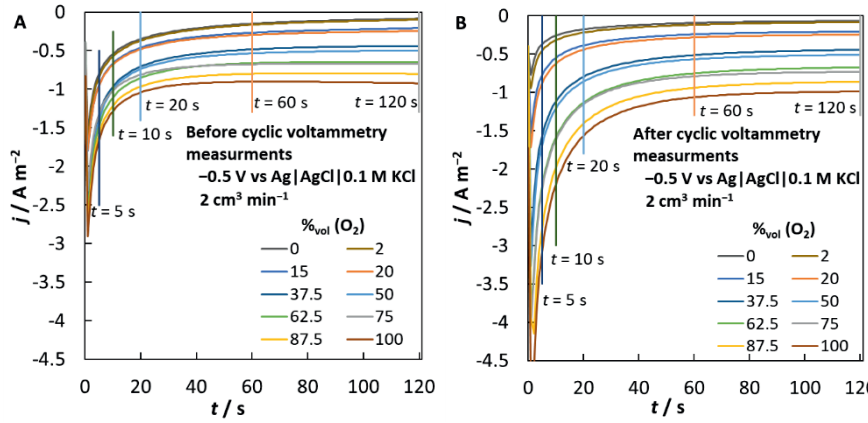

Figure 13. The cronoamperometric measurement of oxygen electroreduction at −0.5 V vs Ag|AgCl|0.1 M KCl in the 0.1 M KCl solution saturated with a mixture of nitrogen and oxygen (p_{tot} = 101 kPa): **A**) before and **B**) after the cyclic voltammetry measurements have been taken. The flow-through cell with membranes was used (**IV**).

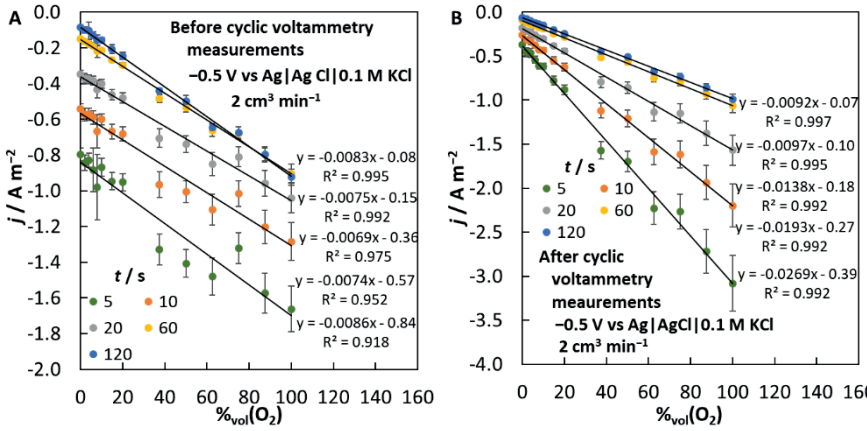

Figure 14. The dependence of oxygen reduction current density on volume percentage of oxygen at different times at −0.5 V vs Ag|AgCl|0.1 M KCl in the 0.1 M KCl solution saturated with a mixture of nitrogen and oxygen (p_{tot} = 101 kPa): **A**) before and **B**) after the cyclic voltammetry measurements have been carried out. The flow-through cell with membranes was used (**IV**).

An optimum measurement time should be found to carry out the analysis. If this time is too long then the sensitivity decreases. However, a stable response is not achieved if the time is too short. A total of two full minutes is enough to get a stationary current density. Even after 60 s

the current density no longer changes in time to any significant degree (Fig. 13). To show how current density changes over time, calibration equations are displayed at different time points during the measurement process. With the longer times, such as 120 s, current density $|j|$ is lower and a pseudo-stationary state is achieved. However, after a shorter measurement time, such as 5 s, sensitivity is better if the CA measurement is performed after the CV measurement has been carried out (Fig. 14B). The CV measurement helps to stabilise the oxygen concentration gradient in the membrane because it takes time for the oxygen to diffuse through the membrane. A time of sixty seconds was chosen as the optimum measurement time because the current density is stable and yet sensitivity is good enough.

As the CV data have shown that cyclic voltammograms are indeed very reproducible, the CA measurements were also carried out at the potential −0.3 V vs Ag|AgCl|0.1 M KCl, which is close to the ORR peak potential where the current density $|j|$ is highest. Better results were obtained if the potential was held at +0.5 V vs Ag|AgCl|0.1 M KCl prior to the application of the measurement potential. The measured CA curves and calibration lines at different measurement times are shown in Fig. 15. These figures display those CA measurements which were carried out after the CV measurement was completed. As in preceding measurements, carrying out the CA measurements after the CV measurements tends to produce more reproducible results. The behaviour of the CA curves in Figs. 14B and 15B are very similar. Current density $|j|$ is slightly lower when compared to the CA measurement at the potential of −0.5 V vs Ag|AgCl|0.1 M KCl. However, the difference is small, and diffusion limited behaviour is achieved at both potentials. As there was no notable difference, the CA measurements were carried out at −0.3 V vs Ag|AgCl|0.1 M KCl in subsequent tests.

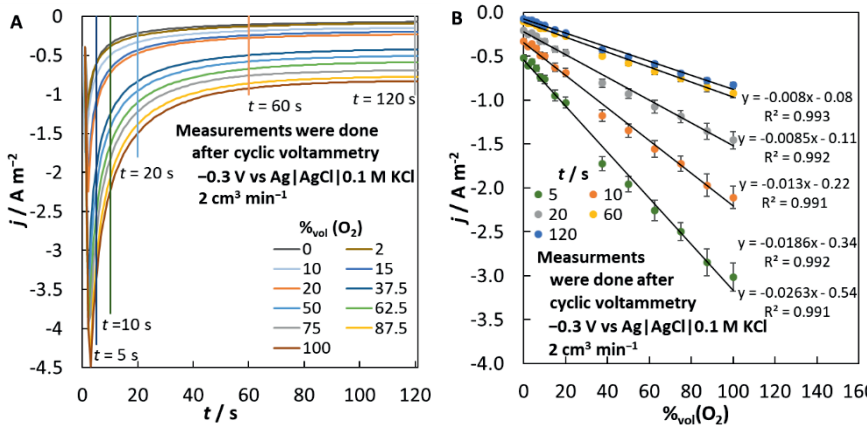

Figure 15. The dependence of the oxygen reduction current density on the volume percent of oxygen at different times at −0.3 V vs Ag|AgCl|0.1 M KCl in a 0.1 M KCl solution saturated with a mixture of nitrogen and oxygen (p_{tot} = 101 kPa): **A**) the chronoamperometry (CA) curves; and **B**) CA data at different times. The flow-through cell with membranes was used (**IV**).

4.3. Testing the DropSens550 screen-printed electrochemical array as a biosensor array

In order to use the sensor array chip as a biosensor, membranes with microorganisms (Section 3.5) were placed on the electrodes (Sections 3.6 and 3.7). In addition, membranes which contained only agarose were used in this process, and one set of electrodes was left without a membrane at all to act as a control set. A flow-through cell (Fig. 5) was used for measurements. A 0.1 M KCl solution was used as a carrier solution for the tests, while calibration was carried out using modified OECD synthetic wastewater (Section 3.8), and a sample of wastewater with an unknown BOD value (Section 3.8) was used to assess the accuracy of the method.

CA was used to measure the current density of the biosensor in the carrier solution, and with synthetic wastewater using different BOD values in the carrier solution (Fig. 16). The figure shows that samples which have different BOD values provide different current density values. After the beginning of the CA measurement process, it can be seen that current density $|j|$ decreases to a certain level and then remains constant. It can be seen that after 60 s, the output signal is stable and is similar to the value at 120 s. The same behaviour was also demonstrated in the previous section in Fig. 13. In the subsequent data

analysis, current densities after a period of 60 s were used. The higher was the BOD value, the lower was the measured current density $|j|$. If the BOD value is higher then there are more organic compounds in the solution which can be bounded by the microorganisms and more oxygen is consumed in the membrane, as a result less oxygen is delivered to the electrode.

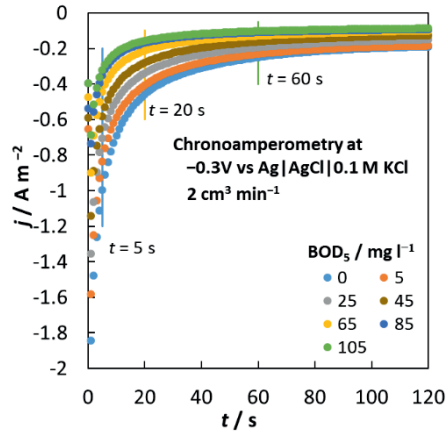

Figure 16. Biosensor signal (current density, j) during the chronoamperometry measurement in a solution of OECD wastewater at different BOD_5 values; at −0.3 V vs Ag|AgCl|0.1 M KCl with a *Pseudomonas putida* membrane (**IV**).

The critical parameters which characterise the BOD sensor include linearity, sensitivity, response time, and the conformance of the traditional BOD_5 to the sensor BOD (as was previously outlined in Section 1.1.1). Fig. 17 shows that sensitivities and linear ranges of the different membranes in the sensor array tend to vary. The difference in sensitivity may be due to different amounts of bacteria in the membranes.

The linear range of the biosensor being used was up to 65-85 mg L^{-1} BOD. In this work, sensitivity was obtained within a range of 0.0018 to 0.0068 $(mg\ L^{-1})^{-1}$. These parameters are compared in Table 1 with other BOD biosensors. The researchers have studied different transducers and sensitive elements. In this study, the response time is rather small when compared to those of the other listed research works. It is hard to compare the sensitivity and the linear range because every author provides results in different units.

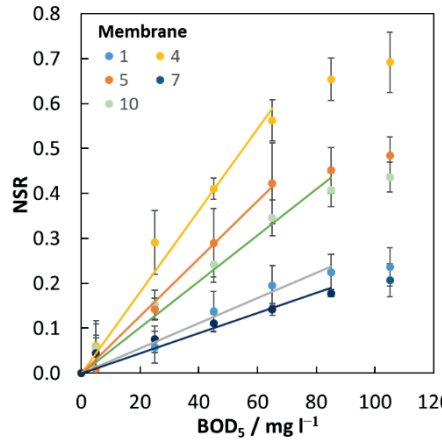

Figure 17. Calibration graphs for different biosensor membranes at a measurement 60 s when OECD wastewater was used for calibration purposes. The different colours indicate different biosensor membranes, while the linear line shows the linear range in which measurements could be conducted. The membranes 1, 4, 5, 7, and 10 were modified with *Pseudomonas putida* (**IV**).

The commercial BOD biosensors often have a measurement range of more than 300 mg BOD L^{-1} (Bahadır and Sezgintürk, 2015).

Table 1. A comparison of BOD biosensor parameters.

Transducer	Sensitive element	Response time (min)	Sensitivity	Linear range	References
Pt electrodes as a dissolved oxygen (DO) sensor	*Pseudomonas putida* Pc15 strain	1	0.0018-0.0068 $(mg\ L^{-1})^{-1}$	5-65 (85) $(mg\ L^{-1}$ BOD)	This work
PdNPs/rGN-COOH/ UMEA as a DO sensor	Fe_3O_4 functionalised *Bacillus subtilis*	5	2.093 $nA/\ (mg{\cdot}L^{-1})$	2-15 $(mg\ L^{-1})$	Wang et al., 2017
A reagent-free tubular biofilm reactor	Activated sludge	–	–	0.25-30 $(mg\ O_2\ L^{-1})$	Liu et al., 2013
A modified ultramicro-electrode array	*Bacillus subtilis* carboxyl graphene	3	3.04 $(nA\ (mg\ L^{-1})^{-1})$	2-15 $(mg\ L^{-1})$	Li et al., 2017
A glassy carbon electrode	Mixed culture	9	0.19 $(\mu A\ (mgO_2\ L^{-1})^{-1})$	1-100 $(mg\ O_2\ L^{-1})$	Niyomdecha et al., 2017
Gold-modified boron-doped diamond electrodes	*Rhodotorula mucilaginosa* UICC Y-181	20	1.4 $\mu A\ mg^{-1}$ L oxygen	10-50 $mg\ L^{-1}$ BOD	Ivandini et al., 2012
Au working electrode (reduced graphene oxide-based hydrogel)	Microbe	<10	–	2-64 $mg\ O\ L^{-1}$	Liu et al., 2015
Gold-disk working electrode	*Bacillus subtilis*	5	1.58 $nA\ (mg\ L^{-1})^{-1}$	5-30 $mg\ L^{-1}$ BOD	Li et al., 2016

In order to check the suitability of the biosensor array for the measurement of BOD in wastewater, actual wastewater (Section 3.8) was also analysed. The results are shown in Fig. 18. The sensor BOD is compared to the BOD_5 value, which was obtained by means of the standard method (Section 3.8).

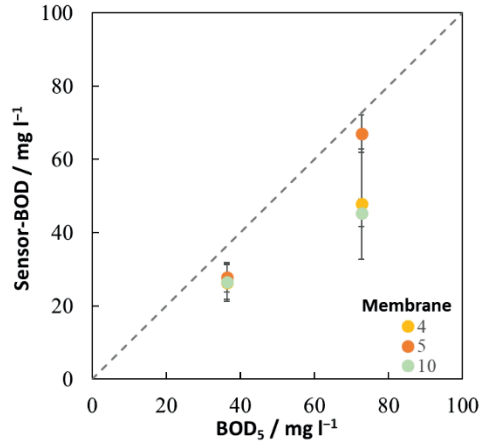

Figure 18. A comparison of BOD_5 and sensor-BOD, where the dashed line shows a one-to-one correlation between BOD_5 and sensor-BOD. The membranes 4, 5, and 10 were modified with *Pseudomonas putida* (**IV**).

The biosensor array which is the subject of this study generally underestimates the solution's BOD value by 8-37%. This may be due to the presence of complex compounds in the test solution, with those compounds not easily being degradable within a short time during which the sensor array measurement was being carried out. There are other studies available in which the BOD value was also underestimated by the BOD biosensors (Lei and Yi, 2010; Webber et al., 2011). Webber et al. described a 73% underestimation of the BOD value with a *K. oxytoca* culture (Webber et al., 2011). Overall, it is expected that the sensors do tend to underestimate the BOD value. This biosensor array can be applied for the assessment of the BOD value of wastewater samples.

5. CONCLUSIONS

The aim of this doctoral thesis was to study different senor arrays in order to construct a BOD biosensor array, which is fast, easy-to-use, and provides reliable results. The following tasks were set out in order to make this gaol achievable:

1. Study the current state of BOD sensor arrays (**I**).
2. Study the usability of the microfabricated and screen-printed sensor array (the DropSens550) in the form of a BOD sensor array (**II**, **III**, and **IV**). Choose the appropriate sensor array for BOD measurements (**III** and **IV**).
3. Test the performance of the BOD sensor array in the standard solution and in the genuine sample (**IV**).

Firstly, the microfabricated senor array which consists of the silicon and borosilicate wafers with Pt electrodes was used. The electrochemical behaviour of the Pt electrodes in the sensor array was studied in the 0.5 M sulphuric acid solution, and in the 1 M potassium chloride solution. The cyclic voltammograms for the platinum electrodes in the sulphuric acid solution had a characteristic shape. Therefore the electrolyte solution and the cell were clean, and the platinum electrodes were working as expected. A test was then carried out to see whether the senor array is sensitive to changes in oxygen content in the solution. The cyclic voltammograms were measured at different partial oxygen pressures (at 0, 25, 49, 74, and 98 kPa) in a 0.5 M sulphuric acid solution. The mass transport limited current density is proportional to the oxygen concentration. For example, the mass transport limited current densities were -0.84 A m^{-2} and -3.3 A m^{-2} at the electrode potential scan rate of 0.1 V s^{-1} if the oxygen partial pressure was at 25 kPa and 98 kPa respectively. Due to the nature of the sensor array's manufacturing process, this sensor array had to be cleaned in a concentrated sulphuric acid solution prior to each measurement. Therefore the immobilisation of microorganisms directly on the sensor array turned out to be impossible, making routine measurements with this sensor entirely impractical.

As an alternative option, the screen-printed sensor array, a DropSens550, was tested. The cyclic voltammetry and chronoamperometry measurements were carried out in a 0.1 M potassium chloride solution which had been saturated with a mixture of oxygen and nitrogen. The

current density measured with the sensor array, a DropSens550, depended on the oxygen concentration in the solution. For example, the averaged mass transport limited current densities were -1.6 A m^{-2} and -5.2 A m^{-2} at the electrode potential scan rate of 0.02 V s^{-1} if the oxygen volume percentage was 20 $\%_{vol}$ and 100 $\%_{vol}$ respectively. Then the dependence of the current density in the mass transport limited area on the solution's pumping speed was investigated. As the mass transport limited current density did not depend too much on the pumping speed when it was above 1.5 cm^3 min^{-1}, a pumping speed of 2 cm^3 min^{-1} was selected for further tests with the flow-through cell when using membranes. The conditions under which the chronoamperometry measurements were to be carried out was determined from the results of the cyclic voltammetry. To determine the oxygen concentration, the electrode potential was stepped from +0.5 V to -0.3 V or -0.5 V vs Ag|AgCl|0.1 M KCl when undertaking chronoamperometry measurements. In both cases, the linear response on oxygen concentration was achieved.

Chronoamperometry at -0.3 V vs Ag|AgCl|0.1 M KCl was carried out in order to calibrate the biosensor array. The calibration was performed with the modified OECD synthetic wastewater. The membranes were modified with the *Pseudomonas putida* Pc15 strain. Different membranes in the biosensor array had different sensitivity levels and linear ranges. This may be due to the different amounts of bacteria in the different membranes. The linear range of the biosensors was up to 65-85 mg L^{-1} BOD. The sensitivity of these biosensors was within the range of 0.0018 to 0.0068 $(mg\ L^{-1})^{-1}$. The fabricated biosensor array was used to analyse the actual wastewater. The biosensor BOD was compared to the BOD_5 value, which was obtained by means of the standard method. The biosensor array which was being studied generally underestimated the solution's BOD value by 8-37%.

Most of the hypotheses were indeed confirmed. All of the tasks which had been set out were indeed completed. It was possible to measure oxygen concentration with both sensor arrays. Due to some technical difficulties, however, it was not possible to measure BOD with the microfabricated senor array. However, the sensor array, the DropSens550, was suitable for BOD measurements. The microbially-modified sensor array, DropSens550, was successfully used to evaluate the BOD value of the calibration solutions and the wastewater samples.

In the future, it may be feasible to measure BOD values with the sensor array which consists of several membranes which have been modified with different pure bacterial cultures.

REFERENCES

Ahmed A. A. M., Shah S. M. A. (2017) Application of adaptive neuro-fuzzy inference system (ANFIS) to estimate the biochemical oxygen demand (BOD) of Surma River. *Journal of King Saud University – Engineering Sciences* 29, 237-243.

APHA (1985) Standard methods for examination of water and wastewater. Washington American Public Health Association (APHA Standard Method 16th Edition Section 507 Oxygen demand (biochemical)).

Arduini F., Cinti S., Scognamiglio V., Moscone D., Palleschi G. (2017) How cutting-edge technologies impact the design of electrochemical (bio)sensors for environmental analysis. A review. *Analytica Chimica Acta* 959, 15-42.

Arlyapov V., Kamanin S., Ponamoreva O., Reshetilov A. (2012) Biosensor analyzer for BOD index express control on the basis of the yeast microorganisms *Candida maltosa*, *Candida blankii*, and *Debaryomyces hansenii*. *Enzyme and Microbial Technology* 50, 215-220.

Arlyapov V. A., Yudina N. Yu., Asulyan L. D., Alferov S. V., Alferov V. A., Reshetilov A. N. (2013) BOD biosensor based on the yeast *Debaryomyces hansenii* immobilized in poly(vinyl alcohol) modified by N-vinylpyrrolidone. *Enzyme and Microbial Technology* 53, 4, 257-262.

Arlyapov V. A., Yudina N. Yu., Asulyan L. D., Kamanina O. A., Alferov S. V., Shumsky A. N., Machulin A. V., Alferov V. A., Reshetilov A. N. (2020) Registration of BOD using *Paracoccus yeei* bacteria isolated from activated sludge. *Biotech* 10, 207.

Bahadır E.B., Sezgintürk M.K. (2015) Review Applications of commercial biosensors in clinical, food, environmental, and biothreat/biowarfare analyses. *Analytical Biochemistry* 478, 107-120.

Baharfar M., Rahbar M., Tajik M., Liu G. (2020) Engineering strategies for enhancing the performance of electrochemical paper-based analytical devices. *Biosensors and Bioelectronics* 167, 112506.

Banerjee R. R., Tudu B., Bandyopadhyay R., Bhattacharyya N. (2016) A review on combined odor and taste sensor systems. *Journal of Food Engineering* 190, 10-21.

Baracu A. M., Gugoasa L. A. D. (2021) Review—Recent Advances in Microfabrication, Design and Applications of Amperometric Sensors and Biosensors. *Journal of The Electrochemical Society* 168, 037503.

Bard A. J. and Faulkner L. R. (2001) *Electrochemical Methods: Fundamentals and Applications*, 2nd ed., p. 864, Wiley & Sons, New York.

Bhalla N., Jolly P., Formisano N., Estrela P. (2016) Introduction to biosensors. *Essays in Biochemistry* 60, 1-8.

Biswas P., Karn A. K. Balasubramanian P., Kale P. G. (2017) Biosensor for detection of dissolved chromium in potable water: A review. *Biosensors and Bioelectronics* 94, 589-604.

Blair E. O., Corrigan D. K. (2019) A review of microfabricated electrochemical biosensors for DNA detection. *Biosensors and Bioelectronics* 134, 57-67.

Blanco C., de la Fuente R., Caballero I., Rodriguez-Mendez M. L. (2015) Beer discrimination using a portable electronic tongue based on screen-printed electrodes. *Journal on Food Engineering* 157, 57-62.

Bourgeois W., Gardey G., Servieres M., Stuetz R. M. (2003) A chemical sensor array based system for protecting wastewater treatment plants. *Sensors and Actuators B: Chemical* 91, 1-3, 109-116.

Bourgeois W., Hogben P., Pike A., Stuetz R. M. (2003) Development of a sensor array based measurement system for continuous monitoring of water and wastewater. *Sensors and Actuators B: Chemical* 88, 3, 312-319.

Bourgeois W., Romain A.-C., Nicolas J., Stuetz R. M. (2003) The use of sensor arrays for environmental monitoring: interests and limitations. *Journal of Environmental Monitoring* 5, 6, 852-860.

Bourgeois W., Stuetz R. M. (2002) Use of a chemical sensor array for detecting pollutants in domestic wastewater. *Water Research* 36, 18, 4505-4512.

Bratov A., Abramova N., Ipatov A. (2010) Recent trends in potentiometric sensor arrays—A review. *Analytica Chimica Acta*, 678, 149-159.

Campos I., Alcañiz M., Aguado D., Barat R., Ferrer J., Gil L., Marrakchi M., Martínez-Mañez R., Soto J., Vivancos J.-L. (2012) A voltammetric electronic tongue as tool for water quality monitoring in wastewater treatment plants. *Water Research* 46, 8, 2605-2614.

Castillo J., Gáspár S., Leth S., Niculescu M., Mortari A., Bontidean I., Soukharev V., Dorneanu S. A., Ryabov A. D., Csöregi E. (2004) Biosensors for life quality Design, development and applications. *Sensors and Actuators B*, 102, 179-194.

Cave J. W., Wickiser J. K., Mitropoulos A. N. (2019) Progress in the development of olfactory-based bioelectronic chemosensors. *Biosensor and Bioelectronics* 123, 211-222.

Cetó X., Voelcker N. H., Prieto-Simón B. (2016) Bioelectronic tongues: New trends and applications in water and food analysis. *Biosensors and Bioelectronics* 79, 608-626.

Chan C., Lehmann M., Chan K., Chan P., Chan C., Gruendig B., Kunze G., Renneberg R. (2000) Designing an amperometric thick-film microbial BOD sensor. *Biosensors and Bioelectronics* 15, 343-353.

Chee G.-J. (2013) Development and characterization of microbial biosensors for evaluating low biochemical oxygen demand in rivers. *Talanta* 117, 366-370.

Chu Z., Peng J., Jin W. (2017) Advanced nanomaterial inks for screen-printed chemical sensors. *Sensors and Actuators* B 243, 919-926.

Ciosek P., Wroblewski W. (2007) Sensor arrays for liquid sensing - electronic tongue systems. *Analyst* 132, 10, 963-978.

Collard D., Kim S. H., Osaki T., Kumemura M., Kim B., Fourmy D., Fujii T., Takeuchi S., Karsten S. L., Fujita H. (2013) Nano bioresearch approach by microtechnology. *Drug Discovery Today* 18, 11/12.

Commault A.S., Lear G., Bouvier S., Feiler L., Karacs J., Weld R.J. (2016) *Geobacter*-dominated biofilms used as amperometric BOD sensors. *Biochemical Engineering Journal* 109, 88-95.

Czolkos I., Dock E., Tønning E., Christensen J., Winther-Nielsen M., Carlsson C., Mojzíková R., Skládal P., Wollenberger U., Nørgaard L., Ruzgas T., Emnéus J. (2016) Prediction of wastewater quality using amperometric bioelectronics tongues. *Biosensors and Bioelectronics* 75, 375-382.

Dai Y., Furst A., Liu C. C. (2019) Review: Strand Displacement Strategies for Biosensor Applications. *Trends in Biotechnology* 37, 12.

Derkus B. (2016) Applying the miniaturization technologies for biosensor design. *Biosensors and Bioelectronics* 79, 901-913.

del Valle M. (2010) Electronic Tongues Employing Electrochemical Sensors. *Electroanalysis* 22, 14, 1539-1555.

D'Souza S. F. (2001) Microbial biosensors. *Biosensors and Bioelectronics* 16, 337-353.

Dutt M. A., Hanif M. A., Nadeem F., Bhatti H. N. (2020) A review of advances in engineered composite materials popular for wastewater treatment. *Journal of Environmental Chemical Engineering* 8, 104073.

Ejeian F., Azadi S., Razmjou A., Orooji Y., Kottapalli A., Warkiani M. E., Asadnia M. (2019) Design and applications of MEMS flow sensors: A review. *Sensors and Actuators* A 295, 483-502.

Ejeian F., Etedali P., Mansouri-Tehrani H.-A., Soozanipour A., Low Z.-X., Asadnia M., Taheri-Kafrani A., Razmjou A. (2018) Biosensors for wastewater monitoring: A review. *Biosensors and Bioelectronics* 118, 66-79.

Estonian Electronic Microbial dataBase (2021) University of Tartu. Retrieved from http://eemb.ut.ee/eng

Fathi F., Rashidi M.-R., Pakchin P. S., Ahmadi-Kandjani S., Nikniazi A. (2021) Photonic crystal based biosensors: Emerging inverse opals for biomarker detection. *Talanta* 221, 121615.

Franssila S. (2006) *Introduction to microfabrication.* Chichester : Wiley, pp.3-15, England.

Ganesan S., Mehta S., Gupta D. (2019) Fully printed organic solar cells – a review of techniques, challenges and their solutions. *Opto-Electronics* 27, 3, 298-320.

Ge S., Ge L., Yan M., Song X., Yu J., Huang J. (2012) A disposable paper-based electrochemical sensor with an addressable electrode array for cancer screening. *Chemical Communications* 48, 9397-9399.

Gonzalez-Sanchez M. I., Valero E., Compton R.G. (2016) Iodine mediated electrochemical detection of thiols in plant extracts using platinum screen-printed electrodes. *Sensor and Actuators B* 236, 1-7.

Głowacz K., Wawrzyniak U. E., Ciosek-Skibińska P. (2021) Comparison of various data analysis techniques applied for the classification of oligopeptides and amino acids by voltammetric electronic tongue. *Sensors and Actuators B: Chemical* 331, 129354.

Gottesfeld S., Raistrick I. D., Srinivasan S. (1987) Oxygen Reduction Kinetics on a Platinum RDE Coated with a Recast Nafion Film. *Journal of the Electrochemical Society* 134, 1455.

Guo F., Liu Y, Liu H. (2021) Hibernations of electroactive bacteria provide insights into the flexible and robust BOD detection using microbial fuel cell-based biosensors. *Science of the Total Environment* 753, 142244.

Gupta N., Renugopalakrishnan V., Liepmann D., Paulmurugan R., Malhotra B.D. (2019) Cell-based biosensors: Recent trends, challenges and future perspectives. *Biosensors and Bioelectronics* 141, 111435.

Ha D., Sun Q., Su K., Wan H., Li H. , Xu N., Sun F., Zhuang L., Hu N., Wang P. (2015) Recent achievements in electronic tongue and bioelectronic tongue astaste sensors. *Sensors and Actuators B* 207, 1136-1146.

Hayat A., Marty J. L. (2014) Review: Disposable Screen Printed Electrochemical Sensors: Tools for Environmental Monitoring. *Sensors* 14, 6, 10432-10453.

Hwa L. C., Rajoo S., Noor A. M., Ahmad N., Uday M.B. (2017) Recent advances in 3D printing of porous ceramics: A review. *Current Opinion in Solid State and Materials Science* 21, 323-347.

Ikumapayi O. M., Akinlabi E. T., Adeoye A. O. M., Fatoba S.O. (2021) Microfabrication and nanotechnology in manufacturing system – An overview. *Materials Today: Proceedings* 44, 1154-1162.

Ivandini A. T., Saepudin E., Wardah H., Dewangga N., Einaga Y. (2012) Development of a biochemical oxygen demand sensor using gold-modified boron doped diamond electrodes. *Analytical Chemistry* 84, 9825-9832.

Janata J., Bezegh A. (1988) Chemical Sensors. *American Chemical Society*, 60, 62R-74R.

Jiawen Y., Wanlei G., Zan Z., Yuliang M., Anbo L., Han J., Jiawen J., Qinghui J. (2020) Batch microfabrication of highly integrated silicon-based electrochemical sensor and performance evaluation via nitrite water contaminant determination. *Electrochimica Acta* 03, 335.

Jouanneau S., Grange E., Durand M.-J., Thouand G. (2019) Rapid BOD assessment with a microbial array coupled to a neural machine learning system. *Water Research* 166, 115079.

Jouanneau S., Recoules L., Durand M. J., Boukabache A., Picot V., Primault Y., Lakel A., Sengelin M., Barillon B., Thouand G. (2014) Review: Methods for assessing biochemical oxygen demand (BOD): A review. *Water Research* 49, 62-82.

Kalkal A., Kumar S., Kumar P., Pradhan R., Willander M., Packirisamy G., Kumar S., Malhotra B. D. (2021) Review: Recent advances in 3D printing technologies for wearable (bio)sensors. *Additive Manufacturing* 46, 102088.

Karube I., Matsunaga T., Mitsuda S., Suzuki S. (1977). Microbial electrode BOD sensors. *Biotechnology and Bioengineering* 19, 10, 1535-1547.

Kashem Md.A., Suzuki M., Kimoto K., Iribe Y. (2015) An optical biochemical oxygen demand biosensor chip for environmental monitooring. *Sensors and Actuators B* 221, 1594-1600.

Kharkova A. S., Aryapov V. A., Turovskaya A. D., Avtukh A. N., Starodumova I. P., Reshetiov A. N. (2019) Mediator BOD Biosensor Based on Cells of Microorganisms Isolated from Activated Sludge. *Applied Biochemistry and Microbiology* 55, 189-197.

Khoshibin Z., Housaindokht M. R., Verdian A., Bozorgmemhr M. R. (2018) Simultaneous detection and determination of mercury (II) and lead (II) ions through the achievement of novel functional nucleic acid-based biosensors. *Biosensors and Bioelectronics* 116, 130-147.

Kibena E., Raud M., Jõgi E., Kikas T. (2013). Semi-specific *M. phyllosphaerae* based microbial sensor for biochemical oxygen demand measurements in dairy wastewater. *Environmental Science and Pollution Research*, 20, 4, 2492-2498.

Kim M.-N., Kwon H.-S. (1999) Biochemical oxygen demand sensor using *Serratia marcescens* LSY4. *Biosensors and Bioelectronics* 14, 1-7.

Kokkinos C., Economou A. (2020) Review Article: Recent advances in voltammetric, amperometric and ion-selective (bio)sensors fabricated by microengineering manufacturing approaches. *Current Opinion in Electrochemistry* 23, 21-25.

Kudr J., Zitka O., Klimanek M., Vrba R., Adam V. (2017) Review article: Microfluidic electrochemical devices for pollution analysis–A review. *Sensors and Actuators B* 246, 578-590.

Kurbanoglu S., Erkmen C., Uslu B. (2020) Frontiers in electrochemical enzyme based biosensors for food and drug analysis. *Trends in Analytical Chemistry* 124, 115809.

Lee J.-H., Seo Y., Lim T.-S., Bishop P. L., Papautsky I. (2007) MEMS Needle-type Sensor Array for in Situ Measurements of Dissolved Oxygen and Redox Potential. *Environmental Science and Technology*, 41, 22, 7857-7863.

Lei H., Yi L. (2010) A novel microbial sensor immobilized *Arxula adeninivorans* for biochemical oxygen demand measure in high salt condition. *IEEE*, DOI:10.1109/ICBBE.2010.5517029.

Lei Y., Chen W., Mulchandani A. (2006) Review Microbial biosensors. *Analytica Chimica Acta* 568, 200-210.

Li M., Li Y.-T., Li D.-W., Long Y.-T. (2012) Recent developments and applications of screen-printed electrodes in environmental assays—A review. *Analytica Chimica Acta* 734, 31-44.

Li M., Li D.-W., Xiu G., Long Y.T. (2017) Review Article Applications of screen-printed electrodes in current environmental analysis. *Current Opinion in Electrochemistry* 3, 137-143.

Li T., Wu Y., Huang J., Zhang S. (2017) Gas sensors based on membrane diffusion for environmentalmonitoring. *Sensors and Actuators: B*, 243, 566-578.

Li Y., Sun J., Wang J., Bian C., Tong J., Li Y., Xia S. (2016) A single-layer structured microbial sensor for fast detection of biochemical oxygen demand. *Biochemical Engineering Journal* 112, 219-225.

Li Y., Sun J., Wang J., Bian C., Tong J., Li Y., Xia S. (2017) A microbial electrode based on the co-electrodeposition of carboxyl graphene and Au nanoparticles for BOD rapid detection. *Biochemical Engineering Journal* 123, 86-94.

Li Y., Sun J., Wang J., Bian C., Tong J., Li Y., Xia S. (2017) A rapid and sensitive BOD biosensor based on ultramicroelectrode array and carboxyl graphene. *IEEE*, DOI: 10.1109/NEMS.2017.8017024.

Lindquist H. D. A. (2020) Microbial biosensors for recreational and source waters. *Journal of Microbiological Methods* 177, 106059.

Liu C., Ma C., Yu D., Jia J., Liu L., Zhang B., Dong S. (2011) Immobilized Multi-Species Based Biosensor for Rapid Biochemical Oxygen Demand Measurement. *Biosensors and Bioelectronics* 26, 5, 2074-9.

Liu C., Zhao H., Gao S., Jia J., Zhao L., Yong D., Dong S. (2013) A reagent-free tubular biofilm reactor for on-line determination of biochemical oxygen demand. *Biosensors and Bioelectronics* 45, 15, 213-218.

Liu J., Mattiasson B. (2002) Microbial BOD sensors for wastewater analysis. *Water Research* 36, 15, 3786-3802.

Liu L., Zhai J., Zhu C., Goa Y., Wang Y., Han Y., Dong S. (2015) One-pot synthesis of 3-dimensional reduced graphene oxide-based hydrogel as support for microbe immobilization and BOD biosensor preparation. *Biosensors and Bioelectronics* 63, 483-489.

Liu M., Zhang C., Liu F. (2015) Understanding wax screen-printing: A novel patterning process for microfluidic cloth-based analytical devices. *Analytica Chimica Acta* 891, 234-246.

Liu W., Li M., Luo Z., Jin G. (2014) Using Electrochemistry - Total Internal Reflection Ellipsometry Technique to Observe the Dissolved Oxygen Reduction on Clark Electrode. *Electrochimica Acta* 142, 371-377.

Lourenco C. F., Ledoa A., Laranjinha J., Gerhardt G. A., Barbosa R. M. (2016) Microelectrode array biosensor for high-resolution measurements of extracellular glucose in the brain. *Sensors and Actuators B* 237, 298-307.

Lv M., Liu Y., Geng J., Kou X., Xin Z, Yang D. (2018) Engineering nanomaterials-based biosensors for food safety detection. *Biosensors and Bioelectronics* 106, 122-128.

Ma D., Gao J., Zhang Z., Zhao H. (2021) Gas recognition method based on the deep learning model of sensor array response map. *Sensors and Actuators*, B, 330, 129349.

Maduraiveeran G., Jin W. (2017) Nanomaterials based electrochemical sensor and biosensor platforms for environmental applications. *Trends in Environmental Analytical Chemistry* 13, 10-23.

Martynko E., Kirsanov D. (2020) Review: Application of chemometrics in biosensing: a brief review. *Biosensors* 10, 100.

Mišlov D., Cifrek M., Krois I., Džapo H. (2015) Measurement of Dissolved Hydrogen Concentration with Clark Electrode. *IEEE,* DOI:10.1109/SAS.2015.7133656.

Moro G., Bottari F., Loon J. V., Bois E. D., Wael K. D., Moretto L. M. (2019) Disposable electrodes from waste materials and renewable sources for (bio) electroanalytical applications. *Biosensors and Bioelectronics* 146, 111758.

Moya A., Gabriel G., Villa R., del Campo F. J. (2017) Review Article: Inkjet-printed electrochemical sensors. *Current Opinion in Electrochemistry* 3, 29-39.

Muňoz J., Pumera M. (2020) 3D-printed biosensors for electrochemical and optical applications. *Trends in Analytical Chemistry* 128, 115933.

Nakamura H. (2018) Current status of water environment and their microbial biosensor techniques – Part II: Recent trends in microbial biosensor development. *Analytical and Bioanalytical Chemistry* 410, 3967-3989.

Nasiria S., Khosravani M. R. (2020) Review Progress and challenges in fabrication of wearable sensors for health monitoring. *Sensors and Actuators* A 312, 112105.

Neves M. M. P. S., González-García M. B., Hernández-Santos D., Fanjul-Bolado P. (2018) Review Article: Future trends in the market for electrochemical biosensing. *Current Opinion in Electrochemistry* 10, 107-111.

Ngoc L .T. B., Tu T. A., Hien L. T. T., Linh D. N., Tri N., Duy N. P. H., Cuong H. T., Phuong P. T. T. (2020) Simple approach for the rapid estimation of BOD 5 in food processing wastewater. *Environmental Science and Pollution Research (international)* 27, 16, 20554-20564.

Niyomdecha S., Limbut W., Numnuam A., Asawatreratanakul P., Kanatharana P., Thavarungkul P. (2017) A novel BOD biosensor based on entrapped activated sludge in aporous chitosan-albumin cryogel incorporated with graphene andmethylene blue. *Sensors and Actuators B* 241, 473-481.

Novodchuk I., Bajcsy M., Yavaz M. (2021) Graphene-based field effect transistor biosensors for breast cancer detection: A review on biosensing strategies. *Carbon* 172, 431-453.

Oliveira J., Correia V., Castro H., Martins P., Lanceros-Mendez S. (2018) Polymer-based smart materials by printing technologies: Improving application and integration. *Additive Manufacturing* 21, 269-283.

Onkal-Engin G., Demir I., Engin S. N. (2005) Determination of the relationship between sewage odour and BOD by neural networks. *Environmental Modelling and Software* 20, 7, 843-850.

Oota S., Hatae Y., Amada K., Koya H., Kawakami M. (2010) Development of mediated BOD biosensor system of flow injection mode for *shochu* distillery wastewater. *Biosensors and Bioelectronics* 26, 262-266.

Panasiuk O., Hedström A., Marsalek J., Ashley R. M., Viklander M. (2015) Review Contamination of stormwater by wastewater: A review of detection methods. *Journal of Environmental Management* 152, 241-250.

Pasco N. F., Weld R. J., Hay J. M., Gooneratne R. (2011) Development and applications of whole cell biosensors for ecotoxicity testing. *Analytical and Bioanalytical Chemistry* 400, 931-945.

Podrażka M., Bączyńska E., Kundys M., Jeleń P. S., Witkowska Nery E. (2018) Electronic Tongue—A Tool for All Tastes? *Biosensors* 8, 1, 3.

Ponomareva O. N., Arlyapov V. A., Alferov V. A., Reshetilov A. N. (2011) Microbial biosensors for detection of biological oxygen demand (a Review). *Applied Biochemistry and Microbiology* 47, 1, 1-11.

Pouvreau L. A. M., Strampraad M. J. F., Van Berloo S., Kattenberg J. H., de Vries S. (2008) Chapter Six NO, N2O, and O2 Reaction Kinetics: Scope and Limitations of the Clark Electrode. *Globins and Other Nitric Oxide-Reactive Proteins, Part A Methods in Enzymology*, 436, 97-112.

Pudas M., Hagberg J., Leppävuori S. (2004) Printing parameters and ink components affecting ultra-fine-line gravure-offset printing for electronics applications. *Journal of the European Ceramic Society* 24, 2943-2950.

Qi X., Wang S., Li T., Wang X., Jiang Y., Zhou Y., Zhou X., Huang X., Liang P. (2021) An electroactive biofilm-based biosensor for water safety: Pollutants detection and early-warning. *Biosensors and Bioelectronics* 173, 112822.

Rastogi S., Kumar A., Mehra N. K., Makhijani S. D., Manoharan A., Gangal V., Kumar R. (2003) Development and characterization of a novel immobilized microbial membrane for rapid determination of biochemical oxygen demand load in industrial waste-waters. *Biosensors and Bioelectronics* 18, 1, 23-29.

Raud M., Linde E., Kibena E., Velling S., Tenno T., Talpsep E., Kikas T. (2010) Semi-specific biosensors for measuring BOD in dairy

wastewater. *Journal of Chemical Technology and Biotechnology*, 85, 7, 957-961.

Raud M., Tenno T., Jõgi E., Kikas T. (2012): Comparative study of semi-specific *Aeromonas hydrophila* and universal *Pseudomonas fluorescens* biosensors for BOD measurements in meat industry wastewaters. *Enzyme and Microbial Technology*, 50, 4-5, 221-226.

Raud M., Tutt M., Jõgi E., Kikas T. (2012): BOD biosensors for pulp and paper industry wastewater analysis. *Environmental Science and Pollution Research*, 19, 7, 3039-3045.

Raud M., Kikas T. (2013) Bioelectronic tongue and multivariate analysis: A next step in BOD measurements. *Water Research* 47, 7, 2555-2562.

Rawal R., Kharangarh P. R., Dawra S., Tomar M., Gupta V., Pundir C. S. (2020) A comprehensive review of bilirubin determination methods with special emphasis on biosensors. *Process Biochemistry* 89, 165-174.

Ribeiro B. V., Cordeiro T. A. R., Freitas G. R. O., Ferreira L. F., Franco D. L. (2020) Biosensors for the detection of respiratory viruses: A review. *Talanta Open* 2, 100007.

Ribeiro B. V., Cordeiro T. A. R., Freitas G. R. O., Ferreira L. F., Franco D. L. (2020) Biosensors for the detection of respiratory viruses: A review. *Talanta* Open 2, 100007.

Rodríguez-Méndez M. L., De Saja J. A., González-Antón R., García-Hernández C., Medina-Plaza C., García-Cabezón C., Martín-Pedrosa F. (2016) Electronic Noses and Tongues in Wine Industry. Frontiers in *Bioengineering and Biotechnology* 4, 81.

Rodriguez-Mozaz S., Lopez De Alda M. J., Marco M.-P., Barcelé, D. (2005) Biosensors for environmental monitoring A global perspective. *Talanta* 65, 291-297.

Sakaguchi T., Morioka Y., Yamasaki M., Iwanaga J., Beppu K., Maeda H., Morita Y., Tamiya E. (2007) Rapid and onsite BOD sensing system using luminous bacterial cells-immobilized chip. *Biosensors and Bioelectronics* 22, 7, 1345-1350.

Scampicchio M., Ballabio D., Arecchi A., Cosio S. M., Mannino S. (2008) Amperometric electronic tongue for food analysis. *Microchimica Acta* 163, 1, 11-21.

Scott S., James D., Ali Z. (2007) Review Data analysis for electronic nose systems. *Microchimica Acta* 156, 183-207.

Serrano N., Alberich A., Díaz-Cruz J. M., Ariño C., Esteban M. (2013) Coating methods, modifiers and applications of bismuth screen-printed electrodes. *Trends in Analytical Chemistry* 46, 15-29.

Sharma S., Kumari R., Varshney S. K., Lahiri B. (2020) Optical biosensing with electromagnetic nanostructures. *Reviews in Physics* 5, 100044.

Shi H., Zhang M., Adhikari B. (2018) Advances of electronic nose and its application in fresh foods: A review. Critical Reviews in *Food Science Nutrition* 58, 16, 2700-2710.

Shinozaki K., Zack J. W., Richards M., Pivovar B. S., Kocha S. S. (2015) Oxygen Reduction Reaction Measurements on Platinum Electrocatalysts Utilizing Rotating Disk Electrode Technique: I. Impact of Impurities, Measurement Protocols and Applied Corrections. *Journal of the Electrochemical Society* 162, F1144.

Sochol R. D., Sweet E., Glick C. C, Wu S.-Y., Yang C., Restaino M., Lin L. (2018) Review article 3D printed microfluidics and microelectronics. *Microelectronic Engineering* 189, 52-68.

Song C., Zhang J. (2008) in PEM Fuel Cell Electrocatalysts and Catalyst Layers, J. Zhang, Editor, p. 89, Springer, London.

Sousa L. P. O., Fukushima K. L., Scagion V. P., Facure M. H. M., Correa D. S., Oliveira J. E., Ferreira D. D. (2021) A Principal Curves-Based Method for Electronic Tongue Data Analysis. *IEEE Sensors Journal* 21, 4, 4957-4965.

Su L., Jia W., Hou C., Lei Y. (2011) Microbial biosensors: A review. *Biosensors and Bioelectronics* 26, 5, 1788-1799.

Sun M., Wang W., Yu D. (2011) Research Progress of Biosensors for Environmental Monitoring. *5th International Conference on Bioinformatics and Biomedical Engineering (IEEE) DOI: 10.1109/icbbe.2011.5780803.*

Suzuki H. (2000) Microfabrication of chemical sensors and biosensors for environmental monitoring. *Materials Science and Engineering: C*, 12, 1-2, 55-61.

Štulík K., Amatore C., Holub K., Mareček V., Kuntner W. (2000) Microelectrodes. Definitions, characterization, and applications (Technical report). *Pure and Applied Chemistry* 72, 8, 1483-1492.

Taleat Z., Khoshroo A., Mazloum-Ardakani M. (2014) Screen-printed electrodes for biosensing: a review (2008-2013). *Microchimica Acta* 181, 9-10, 865-891.

Tan J., Xu J. (2020) Applications of electronic nose (e-nose) and electronic tongue (e-tongue) in food quality-related properties determination: A review. *Artificial Intelligence in Agriculture* 4, 104-115.

Tan T. C., Wu C. (1999) BOD sensors using multi-species living or thermally killed cells of a BODSEED microbial culture. *Sensors and Actuators B: Chemical* 54, 3, 252-260.

Thévenot D. R., Toth K., Durst R. A., Wilson G. S. (2001) Electrochemical biosensors: Recommended definitions and classification. *Biosensors and Bioelectronics* 16, 121-131.

Tønning E., Sapelnikova S., Christensen J., Carlsson C., Winther-Nielsen M., Dock E., Solna R., Skladal P., Nørgaard L., Ruzgas T., Emnéus J. (2005) Chemometric exploration of an amperometric biosensor array for fast determination of wastewater quality. *Biosensors and Bioelectronics* 21, 4, 608-617.

Tran T. S., Dutta N. K., Choudhury N. R. (2018) Historical Perspective Graphene inks for printed flexible electronics: Graphene dispersions, ink formulations, printing techniques and applications. *Advances in Colloid and Interface Science* 261, 41-61.

Vasiliev A.A., Pisliakov A.V., Sokolov A. V., Samotaev N. N., Soloviev S. A., Oblov K., Guarnieri V., Lorenzelli L., Brunelli J., Maglione A., Lipilin A. S., Mozalev A., Legin A. V. (2016) Non-silicon MEMS platforms for gas sensors. *Sensors and Actuators* B 224, 700-713.

Vlasov Y., Legin A., Rudnitskaya A., Natale C. D., D'Amico A. (2005) Nonspecific sensor arrays ("electronic tongue") for chemical analysis of liquids (IUPAC Technical Report). *Pure and Applied Chemistry* 77, 11 1965-1983.

Vlasov Y. G., Legin A. V., Rudnitskaya A. M. (2008) Electronic Tongue: Chemical Sensor Systems for Analysis of Aquatic Media. *Russian Journal of General Chemistry* 78, 12, 2532-2544.

Wang J., Li Y., Bian C., Tong J., Fang Y., Xia S. (2017) Ultramicroelectrode array modified with magnetically labelled Bacillus subtilis, palladium nanoparticles and reduced carboxy graphene for amperometric determination of biochemical oxygen demand. *Microchim Acta* 3, 3, 184, 763-771.

Wang W.-D, Wolfbeis O. S. (2014) Optical methods for sensing and imaging oxygen: materials, spectroscopies and applications. *The Royal Society of Chemistry*, 43, 3666-3761.

Wang X.-X., Yu G.-F., Zhang J., Yu M., Ramakrishna S., Long Y.-Z. (2021) Conductive polymer ultrafine fibers via electrospinning: Preparation, physical properties and applications. *Progress in Materials Science* 115, 100704.

Wasilewski T., Migoń D., Gębicki J., Kamysz W. (2019) Review Critical review of electronic nose and tongue instruments prospects in pharmaceutical analysis. *Analytica Chimica Acta* 1077, 14-29.

Webber J. B, Noonan M., Pasco N. F., Joanne H. M. (2011) Appraising bacterial strains for rapid BOD sensing – an empirical test to identify bacterial strains capable of reliably predicting real effluent BODs. *Applied Microbiological Biotechnology* 89, 179-188.

Wesoły M., Ciosek − Skibińska P. (2018) Comparison of various data analysis techniques applied for the classification of pharmaceutical samples by electronic tongue. *Sensors and Actuators B: Chemical* 267, 570-580.

Xiao-wei H., Xiao-bo Z., Ji-yong S., Zhi-hua L., Jie-wen Z. (2018) Colorimetric sensor arrays based on chemo-responsive dyes for food odor visualization. *Trends in Food Science and Technology* 81, 90-107.

Xu L., Hu C., Huang Q., Jin K., Zhao P., Wang D., Hou W., Dong L., Hu S., Ma H. (2021) Trends and recent development of the microelectrode arrays (MEAs). *Biosensors and Bioelectronics* 175, 112854.

Xu X., Ying Y. (2011) Microbial biosensors for environmental monitoring and food analysis. *Food Reviews International* 27, 300-329.

Ye Y., Guo H., Sun X. (2019) Recent progress on cell-based biosensors for analysis of food safety and quality control. *Biosensors and Bioelectronics* 126, 389-404.

Zaitseva A. S., Arlyapov V. A., Yudina N. Yu., Alferov S. V., Reshetilov A. N. (2017) Use of one- and two-mediator systems for developing a BODbiosensor based on the yeast *Debaryomyces hansenii*. *Enzyme and Microbial Technology* 98, 43-51.

Zhao F., Yao Y., Jiang C., Shao Y., Barceló D., Ying Y. (2020) Self-reduction bimetallic nanoparticles on ultrathin MXene nanosheets as functional platform for pesticide sensing. *Journal of Hazardous Materials* 384, 121358.

Zheng Y.-H., Hua T.-C., Xu F. (2005) A thermal biosensor based on enzyme reaction. *Conference proceedings - IEEE engineering in medicine and biology society* 1909, 12.

SUMMARY IN ESTONIAN

Töö pealkiri eesti keeles on: Biosensor-rivi erinevate reovete biokeemilise hapnikutarbe uurimiseks.

Puhta vee varud on piiratud ja seega tuleks jälgida, et ei toimuks puhastamata reovee vabastamist keskkonda. Vee reostus mõjutab nii inimesi (Panasiuk et al. 2015) kui ka keskkonda (Maduraiveeran and Jin 2017).

Vee kvaliteedi määramiseks kasutatakse erinevaid keemilisi, füüsikalisi kui ka bakterioloogilisi analüüse ja teste. Üks oluline parameeter on vee biokeemiline hapnikutarve (BHT). BHT analüüsi kaudu määratakse vee suhteline hapnikutarve ning selle kaudu on võimalik hinnata lagundatava orgaanilise ja oksüdeeritava anorgaanilise aine hulka vees. Traditsioonilise BHT testi käigus mõõdetakse proovi lahustunud hapniku kontsentratsioon enne ja pärast inkubeerimist ning tulemuste saamiseks kulub olenevalt standardist 5 või 7 päeva aega. Nii pikk aeg ei võimalda reoveepuhastis protsesse kontrollida või reostuse korral koheselt reageerida. Lahenduseks võivad olla biosensorid, mis annavad BHT väärtusele hinnangu minutitega.

Erinevatest töödest on ilmnenud, et biosensorid alahindavad BHT väärtust, kuna lühikese ajaga ei suuda üks bakterikultuur kõiki aineid lagundada. Katsetatud on ka mitmesuguseid segakultuure, aga neil on väiksem stabiilsus, kuna erinevate bakterikultuuride arvukus ja proportsioon ajas muutub.

Käesoleva töö eesmärgiks oli uurida erinevaid sensor-rivi kiipe, selleks et koostada BHT sensor-rivi, mis oleks kiire, lihtne kasutada ja annaks usaldusväärseid tulemusi. Selle eesmärgi täitmiseks püstitati järgnevad ülesanded:

1. Tutvuda BHT sensor-rivide hetke olukorraga teadusmaastikul (**I**)
2. Uurida varem tehtud sensor-rivi ja ostetud sensor-rivi (DropSens550) rakendatavust (**II**, **III**, **IV**) ning valida sobiv sensor-rivi BHT mõõtmiseks (**III**, **IV**)
3. Kontrollida, kas BHT sensor-rivi töötab standardlahuses ja võimaldab mõõta tegelikku reovett (**IV**)

Esmalt kasutati mikrotöötlemise teel valmistatud sensor-rivi, mis koosnes räni ja klaas tahvlitest ning Pt elektroodidest. Kirjeldati sensor-rivi Pt elektroodide käitumist 0.5 M väävelhappe lahuses ja 1 M kaaliumkloriidi lahuses. Saadi plaatinale iseloomulikud kõverad väävelhappe lahuses, mis näitas, et elektrolüüdi lahus ja mõõterakk on puhtad ning plaatina elektroodid töötavad ootuspäraselt. Järgnevalt uuriti, kas sensor-rivi on tundlik hapniku sisalduse muutuse suhtes lahuses. Mõõdeti tsüklilised voltammogrammid 0.5 M väävelhappe lahuses erinevatel hapniku osarõhkudel: 0, 25, 49, 74 ja 98 kPa. Kalibreeriti Pt elektrood hapniku sisalduse muutusega. Hapniku osarõhul 25 kPa ja laotuskiirusel 0.1 V s^{-1} oli massiülekande alas voolutihedus −0.84 A m^{-2}. Samas kui hapniku osarõhul 98 kPa oli voolutihedus −3.3 A m^{-2}. Sensor-rivi valmistamise protsessi eripära tõttu vajas antud kiip enne mõõtmisi puhastamist väävelhappe lahuses seetõttu polnud võimalik baktereid otse kiibile immobiliseerida ning kasutada sensor-rivi pikema aja jooksul mitu korda.

Alternatiivina katsetati täiendavalt siiditrüki meetodil valmistatud DropSens550 sensor-rivi. Viidi läbi mõõtmised hapniku ja lämmastiku seguga küllastatud 0.1 M kaaliumkloriidi lahuses kasutades tsüklilist voltamperomeetriat ja koronoamperomeetriat. DropSens550 sensor-riviga mõõdetud voolutihedus sõltus hapniku sisaldusest lahuses. Lahuses, mis oli küllastatud 20% hapniku sisaldusega, oli massiülekande alas keskmine voolutihedus −1.6 A m^{-2} laotuskiirusel 0.02 V s^{-1}. Samas kui 100% hapnikuga küllastatud lahuses oli keskmine voolutihedus −5.2 A m^{-2}. Seejärel, uuriti massiülekande alas voolutiheduse sõltuvust lahuse pumpamiskiirusest rakkus. Alates kiirusest 1.5 cm^3 min^{-1} tulemused enam oluliselt ei muutunud, seega valiti edasisteks katseteks pumpamiskiirus 2 cm^3 min^{-1}. Tsüklilise voltamperomeetria tulemuste põhjal määrati kronoamperomeetria läbi viimise tingimused. Hapniku hulga määramisel kasutati kronoamperomeetriat nii −0.3 V kui ka −0.5 V vs Ag|AgCl|0.1 M KCl. Mõlema lõpp-potentsiaali korral täheldati lineaarset sõltuvust hapniku kontsentratsioonist.

Biosensor rivi kalibreerimiseks valiti kronoamperomeetria −0.3 V vs Ag|AgCl|0.1 M KCl juures. Kalibreerimiseks kasutati muudetud koostisega OECD sünteetilist reovett. Membraanidele sidumiseks valiti *Pseudomonas putida* Pc15 kultuur. Erinevatel membraanidel oli erinev lineaarse ala ulatus ja tundlikkus, see võis tuleneda erinevast bakterite hulgast erinevatel membraanidel. Lineaarse ala ulatus oli kuni 65-85 mg L^{-1} BHT. Nende biosensorite tundlikkus oli vahemikus 0.0018-

0.0068 $(mg\,L^{-1})^{-1}$. Koostatud biosensor-riviga mõõdeti ka reaalset reovee proovi. Selle tulemust võrreldi traditsioonilise BHT_5 testi tulemusega. Koostatud sensor-rivi alahindas BHT väärtust 8-37% võrra.

Enamus hüpoteesidest leidis kinnitust. Kõik püstitatud ülesanded said täidetud. Mõlemad sensor-rivid olid võimelised määrama hapniku sisalduse erinevust lahuses. Tehniliste raskuste tõttu ei jõutud varem tehtud sensor-riviga BHT mõõtmiseni. DropSens550 sensor-rivi sobis BHT mõõtmiseks. DropSens550 sensor-riviga oli võimalik mõõta kalibreerimislahuseid ja tegeliku reovee BHT väärtust.

Tulevikus võib proovida mõõta BHT väärtusi sensor-riviga, mis koosneb mitmest erineva puhta bakteri kultuuridega membraanidest.

ACKNOWLEDGEMENTS

I would like to acknowledge my supervisors, Professor Timo Kikas, Associate Professor Jaak Nerut, and Dr Merlin Raud. Thank you all for believing in me and giving me the best guidance you could. It has been a long journey, but for the most part I enjoyed it.

My warmest thanks go to Professor Enn Lust for allowing me into the University of Tartu's well-arranged laboratory and giving me detailed feedback.

I gratefully acknowledge the support of the Estonian Science Foundation (Grant ETF 9136), the European Regional Development Fund (TK 141: 'Advanced materials and high-technology devices for energy recuperation systems' (2020.4.01.15 0011)), Institutional Research Grant IUT20-13, the Estonian University of Life Sciences (base financed project P170025), and the Estonian Research Council (grant No. PRG676). I would like to acknowledge the help of the Doctoral School of Energy and Geotechnology III (Estonian University of Life Sciences ASTRA project "Value-chain based bio-economy"). Publication of this thesis is supported by the Estonian University of Life Sciences.

I would also like to thank the European Regional Development Fund and the Archimedes Foundation for their travel grant. Special thanks should go to Rutha Jäger and Elo Kibena-Põldsepp who helped me to travel.

I would like to thank Associate Professor Kaja Orupõld, Milvi Purgas, and Vanessa Friedl for helping to measure traditional BOD values. I would also like to acknowledge the support of Assistant Professor Helena Anderson, Professor Mati Roasto, Kaarel Soots, Fiaz Ahmad, and Kaie Ritslaid. I am additionally grateful to Krista Liin for her help.

Last but not least, I would like to thank my family and friends. Without you I would not be who I am.

I

ORIGINAL PUBLICATIONS

ETIS 1.1: **Pitman, K.**; Raud, M.; Kikas, T. (2015) Biochemical oxygen demand sensor arrays. *Agronomy Research*, 13 (2), 382−395.

Agronomy Research **13**(2), 382–395, 2015

Biochemical oxygen demand sensor arrays

K. Pitman, M. Raud and T. Kikas*

Estonian University of Life Sciences, Institute of Technology, Kreutzwaldi 56, EE51014 Tartu, Estonia. *Correspondence: timo.kikas@emu.ee

Abstract. Biochemical oxygen demand (BOD) is one of the most widely utilized parameters in water quality evaluation. BOD as a parameter illustrates the amount of organic compounds susceptible to biochemical degradation in the water. The BOD test lasts for at least 5–7 days or even up to 21 days. An incubation time this long is not acceptable for monitoring purposes or system control. In order to shorten the BOD measurement time, a multitude of biosensors have been proposed. Unfortunately, BOD biosensors have several limitations, such as short lifetime, limited substrate range, precision etc. Some of those limitations can be overcome by using microbial sensor-arrays. Such bioelectronic tongues can achieve the much wider substrate range usually attributed to multiculture sensors and still maintain the long lifetime of a single culture sensor. This is achieved by separating different cultures from each other in the array and using the signals of separate sensors to produce summarised information via statistical analysis. The purpose of this review is to give a short overview of BOD measurements and discuss the potential of using sensor-arrays for BOD measurements.

Key words: sensor-array, BOD sensor-array, electronic tongue, biosensor, biochemical oxygen demand.

INTRODUCTION

Water quality monitoring is an important aspect of water management with regard to pollution control. One of the most important water quality parameters is biochemical oxygen demand (BOD). This parameter was first introduced in 1917 and published in *Standard Methods* (Bourgeois, 2001). BOD is determined by means of an empirical test in which standardized laboratory procedures are used to determine the relative oxygen requirements of wastewater, effluents and polluted waters (APHA, 1985; Tan & Wu, 1999; Bourgeois, 2001). The standardized test measures the oxygen required for the biochemical degradation of organic material and the oxygen used to oxidize inorganic material, such as sulphides, ferrous iron and reduced forms of nitrogen, unless their oxidation is prevented by an inhibitor (APHA, 1985). The results of a BOD test characterize the total content of biochemically oxidizable organic substances in the water as well as the ability of the water to self-cleanse (Ponomareva, 2011).

In a standardized BOD test, a sample is placed in a full, airtight bottle and incubated under the specified conditions (20 ± 1 °C, in the dark) for a specific time (APHA, 1985). The incubation period is 5 or 7 days according to the American (APHA, 1985) or Swedish standard (Liu & Mattiasson, 2002), respectively. The BOD value is calculated based on the difference between the initial and final dissolved oxygen concentrations (APHA, 1985; Liu & Mattiasson, 2002). The BOD value is measured in milligrams of

oxygen per litre or cubic decimetre ($mgO_2\ l^{-1}$ or $mgO_2\ dm^{-3}$). The BOD_5 values in surface water layers usually fall into the range of 0.5–4 mg l^{-1} (Ponomareva, 2011), while in industrial wastewaters BOD_5 may be as high as 30,000 mg l^{-1}. The precision of the method is around 15–20% (Namour & Jaffrezic-Renault, 2010).

The BOD test has been the most widely used method to measure organic pollution in water samples because of its wide applicability to different type of samples as well as its simplicity (Liu, 2014), since it requires no expensive equipment. However, due to the prolonged incubation time, it is not suitable for the monitoring or control of wastewater treatment systems where fast feedback is necessary (Raud, 2012a).

One way to overcome the long delay between the measurements and the results is to use biosensors. Depending on the measurement method, BOD biosensors can give results within 5 to 30 minutes (Kim, 2006; Kibena, 2012). Many papers on BOD biosensors have been published and these biosensors have been developed and marketed by various manufacturers in both biofilm and bioreactor-type configurations (Rodriguez-Mozaz, 2006). The purpose of this paper is to give an overview of the biosensors used in BOD measurements and to direct more attention to the possibility of using sensor-arrays for BOD measurements.

BIOSENSORS FOR BOD

A biosensor is defined as a self-contained integrated device capable of providing specific quantitative analytical information. A biosensor consists of a biological recognition element (Luong, 2008; Lagarde & Jaffrezic-Renault, 2011; Su, 2011), which is in direct spatial contact with a transduction element (Thévenot, 2001; Xu & Ying, 2011). A variety of transducers have been used in biosensors, such as electrochemical, colorimetric, optical, acoustic, luminescence, and fluorescence transducers. Furthermore, different biological sensing materials have also been used, such as microorganisms, tissues, organelles, receptors, enzymes, antibodies, nucleic acids, aptamers, cofactors, etc. The most frequently used ones are enzymes and microorganisms (D'Souza, 2001; Kissinger, 2005; Su, 2011).

The first BOD biosensor was reported by Karube in 1977 (Karube, 1977). It consisted of a dissolved oxygen electrode and a membrane impregnated with the yeast *T. cutaneum*. Since then, many BOD biosensors based on various measurement principles and biological sensing elements have been reported. Various microorganisms, including yeasts and viable cells of bacteria such as *Arxula adeninivorans, Bacillus polymyxa, Bacillus subtilis, Candida, Escherichia coli, Hansenula anomala, Issatchenkia, Klebsiella, Pseudomonas fluorescens Pseudomonas putida, Saccharomyces cerevisiae, Serratia marcescens, Torulopsis candida, Trichosporon* etc., have been used for the construction of BOD biosensors (Liu & Mattiasson, 2002; Raud, 2010b; Lagarde & Jaffrezic-Renault, 2011; Ponomareva, 2011). Microorganisms have been used in the form of a single pure culture, mixtures of several pure cultures, or mixed cultures, such as activated sludge or the BODSEED culture (Tan & Wu, 1999; Rastogi, 2003). BOD sensors based on a single strain have relatively good stability and a long service life (Kim, 2006), but the sensor-BOD value will be limited due to the narrow substrate spectrum of one microbial strain (Liu & Mattiasson, 2002; Raud, 2012), which may lead to an underestimation of BOD. In order to construct a BOD biosensor with a wider substrate spectrum, mixtures of several microbial strains or mixed cultures have

been used (Suriyawattanakul, 2002). However, compared to single strain biosensors, mixed culture biosensors have decreased stability and a shorter service life due to the different life-spans and growth rates of various microorganisms used in consortia (Liu & Mattiasson, 2002). Thermally killed cells have been used to overcome the instability of microbial consortia and to achieve a longer service life for biosensors (Ponomareva, 2011). Thermally killed cells do not need a periodic nutrients supply. On the other hand, living cells need careful maintenance and a supply of nutrients and minerals during storage (Liu & Mattiasson, 2002).

Most of the reported BOD biosensors fall into one of two types – biofilm and respirometric (also called bioreactor-type) biosensors. Biofilm-type BOD biosensors are based on measuring the change in the dissolved oxygen concentration due to the respiration of microorganisms in the proximity of the transducer (Ponomareva, 2011). Microorganisms may be immobilized directly onto the transducer or immobilized and placed as a separate film or membrane in close proximity to the transducer. The transducer is most commonly a dissolved oxygen sensor. Respirometric or bioreactor-type biosensors, on the other hand, are biosensors where the microorganisms are not attached to the transducer but float freely in the measurement solution and the dissolved oxygen concentration is measured directly from the solution. These systems provide a constant measurement of the respiratory activity of a microbial suspension (Ponomareva, 2011).

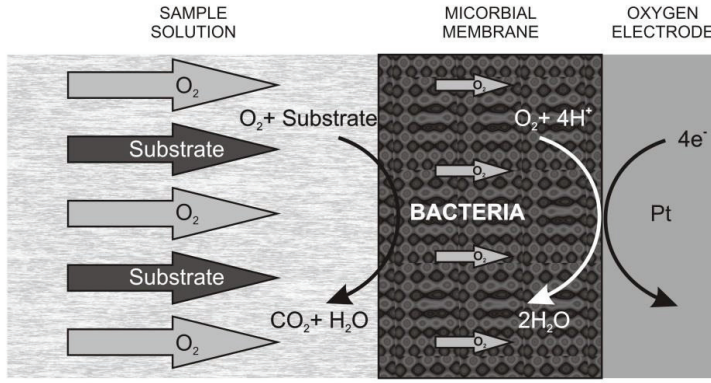

Figure 1. The basic principle of a microbial biosensor based on an amperometric transducer.

The working principle of a typical biofilm-type BOD biosensor is illustrated in Fig. 1. The microorganisms are immobilized or placed onto the oxygen electrode and the biosensor in immersed in the measurement solution. In a clean measuring solution the biosensor achieves a steady state current slightly lower than in the measurement medium, as most of the dissolved oxygen diffuses through the membrane but some is used up by microorganisms. When a sample containing biodegradable substrates is added to the measuring solution, the microorganisms start using oxygen for the assimilation of substrates at a certain rate and the measured oxygen concentration

decreases to a new and lower steady state. The decrease in the concentration of dissolved oxygen is proportional to the concentration of added biodegradable substrates. Based on the decrease in measured oxygen concentration, BOD can be calculated (Liu & Mattiasson, 2002).

With both biosensor types, the signal can be analysed using either the steady-state method or the kinetic method. The first one derives BOD from the current difference between two steady states, before and after adding the sample. It is often also called the end-point method. The kinetic method, on the other hand, uses the time derivative of the current right after the addition of the sample, and is also known as the initial rate, quasi-kinetic or dynamic transient method (Pasco, 2011).

The duration of measurement is 5–25 min in the stationary mode and 15–30 s with the initial rate method (Ponomareva, 2011). Recovery time is 15–60 min in the stationary mode and more than 10 min when using the initial rate method (Liu & Mattiasson, 2002). Hence, the initial rate method is preferable where a constant BOD monitoring is necessary, for example, when controlling a wastewater treatment plant or analysing a large number of samples (Ponomareva, 2011). The sensitivity of the initial-rate method, however, is twice as high as that of the stationary mode (Liu & Mattiasson, 2002).

The BOD values gained from BOD sensors do not always match the conventional BOD results due to differences in the measuring principles. The conventional BOD test has an incubation time of 5 or 7 days. In the course of this time the microorganisms can assimilate easily degradable compounds but also they have time to induce the necessary enzymes for the degradation of refractory compounds. However, during the short measurement time of a biosensor, the immobilized microorganisms are able to assimilate and thereby detect only easily degradable compounds, which may result in an underestimation of BOD values.

The problem with the underestimation of BOD could be overcome by choosing a suitable calibration solution. The most common calibration solutions are: a solution of equal parts of glucose and glutamic acid (GGA) (Ponomareva, 2011) and a synthetic wastewater according to the recipe established by the Organisation for Economic Cooperation and Development (OECD). Due to its simple composition, the GGA solution is unsuitable for studying samples of a more complicated composition (Liu & Mattiasson, 2002). Better results have been obtained with the OECD synthetic wastewater, as its composition closely resembles that of municipal wastewater (Liu & Mattiasson, 2002). Other artificial wastewaters have also been used for the calibration of BOD sensors (Chee, 2005; Chee, 2007). The ideal calibration solution would be as close to the composition of the wastewater to be analysed as possible (Liu, 2000; Liu & Mattiasson, 2002). Therefore, there is no universal calibration solution; rather, it must be chosen based on the composition of the sample to be later analysed.

Other ways to achieve a better match between the BOD values measured by different methods consist in preselecting microorganisms that have wide substrate spectra and are able to assimilate specific refractory compounds found in wastewater, or pre-incubating the living cells in a solution whose composition is similar to the sample to be analysed (Liu & Mattiasson, 2002). The pre-incubation helps living cells to start producing the enzymes that otherwise would not be present in the cells, thus widening their substrate spectrum.

BIOSENSOR ARRAYS

The principle of sensor-arrays is based on an analogy to the biological organization of the olfactory and taste systems of mammals, where millions of nonspecific receptors in nose and taste systems respond to different substances. The idea of artificially reproducing the natural response of a human to environmental stimuli was first published in 1943 (Vlasov, 2005); however, the first attempts to design an artificial olfactory system for smell were made in the 1960s (Vlasov, 2008), while non-specific sensor-arrays became commercially available in the mid-1990s (Bourgeois, 2003). According to the IUPAC (The International Union of Pure and Applied Chemistry) definition, 'an electronic tongue is a multisensor system, which consists of a number of low-selective sensors and uses advanced mathematical procedures for signal processing based on pattern recognition and/or multivariate data analysis' (Vlasov, 2005; del Valle, 2010). The basic principle of a sensor-array is shown in Fig. 2. Each sensor in an array produces an individual signal, which may not always correlate with the samples' composition. The summarised signal of the sensor-array is analysed using statistical multivariate analysis methods, which enable extracting qualitative and quantitative information about the samples. Arrays of gas sensors are termed 'electronic noses' while arrays of liquid sensors are referred to as 'electronic tongues' (Escuder-Gilabert & Peris, 2010).

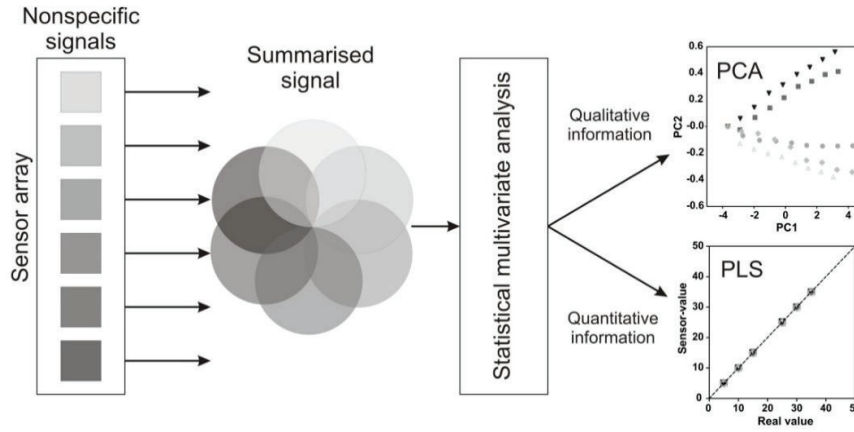

Figure 2. The working principle of a sensor array.

The most typical feature shared by electronic nose and electronic tongue systems is that an array of low selective and cross-sensitive sensors is conjugated with data processing and pattern recognition methods (Vlasov, 2008). Cross-sensitivity in this context is the ability of a sensor to respond to a number of different compounds in a solution and produce a stable response in the sample (Vlasov, 2005). Thereby, when the sensors are responding to several different substrates, the sensor-array creates a chemical image of the sample (Hruškar, 2010) or a signal pattern, which can be related to certain features or qualities of the sample (Krantz-Rülcker, 2001). In this way, the limited selectivity of each individual sensor will be compensated by the data processing, which

allows the determination of a species in the presence of its interference (del Valle, 2010). Electronic tongues are a powerful tool in the rapid assessment of information of complex solutions (Riul Jr, 2010).

Various sensing principles can be employed in sensor-arrays. The most widespread are electrochemical (del Valle, 2010) and optical sensors (Krantz-Rülcker, 2001; Vlasov, 2005; Witkowska, 2010); however, other techniques, such as surface acoustic waves (Krantz-Rülcker, 2001), piezoelectric mass sensors (del Valle, 2010) etc. have been reported. Usually, a single sensor-array consists of sensors of the same type; however, sensors based on different principles of signal transduction may be used in the same sensor-array. The number of sensors in the array may vary from 4 to 40 (Vlasov, 2005), depending on the analytical task and the number of different sensing materials available. Usually, a sensor-array consists of an excessive number of sensors compared to the analytes to be detected and is thereby applicable to different analytical tasks (Vlasov, 2005).

Various biosensor-arrays have been developed for different purposes. Several biorecognition elements can be used for biosensor-arrays, for example, microorganisms, cofactors or enzymes. The most widely used biorecognition elements are enzymes belonging to the classes of oxidoreductases and hydrolases (Solna, 2005). Enzymatic biosensor-arrays are promising pre-screening methods for rapid and simple measurements and an express analysis of many pollutants, which can function either directly as substrates or as inhibitors of the enzymes selected for the sensing array (Solna, 2005).

Multisensor electronic tongue systems are suitable for a diversity of analytical tasks, both conventional and nonconventional for chemical sensors. In recent years, much attention has been given to electronic tongue applications such as industrial and environmental monitoring, and quality control (Vlasov, 2008) (e.g. fermentation processes), as electronic tongues are capable of fast, inexpensive, automated and on-line control (Witkowska, 2010).

SENSOR-ARRAY DATA ANALYSIS

In case of a single biosensor, the linear regression model (LRM) is often used for data analysis (Badertscher & Pretsch, 2006). However, since sensors used in the array may respond to all analytes, a vast amount of multidimensional information is generated (del Valle, 2010). This complex data can be processed using multivariate analysis methods (del Valle, 2010; Vlasov, 2008). Multivariate treatment makes it possible to transform the complex responses of a sensor-array into a format that is easier to interpret. It has been shown that the use of biosensor-arrays with multivariate analysis can be a promising approach for simple, fast, reproducible, selective and sensitive detection of different compounds in various samples and provides both a qualitative and quantitative overview of sample compositions (Solna, 2005).

Qualitative information from sensor-array data is used for the classification and identification of samples. The most commonly used method for this purpose is the principal component analysis (PCA), which is widely used in statistical analysis to present the data (Riul Jr, 2010). PCA makes it possible to explore multivariate data and reduce its noise without loss of information; in addition, the significance of individual components can be assessed (Riul Jr, 2010). PCA is a linear multivariate analysis method

(Hines, 1999; Solna, 2005) whose mathematics is based on matrix algebra (Massart, 2004). PCA decomposes the initial data matrix into latent variables in such a way as to preserve as much variance as possible in the first principal components (PCs). Through this method, loading and score plots can be produced which show the relationship between the variables and the samples, respectively, as well as their influence on the system. The groupings in the score plot can be used for classification, since the more similar samples are grouped together (Krantz-Rülcker, 2001). PCA requires no prior knowledge of the samples and the data is presented in as few variables as possible.

In order to extract quantitative information from biosensor-array signals, a multivariate calibration method must be applied to connect the observed signals with the identity of an analyte and its concentration. However, for the calibration of sensor-arrays, a large amount of various samples are needed in order to divide the samples into two sets: training and test samples. There are several multivariate regression models for calibration available – these can be either linear or non-linear methods (Nascu, 1999). The most widely used methods are partial least squares (PLS) and principal component regression (PCR), which are both factor-based (Correia, 2005) linear calibration methods. PCR is conducted in a similar manner to PCA; however, when used in calibration, PCR performs a linear least squares regression of the dependent variable against the scores of the significant PCs (Hibbert, 1998). On the other hand, in PLS, a principal component analysis is performed on both the dataset and the corresponding actual values (Krantz-Rülcker, 2001). The difference between PCR and PLS is that PLS includes information about the function vector in the model while PCR does not (Hines, 1999). PLS is specially devised for quantification purposes and mainly used in multi-determination applications (del Valle, 2010). The partial least square (PLS) regression method is very useful in predicting a set of dependent variables from a large set of independent variables (Hruškar, 2010).

In case of non-linear data, other methods for data treatment are required. For non-linear data, artificial neural networks (ANNs) methods are widely used. ANN is a massively parallel computing technique, especially suited to non-linear sensor responses and very similar to human pattern recognition (del Valle, 2010). ANNs are distributed computing systems composed of processing units connected by weighted links that can be assembled in one or more layers, resembling the structure and functioning of the human brain (Hruškar, 2010; Riul Jr, 2010). Thereby, ANN creates models that are non-linear (Hibbert, 1998; Krantz-Rülcker, 2001; Hruškar, 2010) and non-parametric (Hines, 1999).

BOD SENSOR-ARRAYS

Various types of BOD sensor-arrays have been reported. Not all of them are based on biosensors but also chemical sensors have been applied. Some BOD sensor-arrays are outlined in Table 1.

Table 1. Overview of BOD sensor-arrays

Transducer	Sensor modification method	Immobilization method	Calibration solution	Application	Data analysis
Clark-type oxygen electrodes (Yang, 1997)	*Trichosporon cutaneum*	Photo-crosslinkable resin ENT-3400	GGA	BOD	Calibration graph
Polypyrrole conducting polymer sensors (Stuetz, 1999) (Bourgeois & Stuetz, 2002)	N/A	N/A	Wastewater samples	BOD	ANN, PCA
The sensor chip with four platinum containment electrodes (König, 2000)	*Sphingomonas yanoikuyae* B1, *Candida parapsilosis,*	Poly(vinyl alcohol) - PVA	Synthetic wastewater	BOD, PAH*	Calibration graph
Polypyrrole conducting polymer sensors (Onkal-Engin, 2005)	N/A	N/A	Wastewater samples	BOD	Multiple discriminant analysis, canonical correlation analysis, ANN
8 screen printed Pt and Pt-graphite electrodes (Tønning, 2005)	Enzymes: tyrosinase, horseradish peroxidase, acetyl cholinesterase and butyryl cholinesterase	cross-linking with glutaraldehyde	N/A	N/A	Drift correction, PCA
CCD camera (Sakaguchi, 2007)	*Photobacterium phosphoreum* IFO 13896	Sodium alginate gel	GGA	BOD	Linear calibration graphs
8 metal electrodes (Au, Pt, Rh, Ir, Ag, Ni, Co, Cu) (Campos, 2012)	N/A	N/A	Wastewater samples	BOD, COD*, NH_4-N, PO_4-P, SO_4-S, acetic acid, alkalinity	PLS
Clark-type oxygen electrodes (Raud & Kikas, 2013)	7 different microorganisms	Agarose	OECD synthetic wastewater	BOD	Sheffe test, PCA, PLS

*PAH – polycyclic aromatic hydrocarbons, COD – chemical oxygen demand.

Stuetz and colleagues used a non-specific electronic nose, which consisted of 12 electrodes coated with a polypyrrole-based conducting polymer doped with different dopants to monitor wastewater samples. The concentration of biodegradable organic matter as determined by BOD was measured in samples collected from different parts of the wastewater treatment facility. The BOD values were derived from the odour profiles of different samples and ANN was applied for data analysis. The results were compared to the corresponding conventional 5-day BOD values and a good correlation was obtained. However, a linear correlation between the sensor responses and BOD was only evident for up to 4 weeks (Stuetz, 1999). A similar approach of using a polypyrrole-based conducting polymer sensor-array for odour analysis was also applied later to a BOD analysis (Bourgeois & Stuetz, 2002; Onkal-Engin, 2005). In that study, a good correlation between odour and the corresponding BOD values as well as good classification accuracy were achieved. However, classification was difficult due to the large variability of wastewater, especially in facilities where domestic and industrial loads frequently alternated (Onkal-Engin, 2005).

Campos and colleagues applied a voltammetric electronic tongue, which consisted of 8 electrodes made of different metals, and PLS was used for data analysis to monitor various parameters in the influent and effluent of the wastewater treatment plant. The sensor-array showed relatively good predictive power for the determination of some parameters; therefore it might be possible to use this technology for semi-quantitative analysis (Campos, 2012).

A biosensor-array utilizing different enzymes was used to extract qualitative information, i.e. to study the quality of the wastewater treatment. However, the sensor performance was not easily characterized due to its decreasing sensitivity over time and the effect of inhibiting compounds. These problems were mitigated by using drift correction algorithms (Tønning, 2005).

One of the first biosensor-arrays with immobilized microorganisms was reported by Yang and colleagues, who used thin film technology to prepare miniaturized Clark-type oxygen electrodes. This dual-type BOD sensor consisted of two oxygen electrodes – one cathode functionalized with yeast and the other without it – and two anodes. The yeast *Trichosporon cutaneum* was immobilized onto the cathode with photo-crosslinkable resin and the GGA solution was used for sensor calibration, while the difference between the outputs of the two oxygen electrodes was used to estimate the BOD. The sensor was also used for an analysis of real samples and the results obtained were in good correlation with the conventional 5-day BOD values (Yang, 1997).

A different approach was employed by Sakaguchi, who used a biosensor-array based on immobilized luminous bacteria in arrayed holes on a microchip. Several different samples were analysed at the same time, since only one strain was used in all the micro-holes. The system used a digital CCD camera to detect the luminescence as well as a mobile PC, making on-site measurements available (Sakaguchi, 2007).

Konig and colleagues immobilized two different microbial strains, one of which was a PAH-degrading bacterium, into separate platinum electrode cavities. The biosensor chip was integrated into a flow-through system to measure the oxygen consumption of the immobilized microorganisms. Good correlations of BOD_5 and sensor-BOD results were achieved. In addition, while both strains responded to glucose, only the PAH-degrading strain gave signals with a naphthalene solution; as a result, the naphthalene concentration was successfully estimated with the sensor-array. Although

high concentrations of toxic substances were supposed to be present, none of the microbial sensors showed any decrease in sensitivity after measurements with these real samples (König, 2000).

Seven microbial cultures were used to construct a biosensor-array to measure BOD in different synthetic wastewater samples containing refractory compounds. The Scheffe test, PCA and multivariate calibration methods were applied to extract qualitative and quantitative information about the different biosensors and wastewater samples. A good correlation between sensor-array measured BOD values and BOD_7 values was obtained. In addition, PCA enabled the separation of samples according to their type and BOD_7 value, making it possible to extract qualitative information about the samples (Raud & Kikas, 2013).

DISCUSSION

Despite the fact that the first BOD biosensor was developed 38 years ago, investigation and development of new devices is still active. The majority of BOD biosensors use microorganisms or a combination of microorganisms as a biological recognition element. Therefore, one main field of study is finding the most suitable microbial cultures for any particular analytical purpose. However, a single culture does not have sufficiently wide substrate spectrum to analyse diverse samples despite the fact that a single culture is more stable than a consortium of several bacterial cultures. To overcome this problem, several sensor-arrays have been proposed for BOD measurements. The first proposed sensor-arrays did not make use of statistical analysis and were thus cast aside. The second wave of sensor-arrays did use statistical analysis, but also utilized chemical sensors with no specificity of the biorecognition element. This led to a summarised signal with no qualitative information. Only in recent years have sensor-arrays been proposed that utilize both statistical multivariate analysis and specific biorecognition elements. Biosensor-arrays utilizing a variety of microorganisms make it possible to conduct measurements with several cultures at the same time, which helps to save time, since information from several biosensors is received simultaneously and a more complex signal is obtained. Applying a multivariate statistical analysis to this kind of signal will yield both more accurate quantitative information and qualitative information.

There is a need for the development of new on-line monitoring techniques, since the standard BOD test is too time-consuming for process control in water treatment systems. On-line measurements are available when automated biosensor-arrays are used. Automated measurements, fully controlled by the computers, are noticeably less labour-intensive and thus measurement precision increases since human error is minimized.

Many new technologies, such as screen-printing and microfabrication, are available that enable the construction of miniaturized biosensor-arrays. Smaller, miniaturized biosensor-arrays lead to less chemical usage and consequently cheaper measuring technology. In addition, using smaller sensors makes it easier to develop portable devices, which enable conducting field measurements. Small but automated on-line biosensor-arrays like these can give real-time information about wastewater parameters and make it possible to operate the treatment plants over the network.

New data analysis methods provide other ways to interpret biosensor-array results. It has been shown that various multidimensional data analysis methods are making it

possible to extract more information from data than ever before. Various classification, calibration and information extraction methods are available, some of which do not require linear models and are even self-learning, such as ANN. Data analysis has become more complex, using sensor-arrays instead of a single biosensor. However, biosensor-arrays with complex data analysis provide more precise results.

Still, there are more problems to be solved. Sensor drift is a big problem with sensor-arrays. It may be caused by the ageing of a sensor, temperature or pressure changes, or the ageing of the biological recognition element (Bourgeois, 2003). Achieving a longer and more stable service life for biological recognition elements, guaranteeing easy and effective maintenance of the measurement system, and overcoming the toxic effect of samples to microorganisms are just a few of those challenges. Another problem, a political one, lies in the fact that it takes time before new devices and methods are accepted by governments and proper legislation is issued to encourage the use of biosensor-array systems.

CONCLUSIONS

Biosensors have been investigated for more than thirty years. Over that time a number of biosensors for the determination of a variety of analytes have been developed, out of which BOD biosensors are probably the most widely reported microbial biosensors. In the past decade various sensor-arrays comprising a set of different sensors and multivariate analysis methods for signal analysis have been developed. Sensor-arrays have been used for BOD measurements; however, there is still room for development. By combining several technologies, such as the application of several specific microorganisms, the miniaturization of sensors and sensor-arrays, the flow-through technology, and the complex multivariate technology for data analysis, superior results could be achieved. A biosensor-array of that kind would be small and fully automated, and precise, multifaceted information could be obtained about the samples.

ACKNOWLEDGEMENTS. Financial support for this research was partially provided by the Estonian Environmental Investment Centre and by 'Integrated Biosystems Engineering', a topic receiving base funding.

REFERENCES

APHA. 1985. *Standard methods for examination of water and wastewater*. Washington American Public Health Association.

Badertscher, M. & Pretsch, E. 2006. 'Bad results from good data'. *TrAC Trends in Analytical Chemistry* **25**(11), 1131–1138.

Bourgeois, W., Burgess, J.E. & Stuetz, R.M. 2001. 'On-line monitoring of wastewater quality: a review'. *Journal of Chemical Technology and Biotechnology* **76**(4), 337–348.

Bourgeois, W., Romain, A.-C., Nicolas, J. & Stuetz, R.M. 2003. 'The use of sensor arrays for environmental monitoring: interests and limitations'. *Journal of Environmental Monitoring* **5**(6), 852–860.

Bourgeois, W. & Stuetz, R.M. 2002. 'Use of a chemical sensor array for detecting pollutants in domestic wastewater'. *Water Research* **36**(18), 4505–4512.

Campos, I., Alcañiz, M., Aguado, D., Barat, R., Ferrer, J., Gil, L., Marrakchi, M., Martínez-Mañez, R., Soto, J. & Vivancos, J.-L. 2012. 'A voltammetric electronic tongue as tool for

water quality monitoring in wastewater treatment plants'. *Water Research* **46**(8), 2605–2614.
Chee, G.-J., Nomura, Y., Ikebukuro, K. & Karube, I. 2005. 'Development of photocatalytic biosensor for the evaluation of biochemical oxygen demand'. *Biosensors and Bioelectronics* **21**(1), 67–73.
Chee, G.-J., Nomura, Y., Ikebukuro, K. & Karube, I. 2007. 'Stopped-flow system with ozonizer for the estimation of low biochemical oxygen demand in environmental samples'. *Biosensors and Bioelectronics* **22**(12), 3092–3098.
Correia, D.P.A., Magalhães, J.M.C.S., Machado, A.A.S.C. 2005. 'Array of potentiometric sensors for simultaneous analysis of urea and potassium'. *Talanta* **67**, 773–782.
D'Souza, S.F. 2001. 'Microbial biosensors'. *Biosensors and Bioelectronics* **16**(6), 337–353.
del Valle, M. 2010). 'Electronic Tongues Employing Electrochemical Sensors'. *Electroanalysis* **22**(14), 1539–1555.
Escuder-Gilabert, L. & Peris, M. 2010. 'Review: Highlights in recent applications of electronic tongues in food analysis'. *Analytica Chimica Acta* **665**(1), 15–25.
Hibbert, D.B. 1998). 'Data Analysis of Multi-Sensor Arrays'. *Electroanalysis* **10**(16), 1077–1080.
Hines, E.L., Llobet, E. & Gardner, J.W. 1999. 'Electronic noses: a review of signal processing techniques'. *Iee Proceedings-Circuits Devices and Systems* **146**(6), 297–310.
Hruškar, M., Major, N. & Krpan, M. 2010. 'Application of a potentiometric sensor array as a technique in sensory analysis'. *Talanta* **81**(1–2), 398–403.
Karube, I., Matsunaga, T., Mitsuda, S. & Suzuki, S. 1977. 'Microbial electrode BOD sensors'. *Biotechnology and Bioengineering* **19**(10), 1535–1547.
Kibena, E., Raud, M., Jõgi, E. & Kikas, T. 2012. 'Semi-specific Microbacterium phyllosphaerae-based microbial sensor for biochemical oxygen demand measurements in dairy wastewater'. *Environmental Science and Pollution Research*, 1–7.
Kim, B.H., Chang, I.S. & Moon, H. 2006. 'Microbial Fuel Cell-Type Biochemical Oxygen Demand Sensor'. *Encyclopedia of Sensors* **X**, 1–12.
Kim, M.-N. & Kwon, H.-S. 1999. 'Biochemical oxygen demand sensor using Serratia marcescens LSY 4'. *Biosensors and Bioelectronics* **14**(1), 1–7.
Kissinger, P.T. 2005. 'Biosensors – a perspective'. *Biosensors and Bioelectronics* **20**(12), 2512–2516.
Krantz-Rülcker, C., Stenberg, M., Winquist, F. & Lundström, I. 2001. 'Electronic tongues for environmental monitoring based on sensor arrays and pattern recognition: a review'. *Analytica Chimica Acta* **426**(2), 217–226.
König, A., Reul, T., Harmeling, C., Spener, F., Knoll, M. & Zaborosch, C. 2000. 'Multimicrobial Sensor Using Microstructured Three-Dimensional Electrodes Based on Silicon Technology'. *Analytical Chemistry* **72**(9), 2022–2028.
Lagarde, F. & Jaffrezic-Renault, N. 2011. 'Cell-based electrochemical biosensors for water quality assessment'. *Analytical and Bioanalytical Chemistry* **400**(4), 947–964.
Liu, C., Zhao, H., Ma, Z., An, T., Liu, C., Zhao, L., Yong, D., Jia, J., Li, X. & Dong, S. 2014. 'Novel Environmental Analytical System based on Combined Biodegradation and Photoelectrocatalytic Detection Principles for Rapid Determination of Organic Pollutants in Wastewaters'. *Environmental Science and Technology* **48**, 1762–1768.
Liu, J., Björnsson, L. & Mattiasson, B. 2000. 'Immobilised activated sludge based biosensor for biochemical oxygen demand measurement'. *Biosensors and Bioelectronics* **14**(12), 883–893.
Liu, J. & Mattiasson, B. 2002. 'Microbial BOD sensors for wastewater analysis'. *Water Research* **36**(15), 3786–3802.
Luong, J.H.T., Male, K.B. & Glennon, J.D. 2008. 'Biosensor technology: Technology push versus market pull'. *Biotechnology Advances* **26**(5), 492–500.

Massart, D.L.H. & Vander, Y. 2004. 'From Tables to Visuals: Principal Component Analysis, Part 1'. *LC – GC Europe* **17**(11), 586–591.
Namour, P. & Jaffrezic-Renault, N. 2010. 'Sensors for measuring biodegradable and total organic matter in water'. *TRAC Trends in Analytical Chemistry* **29**(8), 848–857.
Nascu, H., Jantschi, L., Hodisan, T., Cimpoiu, C. & Cimpan, G. 1999. 'Some applications of statistics in analytical chemistry'. *Reviews in Analytical Chemistry* **18**(6), 409–456.
Onkal-Engin, G., Demir, I. & Engin, S.N. 2005. 'Determination of the relationship between sewage odour and BOD by neural networks'. *Environmental Modelling & Software* **20**(7), 843–850.
Pasco, N., Weld, R., Hay, J. & Gooneratne, R. 2011. 'Development and applications of whole cell biosensors for ecotoxicity testing'. *Analytical and Bioanalytical Chemistry* **400**(4), 931–945.
Ponomareva, O.N.A., Alferov, V.A., Reshetilov, A.N. 2011. 'Microbial Biosensors for Detection of Biological Oxygen Demand (a Review)'. *Applied Biochemistry and Microbiology* **47**(1), 1–11.
Rastogi, S., Kumar, A., Mehra, N.K., Makhijani, S.D., Manoharan, A., Gangal, V. & Kumar, R. 2003. 'Development and characterization of a novel immobilized microbial membrane for rapid determination of biochemical oxygen demand load in industrial waste-waters'. *Biosensors and Bioelectronics* **18**(1), 23–29.
Raud, M. & Kikas, T. 2013. 'Bioelectronic tongue and multivariate analysis: A next step in BOD measurements'. *Water Research* **47**(7), 2555–2562.
Raud, M., Linde, E., Kibena, E., Velling, S., Tenno, T., Talpsep, E. & Kikas, T. 2010. 'Semi-specific biosensors for measuring BOD in dairy wastewater'. *Journal of Chemical Technology and Biotechnology* **85**(7), 957–961.
Raud, M., Tenno, T., Jõgi, E. & Kikas, T. 2012a. 'Comparative study of semi-specific Aeromonas hydrophila and universal Pseudomonas fluorescens biosensors for BOD measurements in meat industry wastewaters'. *Enzyme and Microbial Technology* **50**(4–5), 221–226.
Raud, M., Tutt, M., Jõgi, E. & Kikas, T. 2012b. 'BOD biosensors for pulp and paper industry wastewater analysis'. *Environmental Science and Pollution Research* **19**(7), 3039–3045.
Riul Jr, A., Dantas, C.A.R., Miyazaki, C.M. & Oliveira, Jr, O.N. (2010). 'Recent advances in electronic tongues'. *Analyst* **135**(10), 2481–2495.
Rodriguez-Mozaz, S., Lopez De Alda, M.J. & BarcelĆ, D. 2006. 'Biosensors as useful tools for environmental analysis and monitoring'. *Analytical and Bioanalytical Chemistry* **386**(4), 1025–1041.
Sakaguchi, T., Morioka, Y., Yamasaki, M., Iwanaga, J., Beppu, K., Maeda, H., Morita, Y. & Tamiya, E. 2007. 'Rapid and onsite BOD sensing system using luminous bacterial cells-immobilized chip'. *Biosensors and Bioelectronics* **22**(7), 1345–1350.
Solna, R., Dock, E., Christenson, A., Winther-Nielsen, M., Carlsson, C., Emnéus, J., Ruzgas, T. & Skladal, P. 2005. 'Amperometric screen-printed biosensor arrays with co-immobilised oxidoreductases and cholinesterases'. *Analytica Chimica Acta* **528**(1), 9–19.
Stuetz, R.M., George, S., Fenner, R.A. & Hall, S.J. 1999. 'Monitoring wastewater BOD using a non-specific sensor array'. *Journal of Chemical Technology and Biotechnology* **74**(11), 1069–1074.
Su, L., Jia, W., Hou, C. & Lei, Y. 2011. 'Microbial biosensors: A review'. *Biosensors and Bioelectronics* **26**(5), 1788–1799.
Suriyawattanakul, L., Surareungchai, W., Sritongkam, P., Tanticharoen, M. & Kirtikara, K. 2002. 'The use of co-immobilization of Trichosporon cutaneum and Bacillus licheniformis for a BOD sensor'. *Applied Microbiology and Biotechnology* **59**(1), 40–44.
Tan, T.C. & Wu, C. 1999. 'BOD sensors using multi-species living or thermally killed cells of a BODSEED microbial culture'. *Sensors and Actuators B: Chemical* **54**(3), 252–260.

Thévenot, D.R., Toth, K., Durst, R.A. & Wilson, G.S. 2001. 'Electrochemical biosensors: Recommended definitions and classification'. *Biosensors and Bioelectronics* **16**(1–2), 121–131.

Tønning, E., Sapelnikova, S., Christensen, J., Carlsson, C., Winther-Nielsen, M., Dock, E., Solna, R., Skladal, P., Nørgaard, L., Ruzgas, T. & Emnéus, J. 2005. 'Chemometric exploration of an amperometric biosensor array for fast determination of wastewater quality'. *Biosensors and Bioelectronics* **21**(4), 608–617.

Witkowska, E., Buczkowska, A., Zamojska, A., Szewczyk, K.W. & Ciosek, P. 2010. 'Monitoring of periodic anaerobic digestion with flow-through array of miniaturized ion-selective electrodes'. *Bioelectrochemistry* **80**(1), 87–93.

Vlasov, Y., Legin, A., Rudnitskaya, A., Natale, C.D. & D'Amico, A. 2005. 'Nonspecific sensor arrays ('electronic tongue') for chemical analysis of liquids (IUPAC Technical Report)'. *Pure and Applied Chemistry* **77**(11), 1965–1983.

Vlasov, Y., Legin, A. & Rudnitskaya, A. 2008. 'Electronic tongue: Chemical sensor systems for analysis of aquatic media'. *Russian Journal of General Chemistry* **78**(12), 2532–2544.

Xu, X. & Ying, Y. 2011. 'Microbial Biosensors for Environmental Monitoring and Food Analysis'. *Food Reviews International* **27**(3), 300–329.

Yang, Z., Sasaki, S., Karube, I. & Suzuki, H. 1997. 'Fabrication of oxygen electrode arrays and their incorporation into sensors for measuring biochemical oxygen demand'. *Analytica Chimica Acta* **357**(1–2), 41–49.

II

ETIS 1.1: **Pitman, K.**; Raud, M.; Scotti, G.; Jokinen, V. P.; Franssila, S.; Nerut, J.; Lust, E.; Kikas, T. (2017) Electrochemical Characterization of the Microfabricated Electrochemical Sensor-Array System. *Electroanalysis*, 29, 249−258. 10.1002/elan.201600559.

Full Paper Wiley Online Library ELECTROANALYSIS

DOI: 10.1002/elan.201600559

Electrochemical Characterization of the Microfabricated Electrochemical Sensor-Array System

Kätlin Pitman,[a] Merlin Raud,*[a] Gianmario Scotti,[b, c] Ville P. Jokinen,[b] Sami Franssila,[b] Jaak Nerut,[d] Enn Lust,[d] and Timo Kikas[a]

Abstract: Microfabrication technology has been used to prepare a microchip sensor-array with six sets of platinum electrodes. Chromium/platinum (10 nm/100 nm thick) were sputtered on a borosilicate wafer and patterned by wet etching method. The electrodes were designed with working electrode area of 700×400 μm in the middle and a 200 μm wide and 2600 μm long counter electrode surrounding it from three sides in a U-shape. The connection pads (1000×1500 μm) were located at the edge of a sensor-array chip. Silicon wafer was etched through to form holes with slanting side walls for immobilization cavities. The silicon and the borosilicate wafers were adhesion bonded with SU-8 epoxy resin. The cyclic voltammetry and electrochemical impedance experiments were carried out in a three-electrode electrochemical system to characterize the fabricated sensor-array chip. The results show that the current density depends on the electrode potential sweep rate v. Also, current density depends on the concentration of potassium hexacyanoferrate(III). At slow potential sweep rates ($v \leq 0.01\ V\,s^{-1}$) the steady-state signal is achieved and the electrodes behave as micro-electrodes. Such an array is a promising candidate for fast and simple biochemical oxygen demand (BOD) measurements.

Keywords: Microfabrication · Sensor-array · Electrochemical sensor · Pt electrodes · Micro-electrodes · MEMS

1 Introduction

Application of the micro-electrodes have been in the centre of attention at least for the last forty years [1–2]. If the characteristic dimension of the electrode is less than the diffusion layer thickness, then the electrode behaves as a micro-electrode, i.e. the (pseudo) steady-state conditions could be attained [3]. The field of application of micro-electrodes is very wide: from electroanalytical applications (detection of ultra-low quantities of analyte, biosensors, etc.), kinetic studies of very fast and complex reactions, to measurements in solutions of very low conductivity, etc. [2,4–6]. These applications are based on the following properties of micro-electrodes: (a) the ohmic potential drop, *IR*, is very small because the electrode area is small and therefore the currents measured are also small; (b) the charging current decreases with the dimensions of the electrode and better estimation of the faradaic current is possible at very high potential sweep rate; and (c) the mass-transport rate is enhanced and the steady-state is achievable within usual experimental measurement times because of the radial diffusion of reactants [2,4–6].

Variety of micro-electrode geometries has been exploited, including sphere, hemisphere, cylinder, disk and band type electrodes [6]. In order to increase the signal to noise ratio, improve the sensitivity and lower further detection limits, many individual micro-electrodes could be arranged into array [2,4–5,7]. Both inlaid and recessed disk and band electrodes are used [1,7–12]. The recessed micro-electrode has the advantage that the convection of the bulk solution influences only slightly the mass transport in the hole and therefore linear concentration gradient of electroactive species is more easily achieved in the micro-hole and the overlapping of the diffusion layers of the micro-electrodes in the array is less probable [9]. The recessed micro-electrodes could be used in the flow-through systems, e.g. in liquid chromatographs, various biosensors, etc. [8–10].

Often several sensors are combined into sensor-arrays for simultaneous analysis of various parameters. These sensor-arrays with suitable multivariate analysis can be used for fast, inexpensive and reliable sample characterization – classification, origin recognition, or estimation of properties of complex samples [13–14]. Various electrochemical sensors have been applied in sensor-arrays but

[a] K. Pitman, M. Raud, T. Kikas
Estonian University of Life Sciences, Institute of Technology, Kreutzwaldi 56, EE51014, Tartu, Estonia
*e-mail: merlin.raud@emu.ee

[b] G. Scotti, V. P. Jokinen, S. Franssila
Aalto University, Department of Materials Science and Engineering and Micronova Nanofabriction Centre, PO BOX 13500, FIN-00076 Aalto, Finland

[c] G. Scotti
current address: University of Helsinki, Faculty of Pharmacy, Division of Pharmaceutical Chemistry & Technology, Viikinkaari 5E, FIN-00014 Helsinki, Finland

[d] J. Nerut, E. Lust
University of Tartu, Institute of Chemistry, Ravila 14a, EE50411, Tartu, Estonia

also biosensor-arrays utilizing different enzymes [15], genetically modified single strain microorganisms [16–18] or different strains of microorganisms [19] have been reported. It has been shown that when utilizing differently modified sensors in a biosensor array, better estimation of analyte and additionally, information about the samples' origin can be gained [20].

In practical applications, it is desirable that the analysis is rapid and uses minimal amounts of sample and expensive reagents. Additionally, miniaturization allows the development of portable analytical systems to be used for in-field applications [21–22]. This kind of miniaturized electrodes can be fabricated using microfabrication or screen-printing technologies, which has been widely used for making micro-electrodes for different biosensors and biosensor arrays [19,21,23].

Microfabrication is used to construct physical objects with dimensions in the micrometre to millimetre range [24]. This technology has very high precision in the fabrication process and therefore, it is suitable for preparing micro-electrodes [21] and is based on deposition, lithography and etching steps. Materials like silicon, polymers, metals and silicon oxide or silicon nitride [25] that enable the fabrication of wells, reactors, channels, and electrodes in various sizes and geometries are used [22,26]. Microfabrication technology also enables batch-fabrication, which leads to production of inexpensive sensors and even, disposable, maintenance-free sensors [27].

This paper presents microfabrication and electrochemical characterization of a future sensor-array chip. The sensor-array was based on silicon and borosilicate glass substrates. Sputtered platinum was used for micro-electrodes, and Ag/AgCl/sat. KCl for reference electrodes. The high surface area Pt counter electrode has been used. Electrochemical characterisation was performed on separate sensors of several different sensor-array chips. All individual sensors of different chips performed in a similar fashion within allowed deviation limits (< 1 %).

2 Experimental

2.1 Fabrication of Sensor Array Chip

The sensor array microchips were fabricated using silicon wafers (100 mm diameter double side polished wafer of ⟨100⟩ orientation and thickness of 500–525 μm) and borosilicate wafers (Pyrex glass, also 100 mm, thickness 500 μm). The fabrication process of wafers is illustrated in Figure 1. Before processing, the wafers were cleaned using RCA 1 solution (DI-water, NH_4OH, H_2O_2 in 5 : 1 : 1,4 ratio) for 10 minutes at 70–80°, rinsed with DI-water (deionized water) and dried.

2.2 Pyrex Wafer Processing

Pt electrodes and connection pads were fabricated using 100 nm thick Pt with 10 nm Cr as adhesion layer. Cr and Pt were deposited onto Pyrex wafer using sputtering (Cr 10 nm: 200 W, time 62 sec, 10 rev/min, Ar flow 50, pressure 4 mTorr; Pt 100 nm: 500 W, time 4 min, 6 rev/min, Ar flow 70, pressure 5.2 mTorr) in Plasmalab 400 sputter from Oxford Instruments.

The Cr/Pt Pyrex wafer was baked at 120° for 10 min and primed with HDMS (hexamethyldisilazane) for 10 min in vacuum desiccator. Photoresist (AZ 5214) was spin coated on the wafer (4000 rpm, 30 sec) and baked for 20 min at 90°. The pattern was exposed with mask aligner (MA 6, Karl Süss Microtech) to UV light (λ = 365 nm) through plastic mask with electrode pattern for 4 seconds. During development (developer AZ 351B) the photoresist was removed from areas exposed to UV light while areas covered with dark mask pattern and therefore unexposed to UV light remained covered with photoresist. The wafer was rinsed with DI water and dried and then baked in an oven for 20 min at 120°. The exposed Pt was etched away with hot *aqua regia* (3 : 1 $HCl : HNO_3$ 24°, 4 minutes) followed by Cr etching with Cr etchant

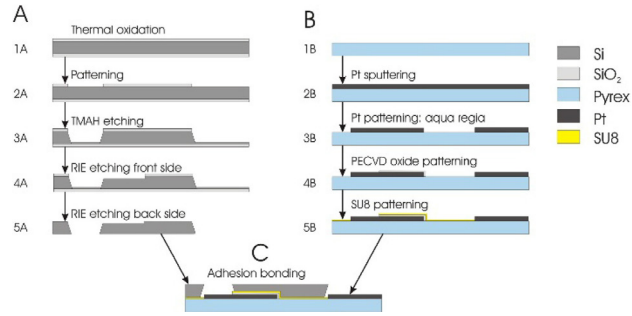

Fig. 1. Process flow of biosensor microchip: A – Si wafer processing; B – Pyrex wafer processing; C – bonding of Si and Pyrex wafer.

(solution of Ceric Ammonium Nitrate, 24°, 10 sec) to fabricate electrode and connection pad patterns into Cr/Pt layer. The remaining resist was then removed with acetone in ultrasonic bath (15 min), followed by rinsing in clean acetone, isopropanol and finally rinsing with DI water and drying.

Plasma-enhanced chemical vapour deposition (PECVD) (Plasmalab 80Plus, Oxford Instruments) was used to deposit 100 nm film of SiO_2 which acts as electrical isolation (time – 105 sec; temp – 300°; pressure – 1000 m Torr; power – 20 W; SiH_4 – 8.5 sccm; N_2O – 710 sccm; N_2 – 161.5 sccm).

Another lithography step, with parameters identical to the above, was carried out to pattern the electrode openings in the oxide layer. Exposed SiO_2 layer was etched away with BHF (buffered hydrofluoric acid) solution (5 sec, 24°). Resist removal, rinsing and drying were identical to the above.

2.3 Silicon Wafer Processing

Silicon wafers were used to make the openings for the electrode areas and cavities for the immobilized microorganisms. Adsorption in an agarose gel matrix was chosen as method of immobilization due to its simplicity and since the direct absorption of whole cells onto the working electrode is not viable [28]. In order to hold the agarose gel with immobilized microorganisms in place, the cavities with slanting side walls in shape of square based frustum pyramid were used. The silicon wafer was chosen for the fabrication of cavities for housing the agarose gel since its crystal structure enables it to be etched anisotropically and results in 54.7° angle cavity walls which formed frustum pyramid based on square base.

Thermal oxidation of silicon wafer was used to fabricate 300 nm thick SiO_2 layer, which was used as a mask to fabricate pattern of through holes in the oxide layer. Lithography process was identical to PECVD oxide patterning above. In order to protect the oxide layer on the back side of the wafer the photoresist was also spun on the back side of the wafer (4000 rpm, 30 sec). The wafer was baked in an oven for 20 min at 120°. The oxide not protected with resist on the front side was etched with BHF (2 min, 35°), and resist removed as above.

The 483 μm deep holes were etched using hot TMAH (tetramethylammonium hydroxide) solution (85°, 15 hours), after which the wafer was rinsed with DI water and dried. The SiO_2 used as a mask was removed in a 49% HF solution (2 min, 24°) and the wafer was rinsed with DI water and dried.

In order to fabricate space for electrical connections between electrode and contact area, RIE (reactive ion etching) was used to etch 433 nm deep patterns, which directly correspond to patterns of electrode connections on Pyrex wafer. Standard lithography was used. Next, RIE (3.5 min, power 70 W, SF_6 flow 100 sccm, pressure 300 mTorr, etch rate 85 nm/min) was used to etch 433 nm deep patterns. Resist was then removed as described.

In order to protect the front side of the wafer during further processing, the 200 nm of SiO_2 was deposited using plasma-enhanced chemical vapour deposition (PECVD) (time – 3.5 min; temp – 300°; pressure – 1000 mTorr; power – 20 W; SiH_4 flow – 8.5 sccm; N_2O flow – 710 sccm; N_2 flow – 161.5 sccm). The through holes for electrode contacts and immobilization cavities were opened using RIE of whole wafer from back side until through holes were gained (etch rate (power 150 W; SF6 – 100 sccm; pressure 100 mTorr; time – 95 min, 420 nm/min) (Plasmalab 80Plus, Oxford Instruments). When the through holes were opened the protective SiO_2 layer was removed with BHF solution. The silicon wafer after through hole etching is shown in Fig. 2.

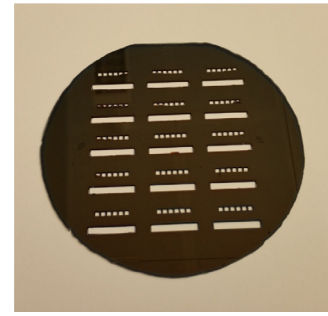

Fig. 2. Silicon wafer after KOH through etching. 15 sensor arrays fit on one 100 mm wafer.

2.4 Bonding

The processed silicon and Pyrex wafers were bonded using adhesive bonding with SU-8 epoxy resin. Before bonding, the silicon wafer was cleaned in RCA-1 solution (10 min, 70–80°), rinsed with DI water and dried. Pyrex wafer with Cr/Pt electrode patterns was baked at 120° for 20 min for dehydration. SU-8-50 was then spin coated on the wafer (45 sec at 9000 rpm), resulting in 10 μm thick layer. The wafer was baked on a programmable hotplate (108 sec from room temp to 65° (21.67°/min); 180 sec at 65°; 120 sec from 65° to 95° (15°/min); 300 sec at 95°). Next, it was exposed to UV light (8 sec) in a mask aligner. Plastic mask, which was previously used to fabricate electrode pattern, was used in the exposure. Post-exposure bake was made using programmable hotplate (300 sec from room temp to 95° (19°/min); 240 sec at 95°; 1200 sec from 95° to room temp (−3.75°/min)). The unexposed SU-8 was removed with SU-8 developer mr-Dev600. The patterns of two wafers were aligned and

wafers were pressed together with a force of 200 N. Reduced pressure 10^{-3} mbar was used in the bond chamber. Temperature was increased at the rate of 10 °C/min to 180° and bonding time of 30 min was used. Temperature was ramped down also at a rate of −10 °C/min until room temperature was reached and the chamber was flushed with nitrogen. The bonded wafer was diced to individual sensor array chips with a diamond blade dicing saw.

2.5 Electrochemical Characterization

2.5.1 Chemicals

Potassium hexacyanoferrate(III) ($K_3[Fe(CN)_6]$) (purity assay 98.7 %) and potassium chloride (KCl) (assay 100.0 %) were purchased from Lach-Ner (Czech Republic). All the solutions were prepared from double distilled water. The concentration of potassium chloride was kept constant (1.0 M) and the concentration of potassium hexacyanoferrate(III) was varied between 2 mM and 15 mM. Prior to the measurements, the solutions were saturated with argon (AGA, 99.9999 %) during 15 minutes.

2.5.2 Instrumentation

3M™ mini D ribbon (MDR) connector with 28 contact pads was used to connect the sensor-array chip with potensiostat. The cyclic voltammetry (CV) and electrochemical impedance (EIS) experiments were carried out in a three-electrode electrochemical system using potentiostat Reference 600 (Gamry Instruments Inc). The working electrode was the inner platinum band electrode and the auxiliary electrode was high surface area platinum electrode. All the potentials were measured against Ag|AgCl| saturated KCl in water reference electrode. The CV was performed from −0.20 V to 0.88 V at different electrode potential sweep rates ν (from 0.01 Vs^{-1} to 1 Vs^{-1}). The EIS data were measured at potentials 0 V and 0.8 V. The ac frequency, *f*, was modulated between 0.1 Hz and 10^6 Hz (10 points per decade) and the ac voltage amplitude was 5 mV (rms). During the electrochemical characterisation step several chips were tested. It was found that different micro-electrodes were electrochemically active and the reproducibility of EIS parameters and (pseudo) steady-state current densities was good. Within one measurement the time stability of cyclic voltammograms and EIS data was very good.

3 Results and Discussion

3.1 Chip Fabrication

The Figure 3A shows a photo of Pt electrodes on Pyrex wafer before bonding. Platinum etching requires an extremely aggressive etchant aqua regia. Therefore, simple room temperature etching, which avoids damage to resist was used. The connection pads are located at the edge of a sensor-array chip so that standard connectors can easily be attached. A layer of PECVD deposited SiO_2 was used as isolation layer to cover the signal lines between electrodes and connection pads. The oxide layer was patterned as a 200 µm wide line directly on top of the 100 µm wide electrode connections with a robust overlap to make the alignment easier.

The silicon wafers were extremely fragile after through etching, especially because the edges were unprotected, and therefore ragged. The cavities were aligned over the electrodes and the top openings of the cavities were of same size as the electrode areas. In addition to the immobilization cavities, the area over connection pads was opened also in order to connect the sensor-array with standard connector to the measurement instrument. As the silicon and Pyrex wafers were initially intended to be bonded using anodic bonding, the 433 nm deep grooves were fabricated, which directly overlapped the Pt and SiO_2 pattern on the Pyrex wafer but because adhesive bonding was eventually adopted, those structures are superfluous.

Adhesive bonding with SU-8 resulted in a bond that is stable in aqueous test solutions. SU-8 is chemically and thermally stable polymer that has been extensively used in chemical microsystems [16]. In order to gain fully bonded and undamaged wafers the force to the wafer and temperature ramps are extremely important. During the bonding the temperature was increased with a small ramp since the perforated silicon wafers were fragile. The fast temperature ramp caused the silicon wafer to break into small pieces. The best bonding quality was gained when the pressure was applied to wafers at first and then the temperature was increased with a slow ramp of 10 °C/min to 180°. After 30 minute of bonding time at 180° the temperature was slowly ramped down to room temperature and then the force to wafers was released. Applying the force after or during the temperature ramp resulted in low bonding quality and releasing the force before the bonded wafers were cooled down resulted in fragmentation of silicon wafer to small pieces. This kind of bonding procedure enabled to obtain nearly perfect bond and all the individual sensor-array chips were usable after dicing. The individual sensor-array chips were separated by dicing. Bare diced chips and chips with standard connector attached are shown in Figures 3B and 3C, respectively.

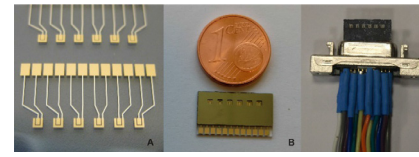

Fig. 3. Photos of the sensor-array chip: **A** – Pt electrodes on Pyrex wafer before bonding; **B** – Bonded and diced sensor-array chip; **C** – Sensor-array chip with standard connector.

3.2 Electrochemical Experiments

The ferrocyanide/ferricyanide redox couple was used to test the electrochemical behaviour of the sensor-array chip. The data of the CV measurements are presented in Figs. 4 and 5. The corrected current density, j_c, was used and analysed, i.e. the current densities, j, measured in the solution of potassium hexacyanoferrate(III) were corrected for currents measured in the 1.0 M KCl base electrolyte solution. In the 1.0 M KCl aqueous solution, there were no apparent indications of faradaic processes in the potential region under study. The slight increase of current density $|j|$ only could be observed at more negative potentials than 0 V during the scans with very slow potential sweep rate ($v \leq 0.01\ V\,s^{-1}$). This could be caused by the slow hydrogen evolution on the platinum electrode.

The electroreduction of the hexacyanoferrate(III) anion starts at less positive potentials than 0.40 V (Fig 4). The hexacyanoferrate(II) anion formed near the electrode is oxidized back during the reversal scan at more positive potentials than 0.25 V. The formal potential of the $[Fe(CN)_6]^{4-}/[Fe(CN)_6]^{3-}$ redox pair is 0.356 V [30–31].

The reduction and oxidation peaks are formed, caused by the linear diffusion-limited process in the solution phase near the electrode surface. The reduction current density, $|j_c|$, and oxidation current density, j_a, increase with the potential sweep rate. At constant concentration of the $[Fe(CN)_6]^{3-}$-anions the dependencies of cathodic peak current density, $j_{p,c}$, on $v^{1/2}$ are non-linear, the ordinates differ from zero and depend systematically on the reactant concentration (insets in Fig. 4), i.e. the classical linear semi-infinite diffusion model does not apply to this system and a kind of steady-state condition could be reached. However, the anodic peak current density, $j_{p,a}$, approaches to zero as the sweep rate becomes zero. The ratio $|j_{p,c}|/j_{p,a}$ is always much higher than 1.2, although, the diffusion coefficients of oxidized and reduced forms of hexacyanoferrate anions in the 1.0 M KCl solution are similar ($D([Fe(CN)_6]^{3-}) = 0.76 \cdot 10^{-5}\ cm^2\,s^{-1}$ and $D([Fe(CN)_6]^{4-}) = 0.63 \cdot 10^{-5}\ cm^2\,s^{-1}$ [32]).

It should be noted that the shape of the cyclic voltammograms depends on the potential sweep rate and it transforms to sigmoidal with decreasing potential sweep rate. This is also theoretically predicted [9] and experimentally observed in case of recessed microdisk electrode arrays [7,9,11,33]. The experimental cyclic voltammograms measured at the recessed micro-band electrode arrays have same characteristics [11]. There is almost no oxidation peak at very slow potential scan rates ($v \leq 0.01\ V\,s^{-1}$) and the oxidation current densities are close to zero, i.e. the pseudo steady-state is achieved [7,33]. The reduction currents in the true steady-state conditions should be exactly the same for the forward and reverse potential scans because the flux of reactants to the surface is constant. This effect is common for the micro-disk electrodes at slow scan rates, if the diffusion step is dominated by the radial component [6,33]. Based on the data in Figs. 4 and 5, in the present case the radial diffusion

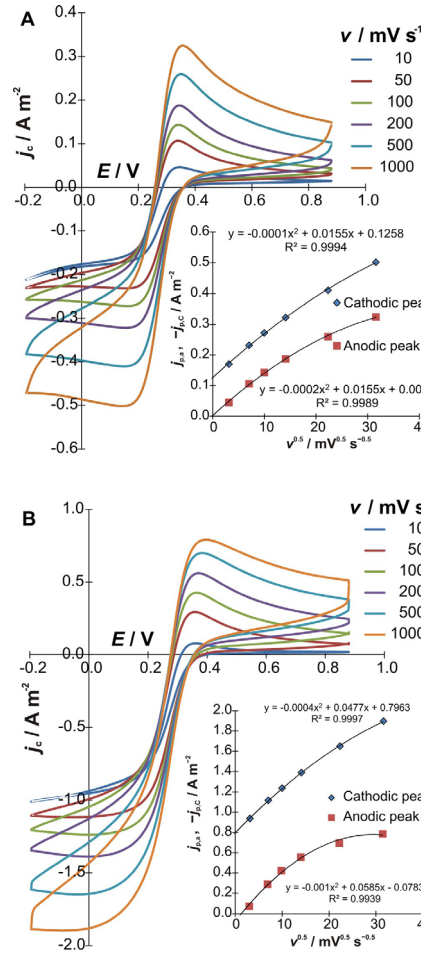

Fig. 4. The dependence of the corrected current density, j_c, on the electrode potential, E, at different electrode potential sweep rates, v, (noted in figure) for the **A** – 1.0 M KCl + 2 mM $K_3[Fe(CN)_6]$ and **B** – 1.0 M KCl + 12.5 mM $K_3[Fe(CN)_6]$ solutions saturated with argon. The working electrode was the inner platinum band electrode on the micro-chip and the auxiliary electrode was high surface area platinum electrode. All potentials were measured against Ag|AgCl| saturated KCl in water reference electrode. Inserts: dependencies of cathodic peak current density, $j_{p,c}$, and anodic peak current density, $j_{p,a}$, on $v^{1/2}$.

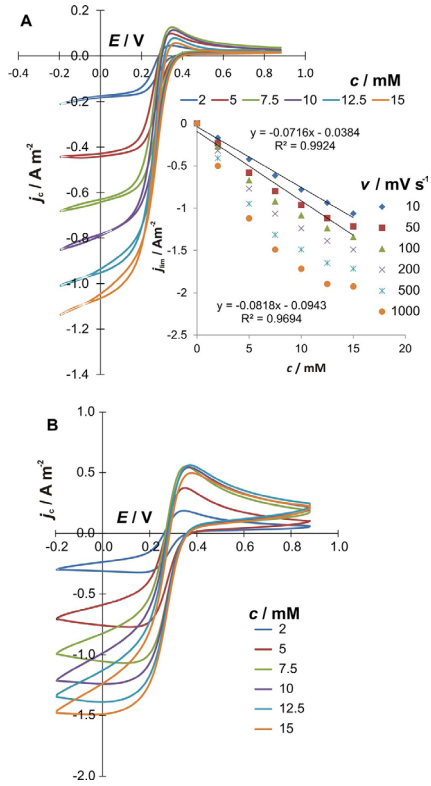

Fig. 5. The dependence of the corrected current density, j_c, on the electrode potential, E, in the 1.0 M KCl solution with different additions of $K_3[Fe(CN)_6]$ (noted in figure) at electrode potential sweep rate: **A** – 0.01 V s^{-1} and **B** – 0.2 V s^{-1}. The working electrode was the inner platinum band electrode on the microchip and the auxiliary electrode was the high surface area platinum electrode. All potentials were measured against Ag | AgCl | saturated KCl in water reference electrode. Insert of part **A** shows dependence of the corrected current density at 0 V on the concentration of $K_3[Fe(CN)_6]$ at different sweep rates.

and linear diffusion components of mass transfer steps are both important. For our systems, the true steady-state is not reached because within the given timescale, size and geometry of the electrode the linear diffusion contributes to the total flux. In addition, the radial diffusion cannot take place as long the diffusion layer is formed within the cavity [7,33].

The steady-state current density, j_{ss}, of the inlaid micro-disk electrode could be calculated according to Eq. 1.1 [1,5–6]. For the recessed micro-disk electrode, Bond et al. derived Eq. 1.2 [8].

$$j_{ss} = \frac{4nFcDr}{A} \tag{1.1}$$

and

$$j_{ss} = \frac{4\pi nFcDr^2}{A(4L + \pi r)}, \tag{1.2}$$

where n is the number of electrons transferred by electrochemical reaction, F is the Faraday constant (96485 C mol^{-1}), c is the bulk concentration of the reactant, D is the diffusion coefficient of the reactant, r is the radius of the disk, A is the electrode area and L is the depth of the recess region. If the disk radius is constant, then the steady-state current density of the recessed micro-disk electrode should be lower compared with that for the inlaid micro-disk electrode. For both electrode types the steady-state current density does not depend on the sweep rate and should be proportional to the concentration of the reactant. The steady-state current of the inlaid micro-band electrode is expressed as [5]:

$$j_{ss} = \frac{2\pi nFcDl}{A\ln(64Dt/w^2)}, \tag{2}$$

where l is the micro-band length, w is the micro-band width and t is the time being equal to value obtained as RT/Fv, where R is the gas constant (8.314 J mol^{-1} K^{-1}) and T is the temperature (K).

There is no exact solution for recessed micro-band electrode. Berduque et al. [11] carried out measurements using recessed micro-band, micro-square and micro-disk array electrodes with the same recess depth ($L = 0.5$ μm) but different dimensions, and performed comparison of experimental currents with calculated currents. (a) It was found that for recessed micro-square electrodes with dimensions: $w = l = 5 \ldots 50$ μm (and micro-disk electrodes with disk radius: $r = 3$ μm) the recessed disk model (Eq. 1.2) yielded best fit and they concluded that smaller electrodes were affected to the greater extent by the depth of the recess. However, for the larger electrodes there were no significant differences between recessed and inlaid disk electrode data calculated, applying mathematical models (Eq. 1.1 vs. Eq. 1.2), i.e. the L/w ratio was sufficiently small. (b) Thereafter, the steady-state currents for the micro-band electrodes with dimensions: $w = 3 \ldots 50$ μm and $l = 500$ μm were compared with theoretical values using the inlaid micro-band model (Eq. 2). The correlation was very good for wide electrodes, whereas for narrow micro-band electrodes, there was negative deviation. Thus, if the critical dimension of the micro-electrode approaches to the recess depth, then the electrochemical signal is influenced to the greater extent. Said et al. [12] studied the recessed micro-band electrode

arrays and came to the same conclusion. Szakaly et al. [10] modelled the electrochemical behaviour of the recessed micro-band electrode and came to the conclusion that the "recession" effect is significant only if the L/w ratio is high.

However, it should be noted that regardless of the model used, the steady-state current (or pseudo steady-state current in case of the micro-band electrode) is proportional to the reactant concentration.

At very high potential sweep rates, the linear diffusion model applies, and in the reversible system the following equation should describe the behaviour of peak current densities on potential sweep rate [6,34]:

$$j_p = 2.69 \cdot 10^5 n^{3/2} D^{1/2} \nu^{1/2} c. \quad (3)$$

At intermediary sweep rates neither steady-state nor linear diffusion models describe the system.

In this paper, the experimentally measured data were compared with the theoretically calculated data using Eqs. 1–3. The results are presented in Table 1. It was established that the best correlation between experimental and calculated current densities could be achieved with the recessed micro-disk electrode geometry. The current densities are overestimated using the inlaid micro-disk (4 times) and micro-band (50 times) electrode models. This is reasonable result, considering the results of work by Berduque et al. [11], as in our study the electrode has rather rectangular with comparable side lengths but not micro-band shape. The current densities calculated using the semi-infinite linear diffusion model are about ten times higher than the experimental values. Thus, under these experimental conditions applied (electrode dimensions and sweep rate) the true steady-state could not be reached. Therefore it is inevitable to perform digital simulations using the correct geometry of the electrode to get deeper insight (diffusion regime, sweep rate dependence, concentration and current profiles, etc.) about the behaviour of the system under study [6,32–34].

Table 1. Comparison of the experimental pseudo steady-state current density values with current densities calculated applying various models at potential sweep rate 10 mV s^{-1} in the aqueous solution of 1.0 M KCl with different concentrations (additions) of $K_3[Fe(CN)_6]$, c. In all calculations the electrode area, A, is taken constant (0.28 mm^2).

Geometry (dimensions)	Equation	Current	c/M	
			2	12.5
Micro-disk (r = 299 μm)	1.1	j_{ss}/A m^{-2}	−0.63	−3.9
Recessed micro-disk (r = 299 μm, L = 483 μm)	1.2	j_{ss}/A m^{-2}	−0.20	−1.3
Micro-band (l = 700 μm, w = 400 μm)	2	j_{ss}/A m^{-2}	−9.0	−56
Infinite plane (A = 0.28 mm^2)	3	j_{pc}/A m^{-2}	−1.5	−9.3
Experimental data		j_{lim}/A m^{-2}	−0.18	−0.94

r – disk radius, L – recess depth, l – band length, w – band width.

For analytical purposes it is very important that in pseudo steady-state, i.e. at very slow electrode sweep rates ($\nu \leq 0.01$ V s^{-1}), the diffusion limited current density, j_{lim}, depends linearly on the concentration of the $[Fe(CN)_6]^{3-}$ anions (inset in Fig. 5A) and electrode behaves as micro-electrode. The intercept of the j_{lim} vs. c dependency is close to zero at potential scanning rate 10 mV s^{-1}. At higher potential sweep rates, the j_{lim} vs. c dependencies are non-linear (inset in Fig. 5A) as both diffusion regimes are determining the mass transfer of the reactants to the electrode surface.

The data of the EIS measurements are presented in Figs. 6–8. There is no electroreduction of hexacyanoferrate(III) anions at potential 0.8 V and the impedance is mainly determined by the charging of the electrical double layer. At this potential, the shape of Nyquist plots (Fig. 6B) depends very weakly on the concentration of potassium hexacyanoferrate(III) in 1.0 M KCl solution. The phase angle, θ, is about −80° at 10 Hz (Fig. 7B), indicating the mainly adsorption limited process. This conclusion is also confirmed by the dependence of imaginary part of impedance, $\log(-Z'')$, on frequency, $\log f$, which slope is close to −0.9. However, more detailed analysis shows that two linear regions can be observed: low frequency region (f = 10 Hz) and high frequency region (f = 100 kHz) (Fig. 8B).

In good agreement with the $\log(-Z'')$ vs. $\log f$ plots data, Fig. 7B demonstrates, that there are two minima in the θ vs. $\log f$ plots at ac frequencies 10 Hz and 100 kHz. Thus, the adsorption is governed by two processes with different time constants, which differ by four orders of magnitude. The same type of behaviour was observed by Ahuja et al. [35] who studied dependence of the EIS response on the micro-disk radius. At high ac frequencies (f > 100 kHz) the impedance was equal to the solution resistance and proportional to the reciprocal value of radius ($Z = R_{el} \sim r^{-1}$) – region of the primary current distribution. Lowering the frequency down to 10 Hz, the impedance became inversely proportional to the electrode area ($Z \sim r^{-2}$). The primary current distribution reduced the amount of charge carriers at the electrode perimeter, thus, the concentration gradient between the electrode perimeter and the centre was formed. As a consequence, the current would flow between the centre and perimeter of the electrode – generating region of the secondary current distribution.

In the region of low frequencies (f < 10 Hz) at potential 0 V, the shape of the Nyquist plots (Fig. 6A) depends on the concentration of hexacyanoferrate(III) anions. Imaginary, $-Z''$, and real part, Z', of the impedance decrease with the increase of concentration of hexacyanoferrate(III) anions.

In the region of high frequencies (f > 100 kHz) the shape of Nyquist plots and Bode plots (θ vs. $\log f$ and $\log|Z|$ vs. $\log f$ dependencies) does not depend on the electrode potential and concentration of the potassium hexacyanoferrate(III). Thus, it is possible to calculate the electrolyte resistance, R_{el}, between the working electrode

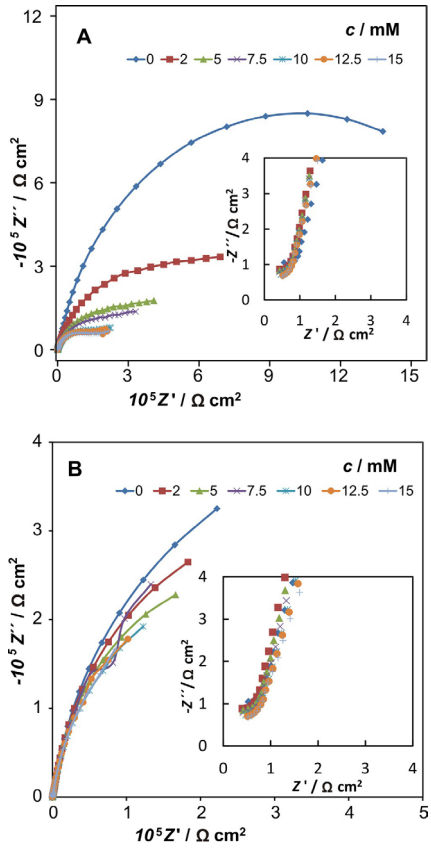

Fig. 6. The dependencies of the imaginary part, Z'', vs. real part, Z', of the impedance in the 1.0 M KCl solution with different additions of $K_3[Fe(CN)_6]$ (noted in figure) at the electrode potentials: **A** – 0 V and **B** – 0.8 V vs. Ag | AgCl | saturated KCl in water.

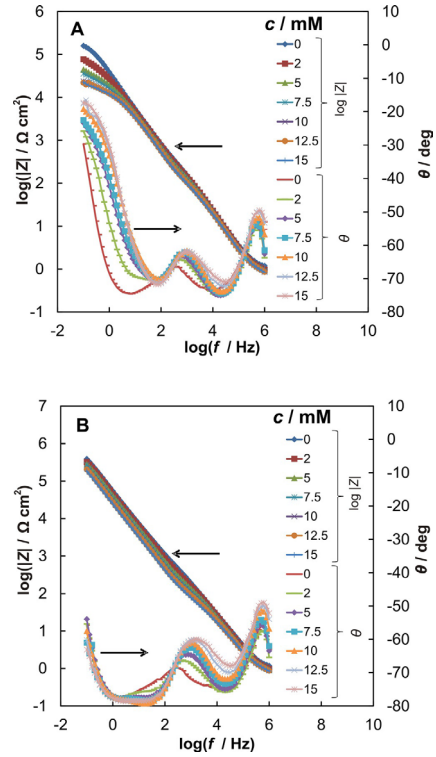

Fig. 7. The dependencies of the magnitude of impedance, $\log|Z|$, and phase angle, θ, on frequency, $\log f$, in the 1.0 M KCl solution with different additions of $K_3[Fe(CN)_6]$ (noted in figure) at the electrode potentials: **A** – 0 V and **B** – 0.8 V vs. Ag | AgCl | saturated KCl in water.

and reference electrode using the extrapolation of the real part of the impedance to infinity ($R_{el} = Z'$ ($f \rightarrow \infty$) = 0.5…0.7 (?) Ω cm^2). The electrolyte resistance calculated is low enough so that the CV measurements are not influenced by the ohmic drop ($jR < 0.2$ mV) and the IR-drop corrections are unimportant. The phase angle values increase with the increase of the concentration of hexacyanoferrate(III) anions (Fig. 7A) from −30° to −20° (at 0.1 Hz) explained by increased rate of the faradaic charge transfer step limited process. This is also accompanied by the decrease of the magnitude of impedance as well as imaginary part of the impedance, $-Z''$, at frequencies less than 10 Hz. Thus, the mixed kinetics faradaic charge transfer and adsorption (or mass transfer) limited steps are determining the electrochemical behaviour of the system under study.

4 Conclusions

In this paper fabrication and electrochemical characterization of the six-channel oxygen sensor-array has been worked out and discussed. The sensor-array has been fabricated of borosilicate wafer containing Pt electrodes and

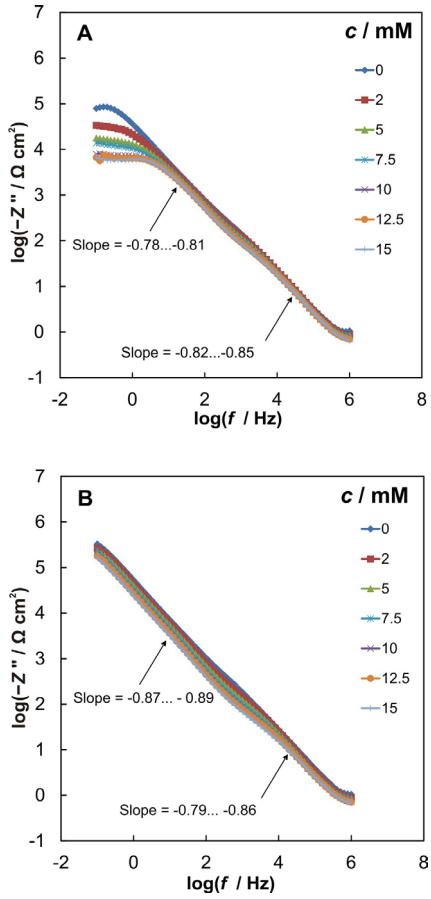

Fig. 8. Dependencies of imaginary part, $-Z''$, on frequency, f, in logarithmic scale in the 1.0 M KCl solution with the different additions of $K_3[Fe(CN)_6]$ (noted in figure) at the electrode potentials: **A** – 0 V and **B** – 0.8 V vs. Ag|AgCl| saturated KCl in water.

connection pads and the silicon wafer with through holes, which were bonded using adhesion bonding method with SU-8. Although the fabrication process of two wafers is simple, the extensively perforated silicon wafer is brittle and can break during bonding step. However, with the customized bonding process, a good bond quality was achieved and all the chips were usable after dicing.

The cyclic voltammetry and electrochemical impedance experiments were carried out in a three-electrode electrochemical system to characterize the prepared sensor-array chips. It was shown that the measured current density depends on the electrode potential sweep rate and both linear and radial diffusion mass transfer components are important at high electrode potential scanning rate. When using slow potential sweep rates ($\nu \leq 0.01\ V s^{-1}$) the pseudo steady-state has been achieved and the electrodes behaved as the micro-electrodes. It was shown that the pseudo steady-state current density depends linearly on the concentration of potassium hexacyanoferrate(III) in the 1.0 M KCl solution. The experimental pseudo steady-state current densities were compared with calculated current densities using different models. The best agreement was established using the model developed by Bond et al. [8] i.e. known as the recessed micro-disk electrode model.

Based on the electrochemical characterisation data it can be concluded that the produced sensor array is suitable for future research including BOD biosensor-array construction. The sensor-array developed can be modified with microorganisms by immobilizing the bacteria into the cavities fabricated onto/into the chip. In future more complex research when modifying the chip, different microbial strains could be used in each cavity, which enables to use this chip as an electronic tongue and thereby, more information could be gathered with one measurement under exactly the same conditions (temperature, pH, etc.).

Acknowledgements

We gratefully acknowledge the support of Estonian Science Foundation (Grant ETF 9136). This research was also supported by the EU through the European Regional Development Fund (Centre of Excellence, 2014-2020.4.01.15-0011) and Institutional Research Grant IUT20-13.

References

[1] K. Aoki, *Electroanalysis* **1993**, *5*, 627–639.
[2] J. Heinze, *Angew. Chem. Int. Ed. Engl.* **1993**, *32*, 1268–1288.
[3] K. Štulík, C. Amatore, K. Holub, V. Mareček, W. Kutner, *Pure Appl. Chem.* **2000**, *72*, 1483–1492
[4] A. M. Bond, *Analyst* **1994**, *119*, 1R–21R.
[5] Israel Rubinstein ed., Christian Amatore, Electrochemistry at Ultramicroelectrodes, in: *Physical Electrochemistry. Principles, Methods and Applications*, Marcel Dekker, Inc., New York, Basel, Hong Kong, **1995**, p. 131.
[6] A. J. Bard, L. R. Faulkner, *Electrochemical Methods: Fundamentals and Applications, 2nd ed*, Wiley & Sons, New York, **2001**.
[7] R. O. Kadara, N. Jenkinson, C. E. Banks, *Sens. Actuators B Chem* **2009**, *142*, 342–346.
[8] A. M. Bond, D. Luscombe, K. B. Oldham, C. G. Zoski, *J. Electroanal. Chem. Interfac.* **1988**, *249*, 1–14.

[9] K. Tokuda, K. Morita, Y. Shimizu, *Anal. Chem.* **1989**, *61*, 1763–1768.
[10] Z. Szakály, L. Daruházi, G. Farsang, *J. Electroanal. Chem. Interfac.* **1991**, *305*, 185–193.
[11] A. Berduque, Y. H. Lanyon, V. Beni, G. Herzog, Y. E. Watson, K. Rodgers, F. Stam, J. Alderman, D. W. M. Arrigan, *Talanta* **2007**, *71*, 1022–1030.
[12] N. A. M. Said, K. Twomey, V. I. Ogurtsov, D. W. M. Arrigan, G. Herzog, *J. Phys. Conf. Ser.* **2011**, *307*, 12052.
[13] E. Witkowska, A. Buczkowska, A. Zamojska, K. W. Szewczyk, P. Ciosek, *Bioelectrochemistry* **2010**, *80*, 87–93.
[14] D. J. Strike, M. G. H. Meijerink, M. Koudelka-Hep, *Fresenius J. Anal. Chem.* **1999**, *364*, 499–505.
[15] R. Solna, E. Dock, A. Christenson, M. Winther-Nielsen, C. Carlsson, J. Emnéus, T. Ruzgas, P. Skladal, *Anal. Chim. Acta B*, *528*, 9–19.
[16] T. Sakaguchi, K. Kitagawa, T. Ando, Y. Murakami, Y. Morita, A. Yamamura, K. Yokoyama, E. Tamiya, *Biosens. Bioelectron. B, 19*, 115–121.
[17] T. Sakaguchi, Y. Morioka, M. Yamasaki, J. Iwanaga, K. Beppu, H. Maeda, Y. Morita, E. Tamiya, *Biosens. Bioelectron.* **2007**, *22*, 1345–1350.
[18] A. Aivasidis, P. Melidis, D. Georgiou, *Bioprocess. Biosyst. Eng.* **2002**, *25*, 29–33.
[19] A. König, T. Reul, C. Harmeling, F. Spener, M. Knoll, C. Zaborosch, *Anal. Chem.* **2000**, *72*, 2022–2028.
[20] M. Raud, T. Kikas, *Water Res.* **2013**, *47*, 2555–2562.
[21] Z. Yang, S. Sasaki, I. Karube, H. Suzuki, *Anal. Chim. Acta* **1997**, *357*, 41–49.
[22] F. Lagarde, N. Jaffrezic-Renault, *Anal. Bioanal. Chem.* **2011**, *400*, 947–964.
[23] S. Heim, I. Schnieder, D. Binz, A. Vogel, U. Bilitewski, *Biosens. Bioelectron.* **1999**, *14*, 187–193.
[24] J. Voldman, M. L. Gray, M. A. Schmidt, *Annu. Rev. Biomed. Eng.* **1999**, *1*, 401–425.
[25] J. Ma, *Displays* **2015**, *37*, 2–10.
[26] H. Ceylan Koydemir, H. Külah, C. Özgen, A. Alp, G. Hasçelik, *Biosens. Bioelectron.* **2011**, *29*, 1–12.
[27] H. Suzuki, *Mater. Sci. Eng.: C* **2000**, *12*, 55–61.
[28] M. A. Alonso-Lomillo, O. Domínguez-Renedo, M. J. Arcos-Martínez, *Talanta* **2010**, *82*, 1629–1636.
[29] D. S. Reuter, A. Bertz, G. Schwenzer, T. Gessner, Vol. 5650, **2005**, pp. 163–171.
[30] F. Scholz, A. M. Bond, *Electroanalytical Methods: Guide to Experiments and Applications: with 100 figures and 31 tables*, Springer Science & Business Media, **2002**.
[31] A. Doménech-Carbó, M. T. Doménech-Carbó, V. Costa, *Electrochemical Methods in Archaeometry, Conservation and Restoration* Springer, **2009**.
[32] R. G. Compton, C. E. Banks, *Understanding Voltammetry, 2nd ed.*, Imperial College Press, London, **2011**.
[33] C. S. Henry, I. Fritsch, *Anal. Chem.* **1999**, *71*, 550–556.
[34] R. G. Compton, E. Laborda, K. R. Ward, *Understanding Voltammetry: Simulation of Electrode Processes*, Imperial College Press, London, **2014**.
[35] A. K. Ahuja, M. R. Behrend, J. J. Whalen, M. S. Humayun, J. D. Weiland, *IEEE Trans. Biomed. Eng.* **2008**, *55*, 1457–1460.

Received: September 1, 2016
Accepted: November 3, 2016
Published online: November 17, 2016

III

ETIS 1.1: **Pitman, K.**; Nerut, J.; Lust, E.; Franssila, S.; Raud, M.; Kikas, T. (2017) Electrooxidation of Hexacyanoferrate(II) Anions and Electroreduction of Oxygen in the Microfabricated Electrochemical Sensor-Array System. *ECS Transactions*, 77 (11), 1771−1782. 10.1149/07711.1771ecst.

ECS Transactions, 77 (11) 1771-1782 (2017)
10.1149/07711.1771ecst ©The Electrochemical Society

Electrooxidation of Hexacyanoferrate(II) Anions and Electroreduction of Oxygen in the Microfabricated Electrochemical Sensor-Array System

K. Pitman[a], J. Nerut[b], E. Lust [b], S. Franssila[c], M. Raud[a], and T. Kikas[a]
[a] Institute of Technology, Estonian University of Life Sciences, Fr.R.Kreutzwaldi 56/1, Tartu 51014, Estonia
[b] Institute of Chemistry, University of Tartu, Ravila 14a, Tartu 50411, Estonia
[c] Aalto University, Otakaari 1 B, Espoo 02150, Finland

The microfabrication technique was used to prepare a six-channel sensor-array chip. The sensor-array has been fabricated using borosilicate wafer containing Pt electrodes and connection pads and the silicon wafer with through holes, which were bonded with SU-8 using adhesion bonding method. To characterize the prepared sensor-array chips the cyclic voltammetry and electrochemical impedance experiments were carried out in a three-electrode electrochemical system. The electrooxidation of ferrocyanide and electroreduction of oxygen were studied. It was shown that the measured current density depends on the electrode potential sweep rate however, both linear and radial diffusion mass transfer components are important at high electrode potential scanning rate. The pseudo steady-state conditions were achieved at slow potential sweep rates (>0.01 V s^{-1}) and the electrodes behaved as the microelectrodes. The pseudo steady-state current density is proportional to the concentration of electroactive species. The recessed microdisc electrode model has been used to describe the system.

Introduction

The field of application of microelectrodes is very wide: from electroanalytical applications (detection of ultra-low quantities of analyte, biosensors, etc.), kinetic studies of very fast and complex reactions, to measurements in solutions of very low conductivity, etc. (1–3). Microelectrodes are very useful for electrochemical sensing in large part because it is possible to achieve (pseudo) steady-state quite quickly compared with larger electrodes (3,4). The microelectrodes could be made of different materials and the geometry of the electrode is limited only by the fantasy and the aim of user. Recessed microelectrodes are used for analytical purposes, e.g. for liquid chromatography (5). Often several microelectrodes are combined into sensor-arrays for simultaneous analysis of various components and kinetic parameters.

Many methods for microelectrode preparation have been proposed however, most of the array electrodes are normally fabricated using microphotolithography and screen-printing (6). Microfabrication is a high precision fabrication technology, which is suitable for preparing microelectrodes. It is based on deposition, lithography and etching steps using materials like silicon, polymers, metals and oxides that enable the fabrication of wells, reactors, channels, and electrodes with dimensions in the micrometer to millimeter

range. Microfabrication technology also enables batch-fabrication, which leads to production of inexpensive sensors and even, disposable, maintenance-free sensors (7).

Microelectrode arrays present an opportunity for the integration in 'lab-on-a-chip' devices, which can be used in a plethora of applications (8). Electrochemical microsensors and sensor-arrays enable to develop inexpensive, on-site and real time analytical methods for measuring various pollutants (9). Environmental monitoring and analysis is widely used field for application of sensor-arrays in samples such as drinking, ground, sea and industrial waters where reliable and robust analytical techniques with low detection limits are required (6). In addition, it has been shown that by applying various multidimensional data analysis methods to sensor-array data it is possible to extract more information from measurement data (7,10).

The previous paper was mainly dedicated to the fabrication of six-channel sensor-array chip (1). The chip was prepared using microfabrication technology and based on silicon and glass wafers and platinum electrodes. The sensor-array chip was designed for the future use for dissolved oxygen measurements in a biochemical oxygen demand (BOD) sensor array.

The aim of this work is to study the electro-oxidation of hexacyanoferrate(II) anions on the platinum microelectrode of the sensor-array in the 1.0 M KCl aqueous solution and use the same sensor-array for determination of oxygen concentration in the 0.5 M H_2SO_4 solution.

Experimental

The preparation of the sensor array microchips is described in our previous paper in detail (11). Shortly for fabrication silicon wafers (100 mm diameter and thickness of 500–525 μm) and borosilicate wafers (Pyrex glass with same dimensions as silicon wafers) were used. Chromium/platinum (10 nm/100 nm thick) were sputtered on a borosilicate wafer and patterned by wet etching method using *aqua regia* (3:1 HCl :HNO_3 24°C, 4 min) and chromium etchant (solution of Ceric Ammonium Nitrate, 248, 10 sec). Silicon wafer was etched through using hot TMAH (tetramethylammonium hydroxide) solution and RIE (reactive ion etching) to form holes with slanting sidewalls for immobilization cavities. The hole depth, L, was 483 μm. The processed silicon and Pyrex wafers were bonded using adhesive bonding with SU-8 epoxy resin. The individual sensor-array chips were separated by dicing. The rectangular platinum working electrode with dimensions 700×400 μm were deposited in the center of the cavity.

The potentiostat Reference 600 (Gamry Instruments Inc) was used for cyclic voltammetry (CV) and electrochemical impedance (EIS) measurements. In the three-electrode configuration the working electrode was inner platinum band electrode, the counter electrode was a large Pt wire mesh separated from the working electrode compartment by a fritted glass membrane. The reference electrode was Ag|AgCl| aqueous saturated KCl (3). The CV data at fixed potentials: 0.0 and 0.7 V were measured at different potential sweep rates, v, from 5 to 1000 mV s^{-1}. The EIS data were obtained within ac frequencies, f, from 100 mHz to 0.1 MHz (12 points per decade) with 5 mV (rms) ac voltage amplitude. The glassware was treated with the hot (80 °C) concentrated

sulfuric acid (95.0-98.0%, Sigma-Aldrich, puriss. p.a.) with small addition of hydrogen peroxide (30%, Merck KGaA, Perhydrol® for analysis) and rinsed carefully with Milli-Q+ (18.2 MΩ cm) water. All solutions were prepared using Milli-Q+ water.

Potassium ferrocyanide ($K_4[Fe(CN)_6]$) (chemically pure) was purchased from Реахим. Potassium chloride (KCl) (assay 100.0%) was purchased from Lach-Ner (Czech Republic). All the solutions were prepared from Milli-Q^+ water. The concentration of potassium chloride was kept constant (1.0 M) and the concentration of potassium ferrocyanide was varied between 0.5 mM and 6 mM. Prior to the measurements, the solutions were deoxygenated with argon (99.9999%, AGA) during 15 minutes.

The oxygen reduction was studied in the 0.5 M H_2SO_4 solution at different partial pressures of oxygen. The 0.5 M H_2SO_4 solution was prepared from the concentrated sulfuric acid solution (≥ 95%, Fluka Analytical, TraceSELECT®, for trace analysis). Before measurements the electrolyte solution was saturated with argon or with mixture of argon and oxygen (99.999%, AGA) during 15 minutes. The partial pressure of oxygen in the mixture of gases was varied from 0 kPa up to 98 kPa with five fixed compositions. The total pressure of gas was 101 kPa. The Brokhorst® mass flow controllers (EL-FLOW Select®) were used to prepare the gas mixtures.

The experiments were performed at room temperature (22±1°C). Three microchips were used. Parallel experiments were conducted and the data were statistically treated. It was found that different microelectrodes were electrochemically active and the reproducibility of EIS parameters and (pseudo) steady-state current densities was good. Within one measurement the time stability of cyclic voltammograms and EIS data was very good.

Results and Discussion

Purification and activation of the sensor-array

It was necessary to clean the platinum electrodes of the sensor-array before the measurements. Without the cleaning step it was impossible to get the electrical contact, i.e. the Pt electrode was covered with isolating film or the shape of the cyclic voltammogramm in the sulfuric acid deviated considerably from the usual behaviour (3,12). The cleaning step consisted of two phases.

Firstly, the sensor-array was sonicated (Bandelin electronic RK 52 H, 60 W, 35 kHz) for 10 min in the acetone (>95%, APC Chemicals). After the sonication, the acetone was poured away and the array was dried in air. This procedure was performed only once with each chip. Continuous treatment with acetone led to decomposition of the sensor-array and the lower part of the array separated from the upper part.

Secondly, the array was cleaned in the hot (50 °C) concentrated sulfuric acid with small addition of hydrogen peroxide (30 wt%). The array was heated up in the sulfuric acid and left to stand overnight. Next morning the array was rinsed with Milli-Q^+ water. Thereafter the array was treated in boiling water from three to five times. Between the

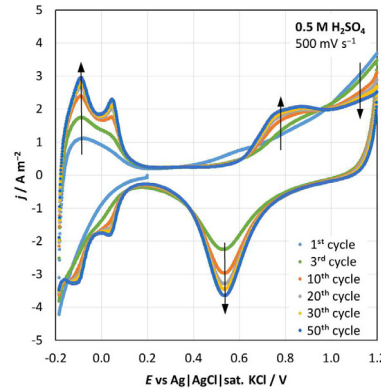

Figure 1. The electrochemical activation of platinum working electrode in the 0.5 M H_2SO_4 solution. The potential sweep rate was 500 mV s^{-1} (50 cycles). The increase of cycle number is indicated with arrows.

boiling steps the array was rinsed with Milli-Q^+ water. The same cleaning method was applied before each measurement.

After the cleaning of the array, the platinum electrodes were electrochemically activated in the 0.5 M H_2SO_4 solution (12). The electrode potential was swept between −0.18 V and 1.20 V 50-100 times (500 mV s^{-1}). The activation process is illustrated in Fig. 1. During the activation process, the current density $|j|$ increased in the region of hydrogen adsorption and desorption (from −0.18 V to 0.20 V), and platinum oxidation and reduction (from 0.40 V to 1.20 V) regions. The cycling was performed until the cyclic voltammogramm was invariant within mentioned potential region. The experiments were performed only with the electrodes that had good electric contact and showed similar characteristics in the 0.5 M sulfuric acid solution.

Electrochemical Experiments

Cyclic voltammetry in 1 M KCl and 0.5 M H_2SO_4 solutions. All sensor-array chip electrodes were characterised in the 0.5 M H_2SO_4 solution and in the 1 M KCl solution. The cyclic voltammograms are presented in Fig. 2. The current density is proportional to the sweep rate (inset in Fig. 2a) i.e. the mainly capacitive processes are taking place at the Pt | 1 M KCl interface. There is slight increase of current density $|j|$ at potentials more negative than −0.05 V that could be caused by the slow hydrogen evolution. At potential more positive than 0.60 V, the increase of current density might be induced by the oxidation of the platinum surface i.e. formation of the oxide layer.

For the sulfuric acid solution, the cyclic voltammetry data (Fig. 2b) are presented as capacitance, C, vs. potential. The capacitance is calculated using equation $C = j/v$. The shape of curves for the Pt | 0.5 M H_2SO_4 interface at different potential sweep rates is typical for polycrystalline platinum (12,13). The hydrogen adsorption/desorption region (below 0.15 V) is very well defined. At potentials more positive than 0.60 V (anodic

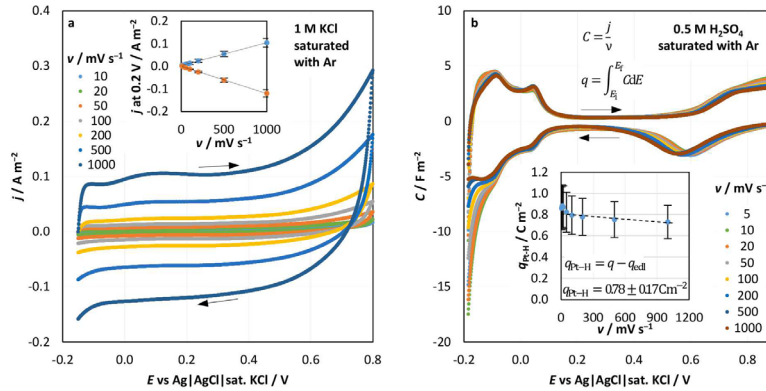

Figure 2. (a) The cyclic voltammogramm of the Pt microchip electrode measured in the 1 M KCl solution and (b) the capacitance, C, vs. electrode potential, E, curves in the 0.5 M H_2SO_4 solution saturated with argon at different potential sweep rates, v (indicated in figure). Inset in part (a): current density vs. v curves at 0.2 V for cathodic and anodic scans and in part (b): calculated charge of adsorbed hydrogen on the Pt electrode, $q_{\text{Pt-H}}$, vs. v dependences.

scan) the surface oxides are formed which are reduced during cathodic scan. Between these two regions, there is so-called electrical double layer (edl) area within this region. The capacitance is almost independent of potential sweep rate expect for lowest sweep rates at potentials more negative −0.10 V. The increase in capacitance is caused by the start of hydrogen evolution at platinum electrode in acid solution.

The real (or working) surface area of platinum electrode, A_{EL}, has been calculated using method in Refs (12,14–16). The area under the hydrogen adsorption-desorption peaks was integrated to get the total charge, q. The charge, q_{edl}, consumed for charging and discharging of the edl in the region of the peaks was estimated from the edl capacitance at 0.2 V and it was assumed to be the same in the region of peaks. The edl charge was subtracted from the total charge to obtain the charge, $q_{\text{Pt-H}}$, used for the formation of the monolayer of adsorbed hydrogen atoms Pt-H on the surface of platinum. T. Biegler et al. (17) evaluated that the charge required to adsorb/desorb a monolayer of hydrogen atoms on the smooth polycrystalline Pt electrode is equal to 2.1 C m^{-2}.Using this approximation, it is possible to estimate the real surface area of the platinum electrode as (14):

$$A_{\text{EL}} = \frac{q_{\text{Pt-H}}}{2.1\ \text{C m}^{-2}} S\,, \qquad [1]$$

where S is the geometric area of the electrode. The results of the calculations of $q_{\text{Pt-H}}$ are presented as inset in Fig. 2b. At slow sweep rates the charge is about 13% higher compared to the value at higher sweep rates. This is caused by the hydrogen evolution

and these sweep rates are left out from the analysis. The real surface area of the platinum electrode were estimated as 0.104±0.023 mm^2.

In further analysis, the current densities measured in the base electrolytes were subtracted from the current densities measured in the solution containing also $K_4[Fe(CN)_6]$ or oxygen to get the current density of the electrode reaction, j_c.

Electrooxidation of ferrocyanide. In the first set of experiments, the ferricyanide/ferrocyanide redox couple was used to test the electrochemical behaviour of the sensor-array chip. The data of the CV measurements are presented in Fig. 3. The oxidation of $[Fe(CN)_6]^{4-}$-anions starts at 0.22 V:

$$[Fe(CN)_6]^{4-} = [Fe(CN)_6]^{3-} + e^-, \quad [2]$$

which is in the region of the formal reduction potential of the $[Fe(CN)_6]^{3-}/[Fe(CN)_6]^{4-}$ redox couple in 1 M KCl ($E^{0'}$ = 0.286 V vs. Ag|AgCl|sat. KCl (18,19)). Clear diffusion limited current plateaus were reached for low concentrations of $[Fe(CN)_6]^{4-}$ anions ($c \leq 3$ mM). However, for highest concentrations clear diffusion limited current plateaus were not achieved. There is no reduction peak of the $[Fe(CN)_6]^{3-}$ anions formed at the surface in the reverse scan (Fig. 3a) (even at the highest sweep rate) indicating that the contribution of the radial diffusion is dominant in the system under study. Although complete stationarity is not achieved as, there is hysteresis between cathodic and anodic scans. The extent of hysteresis is somewhat more pronounced at highest sweep rate although the oxidation peak is not formed. The hysteresis also increases with increasing concentration of ferrocyanide.

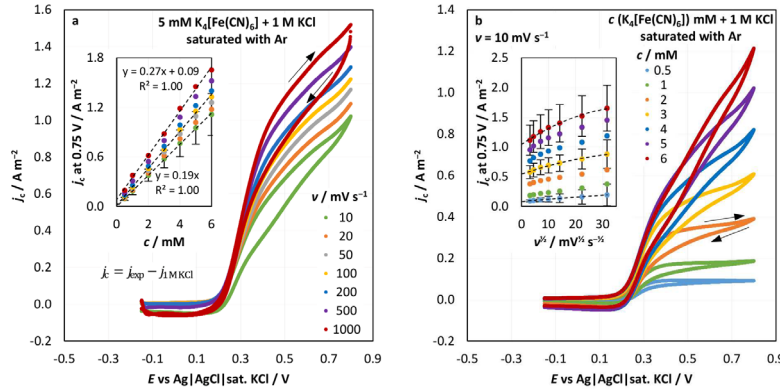

Figure 3. The dependence of the corrected current density, j_c, on the electrode potential, E, (a) at different electrode potential sweep rates, v, (noted in figure) for the 1.0 M KCl + 5 mM $K_4[Fe(CN)_6]$ solution saturated with argon and (b) in the 1.0 M KCl solution saturated with argon with different additions of $K_4[Fe(CN)_6]$ (noted in figure) at $v = 0.01$ V s^{-1}. Inset in part (a): j_c vs. $c(K_4[Fe(CN)_6])$ for different sweep rates and in part (b): j_c vs. v for different additions of $K_4[Fe(CN)_6]$ at 0.75 V.

Inset of Fig. 3a shows at 0.75 V linear dependence of the corrected current density on the concentration of $K_4[Fe(CN)_6]$ at all sweep rates. These dependences are linear at all sweep rates and the intercept is zero in agreement with that expected for the first order reaction. At higher concentrations of ferrocyanide $c > 6$ mM, there is negative deviation from the linearity.

The peak current vs. $v^{½}$ dependencies are expected be to be linear for reactions where the semi-infinite linear diffusion at planar electrode takes place (3). At constant concentration of the $[Fe(CN)_6]^{4-}$ anions, dependences of j_c (at 0.75 V) on $v^{½}$ are non-linear, the ordinates differ from zero and depend systematically on the reactant concentration (inset in Fig. 3b). Thus, the mass transport is dominated by the radial component of diffusion and the electrodes behave as microelectrodes. In these conditions the recessed microdisk electrode model developed by A.M. Bond et al. (20) describes the behavior of experimental current density. The stationary current density, j_{ss}, could be calculated using equation:

$$j_{ss} = \frac{4\pi nFcDr^2}{S(4L + \pi r)}, \quad [3]$$

where n is the number of electrons transferred in electrode reaction, F is the Faraday constant (96485 C mol^{-1}), c is the bulk concentration of the reactant, D is the diffusion coefficient of the reactant and r is the radius of the disk. The theoretical slope of j_{ss} vs. c in these conditions is 0.11 A m^{-2} mM^{-1} if $n = 1$, $D([Fe(CN)_6]^{4-}) = 8.07 \cdot 10^{-6}$ cm^2 s^{-1} (in 1 M KCl) (19) and r is calculated from the surface area of the electrode. The experimental current densities at 0.75 V were extrapolated to sweep rate $v = 0$ and used to calculate the experimental slope in same conditions. The experimental value 0.16 A m^{-2} mM^{-1} is in relatively good agreement with the theoretical calculated value. The slope value is greatly overestimated with models using other geometries (10 mV s^{-1}): microdisk (5 times), microband (50 times), and infinite plane (6 times) and therefore these models cannot be used (11).

Electroreduction of oxygen. The sensitivity of the microchip array was also tested towards oxygen reduction (Fig. 4). The oxygen reduction reaction on the platinum electrode is irreversible and the four-electron process prevails in acid solution (21):

$$O_2 + 4H^+ + 4e^- = 2H_2O \quad [4]$$

As the oxygen electroreduction on the platinum electrode is irreversible, there is no anodic peak during the reverse scan. The hysteresis between anodic and cathodic scans is very small (Fig. 4b) and the clear limiting current plateaus have been achieved, compared with ferrocyanide. At potentials more negative than −0.1 V, the corrected current densities $|j_c|$ started to decrease because the two electron reduction pathway becomes also important and hydrogen peroxide is additionally formed on the electrode (21,22):

$$O_2 + 2H^+ + 2e^- = H_2O_2. \quad [5]$$

The limiting current density is proportional to partial pressure of oxygen at all sweep rates used (inset in Fig. 4a) and the intercept is very close to zero. As in case of ferrocyanide, the corrected current density at 0 V is not proportional to $v^{½}$ (inset in

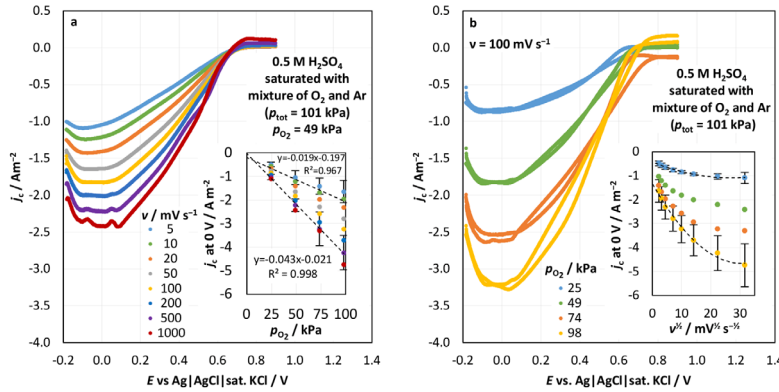

Figure 4. The dependence of the corrected current density, j_c, on the electrode potential, E, for the 0.5 M H_2SO_4 solution saturated with mixture of argon and oxygen (p_{tot} = 101 kPa) (a) at different electrode potential sweep rates, v, (noted in figure) with oxygen partial pressure p_{O_2} = 49 kPa and (b) at different partial pressures of oxygen at v = 0.1 V s^{-1}. Inset in part (a): j_c vs. p_{O_2} for different sweep rates and in part (b): j_c vs. v for different p_{O_2} at 0 V.

Fig. 3b). The propagation of the diffusion layer, δ, in time, t, could be described by simple formula (3,4):

$$\delta = \sqrt{\pi D t} \ . \qquad [6]$$

In case of oxygen reduction, the diffusion layer thickness becomes comparable with the critical dimension of the electrode more quickly and the radial diffusion becomes more important than linear diffusion at higher sweep rate as the diffusion coefficient of oxygen $D(O_2) = 18 \cdot 10^{-6}$ cm^2 s^{-1} (in 0.5 M H_2SO_4) (13) is more than two times higher compared to ferrocyanide. The diffusion limited current density $|j_c|$ for solution saturated with oxygen ($c(O_2)$ = 1.13 mM in 0.5 M H_2SO_4 (13,23)) is 10 times higher if v = 10 mV s^{-1} and 13 times higher at v = 1000 mV s^{-1} higher compared to j_c at 0.75 V in 1 mM $K_4[Fe(CN)_6]$. This could be explained using Eq. 3: the difference in the factor nDc for oxygen and ferrocyanide is ten times. As at slower sweep rate the system is closer to pseudo steady-state, the agreement is also better. The theoretical and experimental slope values of j_c (at 0.1 V) vs. c dependencies are −0.97 and −1.18 A m^{-2} mM^{-1}, respectively. The consistency is reasonable, although for both substances the theoretical values are underestimated. The oxygen reduction process conditions are closer to the pseudo steady-state mode as the diffusion coefficient of oxygen is higher. To get better understanding of the system behavior the simulation should be performed using the right geometry of the working electrode (24).

Electrochemical impedance spectroscopy measurements. The data of the EIS measurements in 1 M KCl solution without and with addition of ferrocyanide are

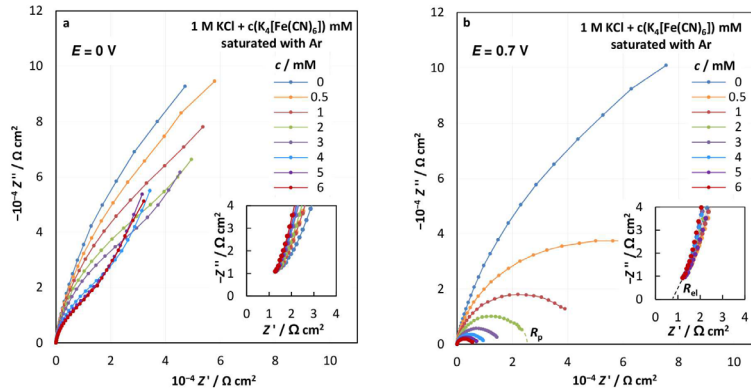

Figure 5. The dependencies of the imaginary part, Z'', vs. real part, Z', of the impedance in the 1.0 M KCl solution with different additions of $K_4[Fe(CN)_6]$ (noted in figure) at the electrode potentials: (a) 0 V and (b) 0.7 V.

presented in Figs. 5-6. The shape of Nyquist plots (Fig. 5) depends on the electrode potential and concentration of the potassium ferrocyanide in 1.0 M KCl solution. The electrolyte resistance, R_{el}, (between the reference electrode and working electrode) is calculated from the extrapolation of real part of impedance to infinity ($R_{el} = Z'(f \rightarrow \infty)$). The electrolyte resistance is equal to 0.9 Ω cm^2 and is independent of potential and concentration of electroactive species (insets in Fig. 5). There are two minima in the θ vs. log f plots at ac frequencies 10 Hz and 10 kHz (Fig. 6), respectively. Two processes with different time constants, which differ by three orders of magnitude, govern the adsorption. A. K. Ahuja et al. (25) also observed two minima in the Bode phase angle plot and the deepening of high frequency minimum becomes with decreasing of the radius of microdisk electrode in the surface inactive electrolyte. The appearance of the high frequency minimum was explained by the step-by-step replacement of "solution resistance regime" with "the area driven capacitive regime" i.e. the RC time constant decreases (25). There are also two linear areas with the same slope in the Bode magnitude plot in 1 M KCl (Fig. 6a) – the transition region is between 100 and 1000 Hz. The appearance of the low frequency maximum could be explained by the increase of relative importance of the secondary current distribution at lower frequencies (25).

After addition of the ferrocyanide to the 1 M KCl solution, the Nyquist and Bode plots do not change remarkably at 0 V (Figs 5a and 6a) as at this potential ferrocyanide does not oxidize (Fig. 3). Some changes in the impedance could be explained by the alternation of the edl capacitance induced by the adsorption of ferrocyanide. The situation is different at 0.7 V. The depressed semicircle is formed as the concentration of the ferrocyanide in the solution increases (Fig. 5a). The Bode plot reveals that at low frequencies ($f < 100$ Hz) the phase angle $-\phi$ and the impedance Z decreases with the increasing concentration of ferrocyanide. The apparent polarization resistance, R_p, could be calculated from the extrapolation of the real part of the impedance to zero frequency ($R_p = Z'(f \rightarrow 0)$). The apparent polarization resistance at 0.7 V (inset in Fig. 6b) decreases

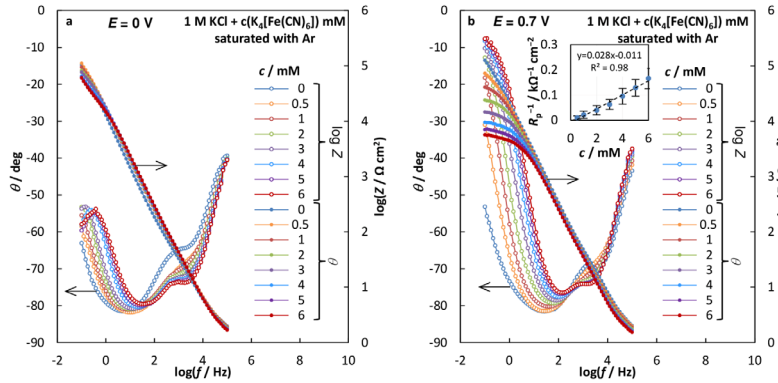

Figure 6. The dependencies of the magnitude of impedance, log Z, and phase angle, θ, on frequency, log f, in the 1.0 M KCl solution with different additions of $K_4[Fe(CN)_6]$ (noted in figure) at the electrode potentials: (a) 0 V and (b) 0.7 V. Inset in part (b): the reciprocal value of polarization resistance R_p^{-1} vs. $c(K_4[Fe(CN)_6])$ at 0.7 V.

with increasing of the concentration of ferrocyanide. The R_p^{-1} vs. $c(K_4[Fe(CN)_6])$ dependence is linear as the j_c (at 0.7 V) vs. $c(K_4[Fe(CN)_6])$ dependences, however the EIS data are measured in stationary state. The interpretation of EIS data at 0.7 V using physical models is challenging task. The mixed charge transfer kinetics: faradaic charge transfer, mass transfer and adsorption limited steps are determining the electrochemical behavior of the system under study. A. Lasia (26) modelled semi-infinite external spherical diffusion and found that, contrary to the semi-infinite linear diffusion, where the Warburg impedance approaches infinity as $f \rightarrow 0$, in the case of spherical diffusion the impedance goes to a real constant as $f \rightarrow 0$. This means that the current passes in the system as it occurs for microelectrodes in stationary state.

Summary

The sensor-array has been fabricated using borosilicate wafer containing Pt electrodes and connection pads and the silicon wafer with through holes, which were bonded with SU-8using adhesion bonding method.

The sensor-array was sensitive towards ferrocyanide and oxygen. The calibration graphics were linear for both reactants (oxygen and ferrocyanide) used.

It was shown that the measured current density depends on the electrode potential sweep rate and both linear and radial diffusion mass transfer components are important at high electrode potential scan rates. For slow potential sweep rates ($v \leq 0.01$ V s^{-1}) the pseudo steady-state has been achieved and the electrodes behaved as the microelectrodes. The recessed microdisk model worked out by Bond et al. was used to describe the behavior of pseudo steady-state current densities. The consistency of theory with experiment was very good for oxygen electroreduction because the pseudo-steady state

was achieved more readily for this system at slow sweep rates. For ferrocyanide oxidation slower sweep rates have to be used to accomplish better agreement.

The EIS was used to describe the system performance in 1 M KCl solution with and without addition of ferrocyanide. For the system with addition of ferrocyanide the depressed semicircle was formed in the Nyquist plot in the region of diffusion limited current densities. The polarization resistance decreased systematically with increasing concentration of ferrocyanide.

Based on the electrochemical characterization data collected, it can be concluded that the produced sensor array is suitable for future research including BOD biosensor-array construction.

Acknowledgments

This research was supported by the EU through the European Regional Development Fund (Centre of Excellence, 2014-2020.4.01.15-0011) and Institutional Research Grant IUT20-13. We also gratefully acknowledge the support of Estonian University of Life Sciences (base financed project P170025). K. Pitman would like to thank the European Regional Development Fund and Archimedes Foundation for travel grant.

References

1. J. Heinze, *Angew. Chem. Int. Ed. Engl.*, **32**, 1268 (1993).
2. A. M. Bond, *Analyst*, **119**, 1R (1994).
3. A. J. Bard and L. R. Faulkner, *Electrochemical Methods: Fundamentals and Applications*, 2nd ed., p. 864, Wiley & Sons, New York, (2001).
4. K. Štulík, C. Amatore, K. Holub, V. Mareček, and W. Kutner, *Pure Appl. Chem.*, **72**, 1483 (2000).
5. Z. Szakály, L. Daruházi, and G. Farsang, *J. Electroanal. Chem. Interfacial Electrochem.*, **305**, 185 (1991).
6. X. Xie, D. Stueben, and Z. Berner, *Anal. Lett.*, **38**, 2281 (2005).
7. K. Pitman, M. Raud, and T. Kikas, *Agron. Res.*, **13**, 382 (2015).
8. F. Tan, J. P. Metters, and C. E. Banks, *Sens. Actuators B Chem.*, **181**, 454 (2013).
9. F. Davis and S. P. J. Higson, *Environ. Sci. Process. Impacts*, **15**, 1477 (2013).
10. M. Raud and T. Kikas, *Water Res.*, **47**, 2555 (2013).
11. K. Pitman, M. Raud, G. Scotti, V. P. Jokinen, S. Franssila, J. Nerut, E. Lust, and T. Kikas, *Electroanalysis*, **29**, 249 (2017).
12. K. Shinozaki, J. W. Zack, R. M. Richards, B. S. Pivovar, and S. S. Kocha, *J. Electrochem. Soc.*, **162**, F1144 (2015).
13. S. Gottesfeld, I. D. Raistrick, and S. Srinivasan, *J. Electrochem. Soc.*, **134**, 1455 (1987).
14. S. Trasatti and O. A. Petrii, *J. Electroanal. Chem.*, **327**, 353 (1992).
15. A. Pozio, M. De Francesco, A. Cemmi, F. Cardellini, and L. Giorgi, *J. Power Sources*, **105**, 13 (2002).
16. F. J. Nores-Pondal, I. M. J. Vilella, H. Troiani, M. Granada, S. R. de Miguel, O. A. Scelza, and H. R. Corti, *Int. J. Hydrog. Energy*, **34**, 8193 (2009).
17. T. Biegler, D. A. J. Rand, and R. Woods, *J. Electroanal. Chem. Interfacial Electrochem.*, **29**, 269 (1971).

18. P. Kulesza, T. Jędral, and Z. Galus, *J. Electroanal. Chem. Interfacial Electrochem.*, **109**, 141 (1980).
19. E. Tourwé, T. Breugelmans, R. Pintelon, and A. Hubin, *J. Electroanal. Chem.*, **609**, 1 (2007).
20. A. M. Bond, D. Luscombe, K. B. Oldham, and C. G. Zoski, *J. Electroanal. Chem. Interfacial Electrochem.*, **249**, 1 (1988).
21. C. Song and J. Zhang, in *PEM Fuel Cell Electrocatalysts and Catalyst Layers*, J. Zhang, Editor, p. 89, Springer, London (2008).
22. N. M. Marković, H. A. Gasteiger, and P. N. Ross, *J. Phys. Chem.*, **99**, 3411 (1995).
23. K. E. Gubbins and R. D. Walker, *J. Electrochem. Soc.*, **112**, 469 (1965).
24. R. G. Compton, E. Laborda, and K. R. Ward, *Understanding voltammetry: Simulation of electrode processes*, p. 260, Imperial College Press, London, (2014).
25. A. K. Ahuja, M. R. Behrend, J. J. Whalen, M. S. Humayun, and J. D. Weiland, *IEEE Trans. Biomed. Eng.*, **55**, 1457 (2008).
26. A. Lasia, *Electrochemical Impedance Spectroscopy and its Applications*, p. 368, Springe, New York, Heidelberg, Dordrecht, London, (2014).

IV

ETIS 1.1: **Pitman, K.**; Nerut, J.; Raud, M.; Kikas, T. (2020) Characterisation of Electrochemical Sensor-array for Utilisation in Construction of BOD Bioelectronic Tongue. *Environmental and Climate Technologies* 24 (3), 39-54. 10.2478/rtuect-2020-0084.

Environmental and Climate Technologies
2020, vol. 24, no. 3, pp. 39–54
https://doi.org/10.2478/rtuect-2020-0084
https://content.sciendo.com

Characterisation of Electrochemical Sensor-Array for Utilisation in Construction of BOD Bioelectronic Tongue

Kätlin PITMAN[1]*, Jaak NERUT[2], Merlin RAUD[3], Timo KIKAS[4]

[1,3,4]*Institute of Technology, Estonian University of Life Sciences, Fr.R.Kreutzwaldi 56/1, Tartu 51014, Estonia*

[2]*Institute of Chemistry, University of Tartu, Ravila 14a, Tartu 50411, Estonia*

***Abstract* – There is need to rapidly measure biochemical oxygen demand (BOD) to estimate organic pollution in wastewater. Biosensors are able to estimate BOD values within 5–30 minutes, but they have some limitations that can be overcome with biosensor-array. This work used sensor-array, which consists of 8 × 3 electrodes. The working electrode was inner Pt circle electrode, counter electrode was a Pt band electrode and the reference electrode was a silver wire. The potentiostat was used to record cyclic voltammetry and chronoamperometry. The pumping speed was set at 1.5 cm^3 min^{-1} or higher, to avoid the interference. Next, sensor-array was tested to measure different oxygen amounts and calibrated accordingly. Lastly, *Pseudomonas putida* membranes were calibrated and used to estimate BOD value. The calibration gave linear range up to 85 mg L^{-1} of BOD and sensitivity from 0.0018 to 0.0068. Real industrial wastewater, from lignocellulosic bioethanol production, was used to test the biosensor-array. It underestimated BOD values from 8 to 37 %. This biosensor-array allows to measure BOD value in less than 15 minutes.**

***Keywords* – Biochemical oxygen demand; biosensor; BOD; BOD sensor-array**

1. INTRODUCTION

Worldwide, more than 310 km^3 of municipal wastewater was produced in year 2010 [1]. In addition, wastewater is also generated in industries [2]. Before releasing it to nature, wastewater needs to be cleaned. In order to assure the quality of the cleaning process, the wastewater to be released also needs to be tested. One of the most important parameters in wastewater quality is biochemical oxygen demand (BOD). BOD is defined as an amount of oxygen required to biooxidize organic compounds in the water [3]. We have described traditional standard BOD test and BOD sensors in earlier work [4], [5]. The BOD traditional test takes at least 5 days of incubation at 20 °C in dark [6]–[8], which makes it of little use in cases where fast feedback is required [9].

Biosensors however, shorten the measuring time to 5–30 minutes [10], [11]. Most BOD biosensors are based on microorganisms that are immobilised on a Clark type oxygen sensor [12]. These sensors measure the change in microbial respiration rate due to the presence of organic compounds [3]. This change in respiration is proportional to the concentration of organic substrate in the solution [13]. However, the BOD values measured

* Corresponding author.
E-mail address: katlin.pitman@student.emu.ee

with biosensors are often not identical to those measured using conventional method. This is due to the fact that during the short measurement time of BOD sensor only substrates that are quickly biodegradable contribute to the signal [14]. Although many bacteria can degrade wide range of substrates, the substrate range assimilable to a single culture is limited. While mixed cultures can cover wider substrate range, the stability of such mixed cultures is low, which makes their utilisation in analytical systems problematic. One solution to these problems could be using spatially separated microorganisms on an oxygen sensor array [4]. Selection of different microorganisms ensures better agreement between sensor BOD and BOD_7, and spatial separation ensures stability and longer lifetime of the microorganisms.

Purpose of this work was to examine if *DropSens 550* screen-printed electrochemical array could be used as a base sensor for a biosensor array to measure BOD. The flow through cell was designed for the measurements. Cyclic voltammetry (CV) and chronoamperometry (CA) were used to study the oxygen reduction reaction (ORR) on the electrochemical array. The measurement conditions were optimized to achieve reliable results.

2. MATERIALS AND METHODS

2.1. Chemicals

Potassium chloride (KCl) (Cas 7447-40-7) (assay 100.0 %) was purchased from *Lach-Ner* (Czech Republic). The concentration of potassium chloride was kept constant (0.1 M). Solution was prepared using Milli-Q^+ water (18.2 MΩ cm). Agarose type I-A Low EEO (Cas 9012-36-6) was purchased from *Sigma-Aldrich* (Spain).

Prior to the measurements, the solution was saturated with oxygen (99.999 %, AGA) or nitrogen (99.999 %, AGA) mixture during 30 minutes. The partial pressure of oxygen in the mixture of gases was varied from 0 kPa up to 98 kPa: 14 compositions. The total pressure of gas was 101 kPa. The *Brokhorst*® mass flow controllers (*EL-FLOW Select*®) were used to prepare gas mixtures.

Tryptone (LOT 62321-70230; Cas 91079-40-2), yeast extract (LOT 175915; Cas 8013-01-2) and sodium pyruvate (LOT 175070; Cas 113-24-6) (≥99 %) was purchased from *Fischer Scientific* (Belgium). Sodium chloride (NaCl) (Cas 7647-14-5), dipotassium phosphate (K_2HPO_4) (Cas 7758-11-4), monopotassium phosphate (KH_2PO_4) (Cas 7778770) was purchased from *Lach-Ner* (Czech Republic). Peptone (LOT 177485; Cas 73049-73-7) was purchased from *Fischer Scientific* (US). Casamino acids (LOT 18F0456060; Cas 65072-00-6) was purchased from *VWR Chemicals* (USA). D-(+)-Glucose (LOT SZBF3070V; Cas 50-997) was purchased from *Sigma-Aldrich* (France). Starch, soluble (LOT 1744617; Cas 9005-25-8) was purchased from *Fischer Scientific* (UK). Beef extract (LOT-59P038) was purchased from *Biolife* (Italy).

2.2. Instrumentation (Including Sensor-Array and Flow Cell)

The custom made flow cell was constructed for the experiments (Fig. 1). The flow cell was sandwich type flow cell which consisted in two sides attached to each other and tightened with three screws. Between the two sides were *DropSens 550* screen-printed electrochemical array, membranes, black distance piece and orange silicone sealing.

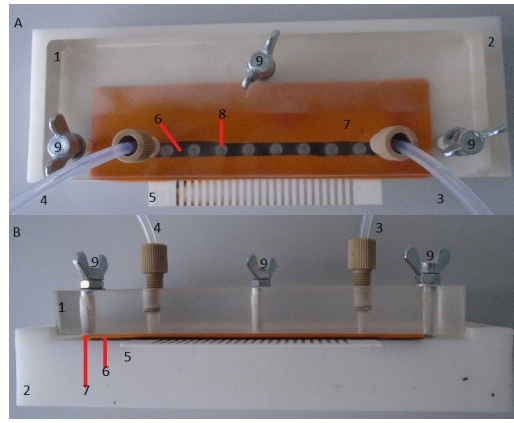

Fig. 1. Custom made flow cell (A) top view and (B) side view. Flow though cell consists of (1) cell top part, (2) cell nether part, (3) inflow tube, (4) outflow tube, (5) DropSens 550 screen-printed electrochemical array, (6) black distance piece, (7) orange silicone sealing, (8) membrane, (9) screw.

Screen-printed electrochemical array formed by eight 3-electrode electrochemical cells (Fig. 2(A)). In the three-electrode configuration, the working electrode was inner platinum circle electrode (2.56 mm diameter), the counter electrode was a Pt band electrode around the working electrode and the reference electrode was silver wire. Distance piece (Fig. 2(C)) had 8 passing through holes with pore diameter 5 mm. Distance piece was 3D printed and preformed with acetone. One side of distance piece was covered with silicone to make the flow through cell leakage free. In the silicone gasket, the holes were cut at the exactly same place with electrodes. Membranes (Fig. 2(D)) were prepared from agarose and immobilized microorganisms according to instructions in chapter 2.5.

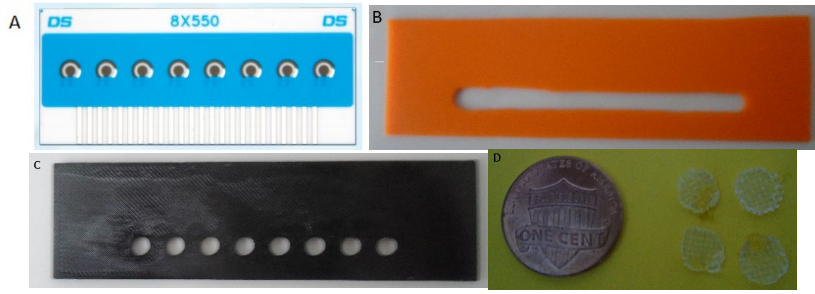

Fig. 2. (A) *DropSens 550* screen-printed electrochemical array, (B) silicone sealing, (C) membrane holder, and (D) membranes.

Master Dual Pump model *AL 1000* was used to pump the electrolyte. 20 cm^3 syringe was used which had diameter 20 mm (lot 15f15c8; ref 4645200v). The pumping speed of the electrolyte was varied from 0 to 3 cm^3 min^{-1}.

The potentiostat PalmSens (*Palm Instruments BV*) was used for CV and CA measurements in part 3.1. and 3.2. The CV data were measured at potential sweep rate, v, 20 Mv s^{-1}. Chronoamperometry was measured at −0.5 V vs Ag|AgCl|0.1 M KCl for 120 s. During the pre-step the electrode potential was held at 0.5 V vs Ag|AgCl|0.1 M KCl for 30 s.

The measurements were carried out simultaneously at all 8 nodes. At first CA was performed, then CV and at the end CA was repeated. The CA measurement were repeated to find out how the cycling of the potential influence the CA response. Between measurements the solution flow was stopped.

Additionally, the potentiostat Reference 600 (Gamry Instruments Inc) was used for cyclic voltammetry (CV) and chronoamperometry measurements in part 3.1.–3.2. The CV data were measured at different potential sweep rates, v, from 10 to 1000 mV s^{-1}. Chronoamperometry was measured at −0.5 V and 120 s after every second.

All electrochemical measurements were performed at room temperature (22 ± 2 °C) in the Faraday cage. Different electrochemical measurements were carried out within 10 months.

2.3. Microbial Material

Pseudomonas putida strain provided by the Collection of Environmental and Laboratory Microbial Strains (CELMS), Institute of Molecular and Cell Biology, University of Tartu, Estonia, (http://eemb.ut.ee), as imposed by the depositor, Eeva Heinaru.

2.4. Cultivation of Microorganisms

The bacteria were grown under aerobic condition in a rotating shaker (*Heidolph*, Germany) at 350 rpm/min at 30 °C in a Luria-Bertan liquid medium. Culture medium (2 mL) was inoculated and incubated for 16 hours. The cell suspension was subcultured into a 250 mL of culture medium in a rotating shaker at 350 rpm at 30 °C. Optical density of the bacterial suspension was measured with spectrophotometer at wavelength 600 nm. After 5 hours there was sufficient number of cells for immobilization.

2.5. Immobilization of Microorganisms

The bacterial suspension was centrifuged (*Thermo Scientific*, *Heraeus Megafuge 40* Centrifuge) at 4000 r/min for 15 min at 25 °C. The supernatant was decanted. The cells were washed three times with phosphate buffer (K_2HPO_4, 7 g/L and KH_2PO_4, pH 6.85) and centrifuged. 0.18 g agarose (Type I-A Low EEO) mixed with 7.5 mL phosphate buffer and heated to 70 °C until complete melting of agarose. Mixture was cooled down to 45 °C and 900 µL cell paste was added. The agarose suspension was mixed rapidly and added to the net discs (*Scrynel*, PE 500 HD, diameter was ¼ inch). The membranes were placed between two glass plates and even force was applied to gain certain and even thickness of membranes. The membranes were maintained at 4 °C in a synthetic wastewater solution with BOD was 5 mg L^{-1}. The agarose membranes without bacteria were made in a similar way, but instead of phosphate buffer the distilled water was used.

2.6. Membranes Calibration

Different solutions have been used for calibration of BOD biosensor and biosensor arrays. GGA solution is widely used for this purpose [15] however, it only consists of two simple components – glucose and glutamic acid [16]. Also good results have been gained when OECD (Organization of Economic Cooperation and Development) synthetic wastewater have

been used since this solution consist of a complex mixture of substrates (complex carbohydrates and peptones) [12], [13], [17], [18]. To calibrate membranes solution of modified OECD synthetic wastewater was used. It consisted of peptone 1.6 g L^{-1}, urea 0.3 g L^{-1}, beef extract 1.1 g L^{-1} in 0.1 M KCl solution. Compared to standard solution the salts (NaCl; $MgSO_4$; $CaCl_2$) were not added since they may interfere electrochemical measurement. The calibration points were calculated form 4 or 5 different measurements.

2.7. Experimental Procedure with Bacterial Membranes

Before measurements membranes were in 0.1 M KCl solution for 1 hour at room temperature. Beaker containing 50 mL 0.1 M KCl was aerated with pump (*Resum*, *Pro Silent a 100*, China) and mixed with magnetic stirrer. The custom-made flow cell was put together as shown in Fig. 1.

During one experiment 5 bacterial membranes, 2 agarose membrane and 1 empty electrochemical cell was used simultaneously. To gain the biosensor signal in clean solution, 0.1 M KCl solution was pumped with pump (*FIAlab Instruments Inc*, USA) through the cell for 10 min with the pumping speed 2 cm^3 min^{-1}. Chronoamperometry was measured at −0.3 V vs Ag|AgCl|0.1 M KCl for 120 s with the potentiostat PalmSens. During the pre-step the electrode potential was held at 0.5 V vs Ag|AgCl|0.1 M KCl for 30 s.

For calibration and measurement of unknown solution the aerated sample and pumped through the biosensor cell for 10 min and then new CA was measured. The measurement period was almost 2 months with bacterial membranes. The bacterial membranes were made on 25.04.2019. The last time they were used to measure on 17.06.2019.

2.8. Wastewater Sample

Experiments with real industrial wastewater were made to test the performance of biosensor-array. Liquid waste from lignocellulosic bioethanol production process was used as an unknown sample. The measurements were made with one sample in two different days with all 10 membranes on both days. The BOD_5 of the sample was measured with conventional APHA method [19], the other method to calculate BOD was given in [20]. The BOD value was 29084 mg L^{-1}.

2.9. Data Analysis

The biosensor output signal was normalized using formula: $NSR = (I_0 - I_S)/I_0$, where I_0 is output in the 0.1 M KCl solution, I_S is output of solutions with synthetic wastewater, NSR is normalized response. Data was gathered using *Microsoft Excel 2013* software.

3. RESULTS AND DISCUSSION

3.1. Optimisation of the Pumping Speed of the Electrolyte for Oxygen Measurements

The custom-made flow though cell (Fig. 1) was used to measure dependence of the current density at different pumping speeds of the solution for the 0.1 M KCl solution saturated with oxygen at the potential sweep rate, $v = 20$ mV s^{-1} (Fig. 3(A)). The averaged data for nodes 3–7 is only shown. It was found that for side nodes the current density |j| was higher because of the additional mixing of the solution i.e. presence of solution vortexes near the entrance and exit of the cell. At all pumping speeds the diffusion-limited current density j_d, plateaus are formed. There is a very small peak in case of pumping speed 0.1 cm^3 min^{-1}. This is

probably caused by the non-stationary diffusion effect i.e. the pumping speed is not high enough for the formation of uniform diffusion layer. If the pumping speed is higher, the current density |j| is also higher (Fig. 3(A) inset). For the anodic and cathodic scans, the diffusion limited current densities are very similar. At pumping speeds higher than 0.9 cm^3 min^{-1} the diffusion-limited current density achieves constant value (Fig. 3(A) inset).

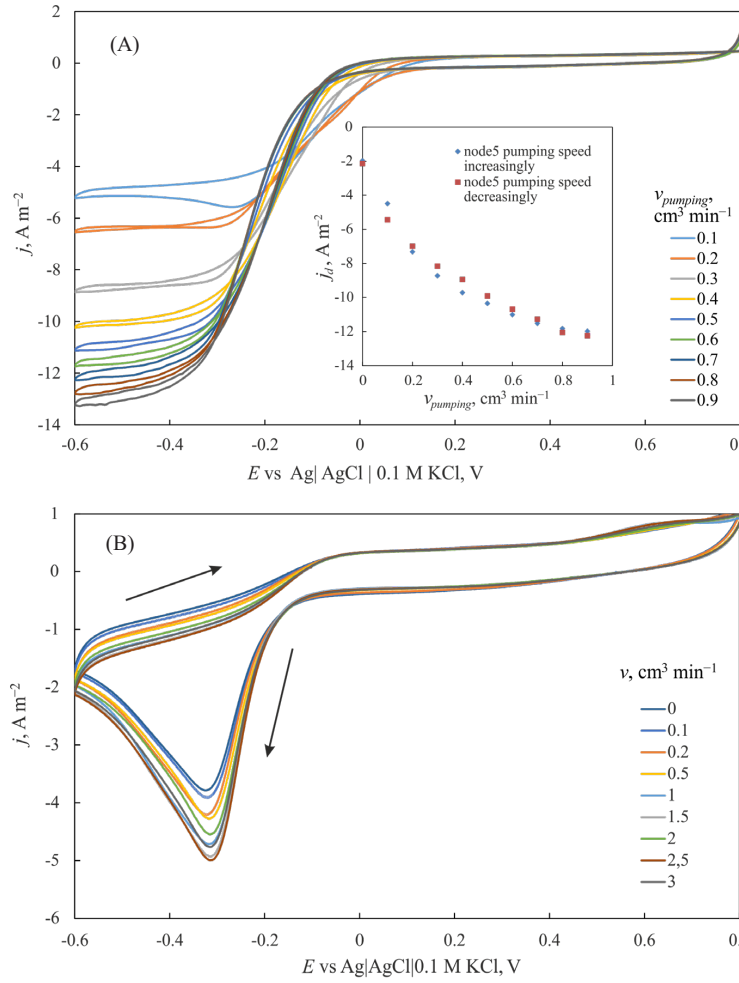

Fig. 3. The dependence of the current density j on the electrode potential E for the 0.1 M KCl solution saturated with oxygen (p_{tot} = 101 kPa) for: (A) the flow through cell only with channel (1st cycle), and (B) oxygen sensor array (2nd cycle) at different pumping speeds. The potential sweep rate was 20 mV s^{-1}. Inset in Fig 3(A): the dependence of the limiting current density j_d, on the pumping speed of the solution, $v_{pumping}$ (node 5).

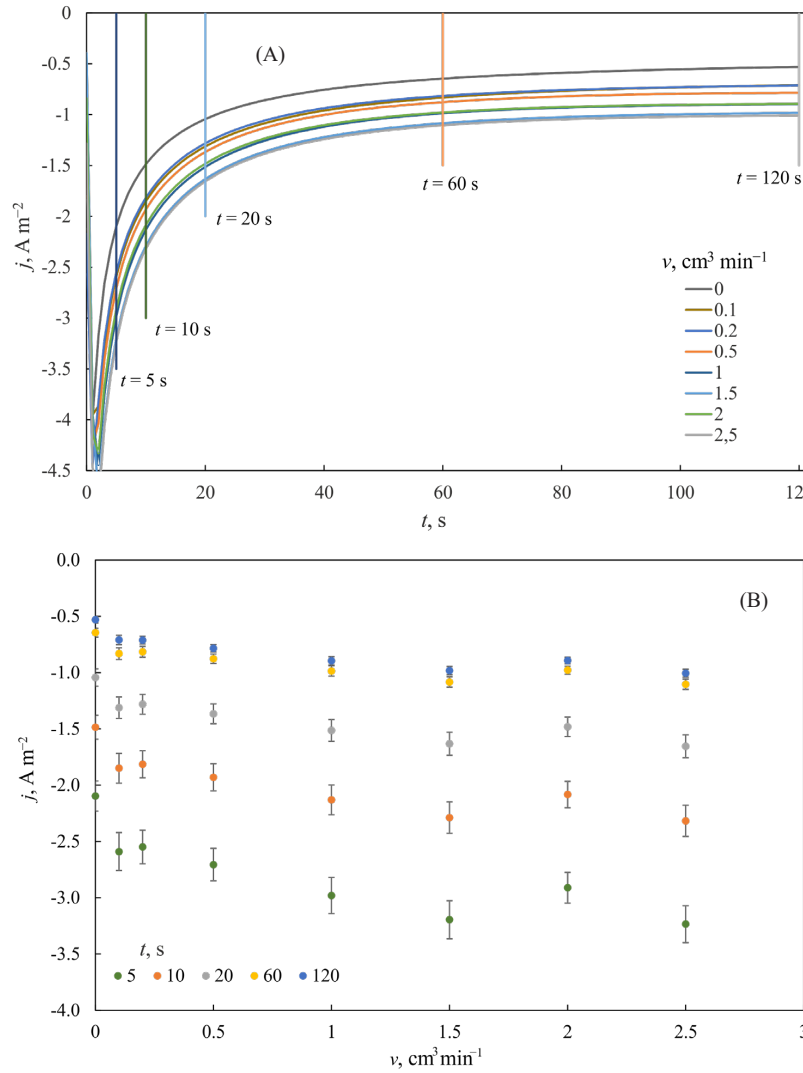

Fig. 4. (A) The dependence of the current density j on the time t and (B) the dependence of the current density on the pumping speed, v, at different moments during the chronoamperometry. The potential of the platinum electrode was stepped from 0.5 V to −0.5 V vs Ag|AgCl|0.1 M KCl. The 0.1 M KCl solution was saturated with 100 % oxygen (p_{tot} = 101 kPa).

To see if the there are any "memory effects" in the system, the CVs were recorded by increasing the pumping speed of the solution step by step from 0 to 0.9 cm^3 min^{-1} and then the pumping speed was reduced from 0.9 to 0 cm^3 min^{-1}. Apparently, there were no memory

effect as the limiting current densities values for both scans were very similar (Fig. 3(A) inset).

To study if it is possible to increase the ORR current density |j| and at the same time the sensitivity of the chemical sensor array (Fig. 1) by increasing the pumping speed of the solution the CV and CA measurements were performed also at different pumping speeds of solution. The pumping speed of the solution was varied between 0 and 3 $cm^3\ min^{-1}$. The second CV scans for solution 100 % saturated with oxygen are given in Fig. 3. Both scans look very similar and it seems some pseudo-stationary state is achieved. More detailed analysis of peak current densities reveals (Fig. 4) that indeed, for the first scan there is no dependence of the peak current density on the pumping speed (not shown). However, for the second scan the peak current density $|j_P|$ increases as the pumping speed increases from 0 to 1.5 $cm^3\ min^{-1}$ and afterwards there is no dependence. Probably during the first scan the oxygen concentration gradient is not as well reproducible and stable as during the second scan. Apparently, it is impossible to get to the true steady state in the system with membranes compared to the system without membranes. At higher pumping speeds the ORR rate is determined with the concentration gradient in the membrane and it is impossible to influence it further by stirring of the solution outside the membrane.

The CA measurement was also performed after the CV measurements (not shown). The results confirm the previously made conclusions as is evident from Fig. 4(A). Therefore, in the following CA measurements pumping speeds above 1.5 $cm^3\ min^{-1}$ were utilised.

In these configurations it was necessary to perform CV before measuring CA in order to clean the electrodes (data not shown).

3.2. Chronoamperometry Measurements

Data of the CA measurements are given in Fig. 5 and Fig. 6. The electrode potential −0.5 V was chosen because according to the CV results at this potential ORR should be mass transport limited process. During the conditioning step, the potential was held in the region (E = 0.5 V) where ORR does not occur. This could help to accomplish more reproducible oxygen concentration near the electrode.

After the potential step, the current density $|j|$ increased sharply because of the EDL charging currents (Fig. 5). After the EDL charging, the current density $|j|$ starts to decrease as the oxygen concentration depletes in the diffusion layer. However, the current density stabilizes after about 120 s. Because the solution is continuously pumped over the electrode and the pseudo-stationary state is achieved. The current density depends on the oxygen concentration. This is visualized in Fig. 6 at different times from the CA step. The current density dependence on oxygen concentration is linear for all times. Although, for longer times the linearity is better. As expected, the peak current densities in the CV experiment (not shown) are higher. The intercepts of the j vs t dependences differ from zero. After the CV measurement the CA response is more stable, the linearity of the j vs t dependences is higher and the reproducibility is better. Probably the cycling of the potential helps to stabilize the concentration gradient in the oxygen it takes time for oxygen to pass through the membranes.

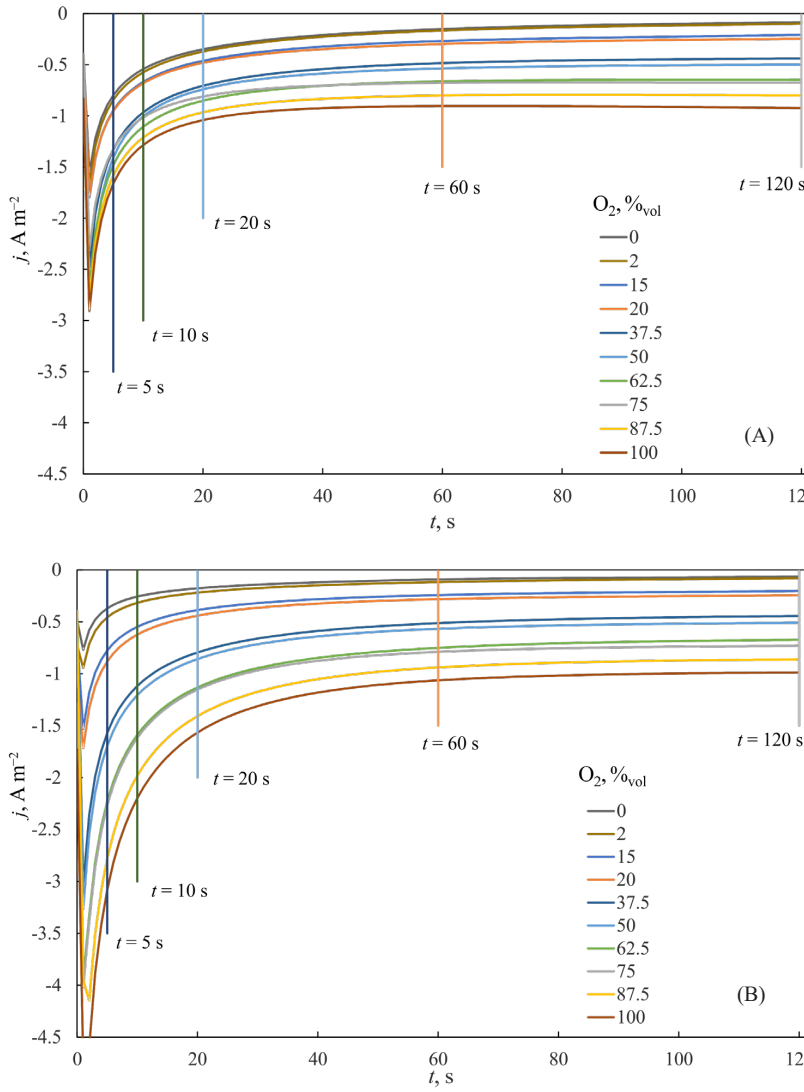

Fig. 5. The dependence of the current density, j, on the time, t, after the potential step of platinum electrode from 0.5 V to −0.5 V vs Ag|AgCl|0.1 M KCl for the 0.1 M KCl solution saturated with mixture of nitrogen and oxygen (p_{tot} = 101 kPa) at different partial pressures of oxygen. The pumping speed of the solution was 2 cm^3 min^{-1}. (A) Before and (B) after cyclic voltammetry measurement.

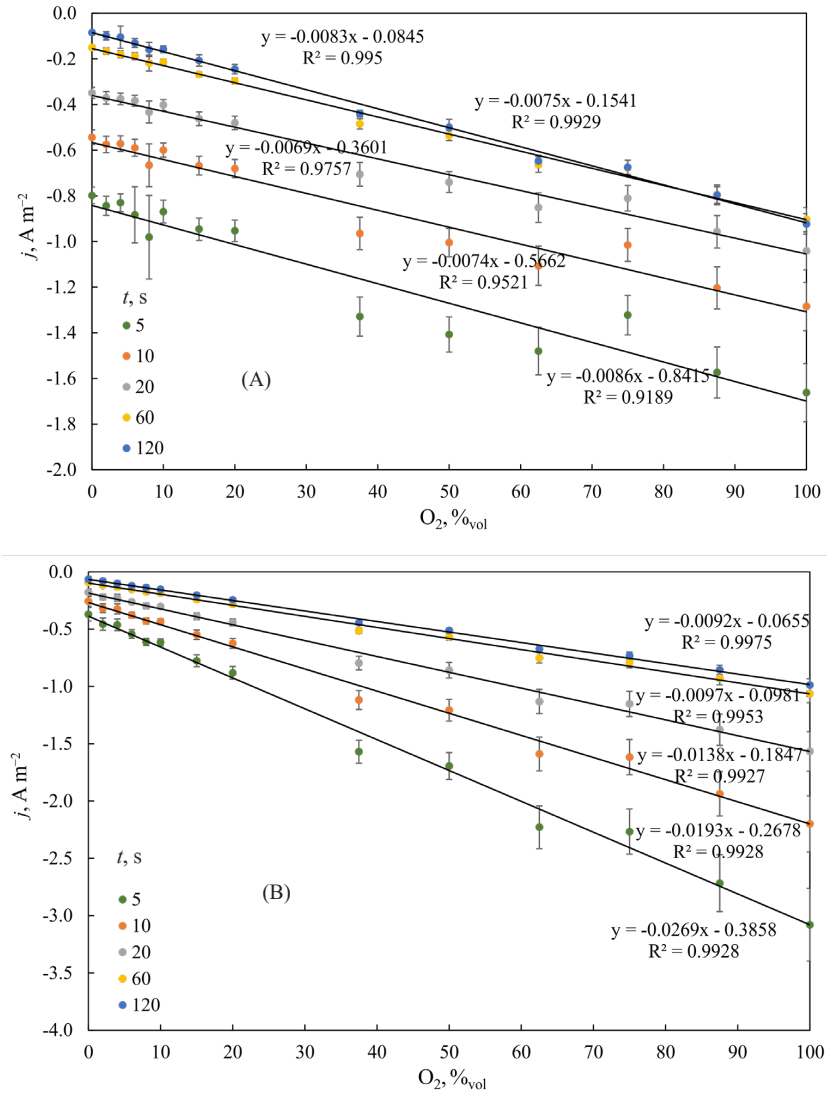

Fig. 6. The dependence of the current density, j, on the oxygen concentration at different moments during the chronoamperometry experiment in the 0.1 M KCl solution saturated with mixture of nitrogen and oxygen (p_{tot} = 101 kPa) at different partial pressures of oxygen. The pumping speed of the solution was 2 cm^3 min^{-1}. (A) Before and (B) after cyclic voltammetry measurement.

As the cyclic voltammogramms showed good stationary behaviour, CA measurements were also performed at potential E = −0.3 V, which is close to peak potential. The CA curves and

the corresponding calibration graphics are shown in Fig. 7. CA was performed after the CV measurement as in previous section. The behaviour of CA curves in Fig. 6(B) and Fig. 7(A) is very similar. This is also confirmed by the data in Fig. 6(B). The absolute values of slopes are slightly higher when the potential was stepped to −0.5 V. Probably because pure diffusion limitation is achieved. The absolute values of intercepts are higher when the potential was stepped to −0.3 V. Probably because in the stationary state the current densities |*j*| were higher in the region of peak (data not shown). The determination coefficient is also slightly better when the potential is stepped to the diffusion-limited region. Therefore, in the CA experiments the potential was stepped into diffusion-limited region (E = 0.5 V).

3.3. Using DropSens 550 Screen-Printed Electrochemical Array as Biosensor

To use the sensor array chip as a biosensor, electrodes were modified with membranes containing immobilized microorganisms. Additionally, membranes containing only agarose was used a blank and one electrode without any membrane was used to see the difference between different conformations. To give membranes durability and enable easy change of membranes the microorganisms were immobilized into agarose gel matrix which was supported by a plastic net. The measurements were conducted in custom made flow cell and solution, either clean buffer solution, buffer solution spiked with OECD synthetic wastewater or unknown sample, was pumped through the flow cell.

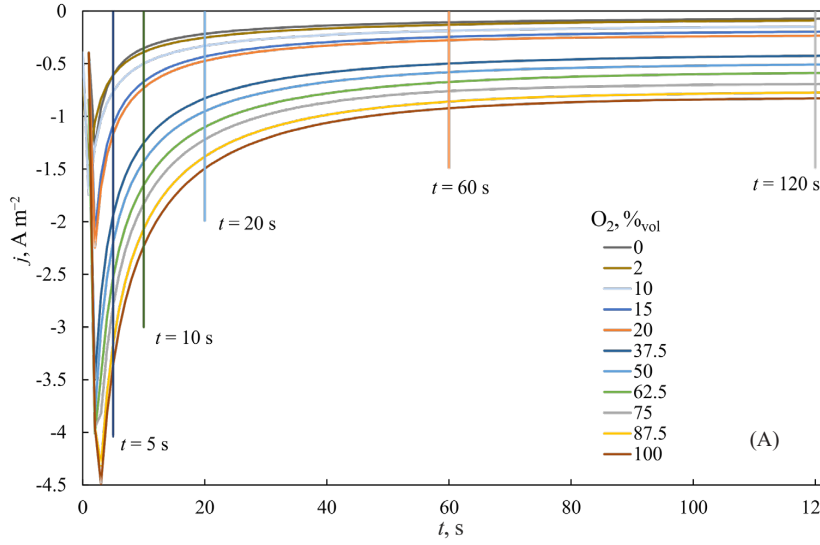

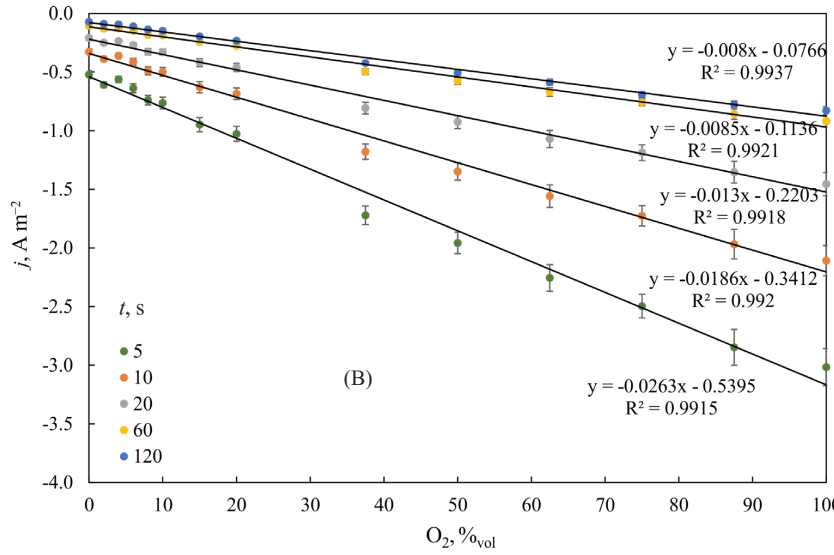

Fig. 7. (A) The dependence of the current density j on the time t at different partial pressures of oxygen and (B) the dependence of the current density on the oxygen concentration at different moments during the chronoamperometry. The potential of the platinum electrode was stepped from 0.5 V to −0.3 V vs Ag|AgCl|0.1 M KCl, the 0.1 M KCl solution was saturated with mixture of nitrogen and oxygen (p_{tot} = 101 kPa) and the pumping speed of the solution was 2 cm^3 min^{-1} using DropSens 550 Screen-Printed Electrochemical Array as Biosensor.

In Fig. 8 the biosensor current density j during measurement with buffer solutions with different BOD values is presented. It can be seen that the current density in case of samples with different BOD values was different. After starting the CA measurement, the current density increases until it stabilises at a certain level. It can be seen that after 60 seconds the sensor output signal can be considered stable and similar to the signal gained at 120 seconds. In all further experiments the output signal was recorded 60 seconds after starting the CA measurement and used in following experiments. From the stable signal, it can be seen that the higher the BOD of sample, the higher current density was measured. When the BOD was higher, less oxygen reached the electrodes since immobilised microorganisms consumed part of the oxygen when assimilating organic compounds diffusing through the membrane.

In this study OECD synthetic wastewater was used for calibration of biosensor array and calibration graphs of different biosensor membranes are presented in Fig. 9.

Important performance characteristics of BOD sensor are linearity, sensitivity, response time and agreement of sensor BOD with BOD_5 values [12]. It can be seen that different membranes conjugated with sensor array chip have different sensitivities and linear ranges. In this work sensitivity was defined as a signal change per unit of concentration of substrate and it is expressed as slope of the calibration curve. On the other hand, linear range was defined as amplitude of substrate concentration where output signal is proportional with known concentration value [8], [21]. The differences between membranes sensitivity may be caused by different bacterial amount in the membrane. During membrane preparation, uneven

number of bacteria was immobilized into an agarose matrix, which later reflects in different sensitivities and linear ranges.

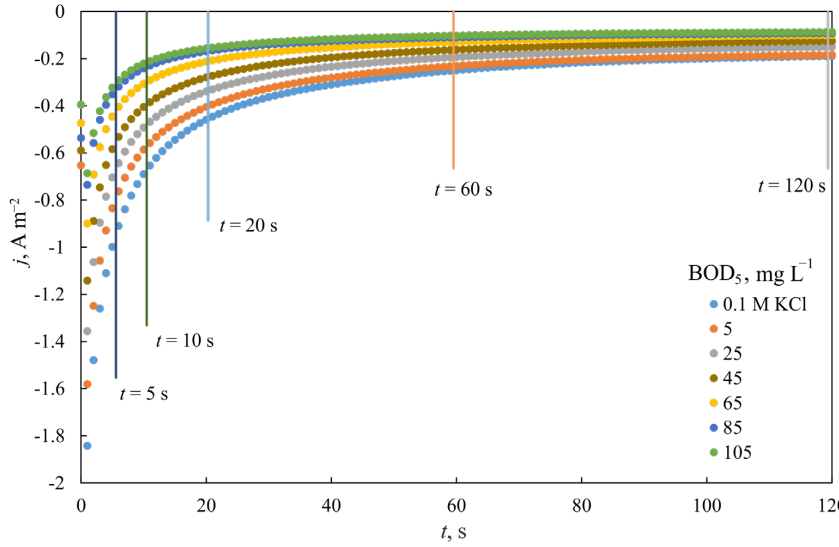

Fig. 8. The biosensor signal (current density, *j*) during measurement of CA in solution of OECD wastewater at different BOD_5 values; 2 mL min^{-1}.

The linear ranges of used biosensors were between 65 to 85 mg L^{-1} of BOD. Linearity depended on sensor fabrication, type and density of the cells [12].

In this work the sensitivities were measured they were between 0.0018 and 0.0068. Wang *et al*. described linear ranges and sensitivities obtained by different authors [22]. There are two works with similar sensitivities as in the case described here. Wang *et al*. show 5 works that have smaller linear ranges, one with a similar one, and 3 works with longer linear ranges [22].

In order to investigate the suitability and performance of biosensor array, a real wastewater sample was analysed. The sample was collected from the liquid stream of second-generation bioethanol production process after lignocellulosic biomass pretreatment step. In the bioethanol production, birch biomass was used and this was pretreated with nitrogen explosion [23], [24] pretreatment method at 200 °C. This kind of sample contains different degradation products from hemicellulose and cellulose hydrolysis, which microorganisms are able to rapidly assimilate and thereby, they are easily detectable with biosensor. The results of biosensor measured BOD and its comparison to standard BOD_5 are shown in Fig. 10.

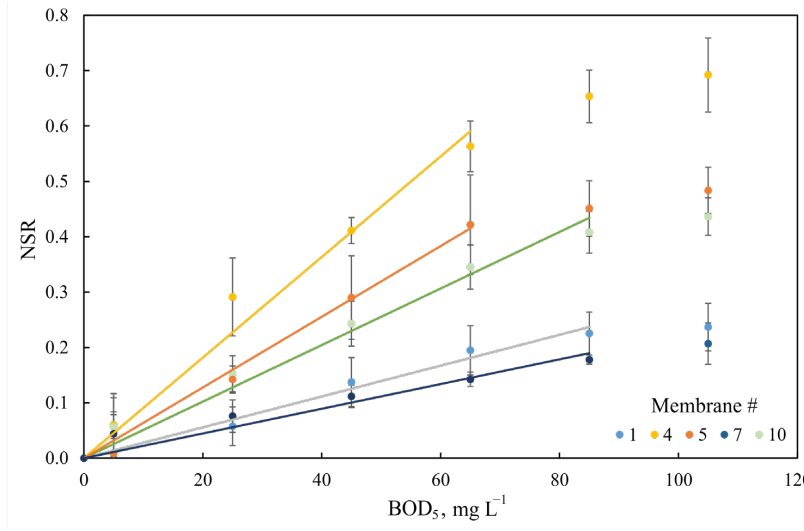

Fig. 9. Calibration graphs of different biosensor membranes at measurement 60 second when OECD wastewater was used for calibration. Different colours indicate different biosensor membranes and linear line indicates the linear range where measurements could be conducted.

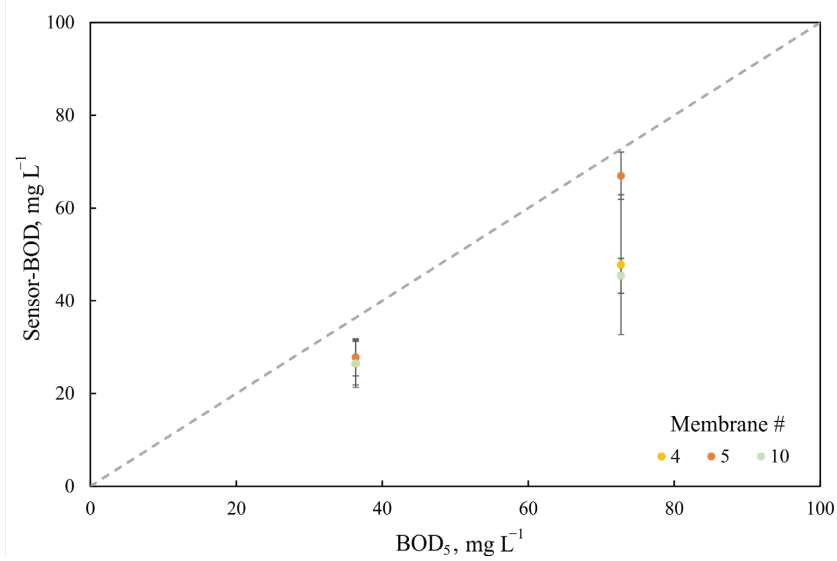

Fig. 10. Comparison of BOD_5 and sensor-BOD, where dashed line shows 1 to 1 correlation between BOD_5 and sensor-BOD.

The biosensor array mostly underestimates solution BOD values from 8 to 37 %. This underestimation is caused by organic components that are biodegradable during the longer BOD_5 measurement but the immobilised cells of the biosensor array did not have suitable enzymes to biodegrade these during the short measurement time of the array.

Underestimation of BOD values was also gained by Webber *et al*, Lei and Yi, Tan and Wu [18], [25], [26]. Tan and Wu studied living cells and thermally killed cells with biofilm sensor. Both underestimated BOD_5 values by 21–28 % [26]. In other study, sensor underestimated food industry wastewater (1 %) and refinery industry wastewater (7 %) [25] with active sludge biosensor. Webber *et al*. used bacteria *Arthrobacter globiformis* in a biosensor that underestimated BOD value by 16 % [18]. In the same study, microbes *K. oxytoca* underestimated BOD value by 73 % [18].

4. CONCLUSIONS

DropSens 550 array showed sensitivity towards oxygen content in the electrolyte solution (0.1 M KCl (aq)). It is possible to use CA and CV methods to estimate the oxygen concentration. According to the CV results, the pseudo stationary state was achieved if the pumping speed of the solution was 2 $cm^3\ min^{-1}$ and the potential sweep rate was 20 $mV\ s^{-1}$. The sensitivity and reproducibility in the CA experiment increased after addition potential cycling of the platinum electrode. Probably the potential cycling helps to achieve more stable and reproducible concentration gradient of oxygen in the agarose.

Based on the electrochemical characterization data it can be concluded that *DropSens 550* screen-printed electrochemical array is suitable for future research including BOD biosensor-array construction.

Biosensor array based on *DropSens 550* with bacterial membranes was calibrated. The linear range was up to 85 $mg\ L^{-1}$ of BOD and sensitivity from 0.0018 to 0.0068 with *Pseudomonas putida* biosensor array. Using this biosensor array, the sensor BOD value was obtained with less than 15 minutes. Although the biosensor array underestimated the BOD value in bioethanol production stillage, it shows promise to be utilised in environmental monitoring.

In the future research different bacterial cultures can be used at the same time and by applying different measurement methods faster results could be obtained. In addition, different kind of wastewaters at different concentrations must be tested to evaluate the performance on biosensor array with real samples.

ACKNOWLEDGEMENT

This work was supported by the EU through the European Regional Development Fund under project TK141 “Advanced materials and high-technology devices for energy recuperation systems” (2014-2020.4.01.15-0011) and by the Estonian Research Council (grant No. PRG676). We also gratefully acknowledge the support of Estonian University of Life Sciences (base financed project P170025)

REFERENCES

[1] Jouanneau S., *et al*. Rapid BOD assessment with a microbial array coupled to a neural machine learning system. *Water Research* 2017:166:115079. https://doi.org/10.1016/j.watres.2019.115079

[2] Rocha-Meneses L., *et al.* Thermodynamic, Environmental and Economic Simulation of an Organic Rankine Cycle (ORC) for Waste Heat Recovery: Terceira Island Case Study. *Environmental and Climate Technologies* 2019:23:2:347–365. https://doi.org/10.2478/rtuect-2019-0073

[3] Li Y., *et al*. A Rapid and Sensitive BOD Biosensor Based on Ultramicroelectrode Array and Carboxyl Graphene. *Proceedings of the 12th IEEE International Conference on Nano/Micro Engineered and Molecular Systems* 2017.

[4] Pitman K., Raud M., Kikas T. Biochemical oxygen demand sensor arrays. *Agronomy Research* 2015:13:2:382–395.

[5] Raud M., Kikas T. Bioelectronic tongue and multivariate analysis: A next step in BOD measurements. *Water Research* 2013:47:2555–2562. https://doi.org/10.1016/j.watres.2013.02.026

[6] Ejeian F., *et al*. Biosensors for wastewater monitoring: A review. *Biosensors and Bioelectronics* 2018:118:66–79. https://doi.org/10.1016/j.bios.2018.07.019

[7] Commault A. S., *et al*. Geobacter-dominated biofilms used as amperometric BOD sensors. *Biochemical Engineering Journal* 2016:109:88–95. https://doi.org/10.1016/j.bej.2016.01.011

[8] Raud M. Study of semi-specific BOD biosensors for Biosensor-array. Tartu: University of Tartu, 2013.

[9] Cêbere B., *et al*. Toxicity Tests for Ensuring Succesful Industrial Wastewater Treatment Plant Operation. *Environmental and Climate Technologies* 2010:3(3):47. https://doi.org/10.2478/v10145-009-0005-8

[10] Kim B. H., Chang I. S., Moon H. Microbial Fuel Cell-Type Biochemical Oxygen Demand Sensor. *Encyclopedia of Sensors X* 2006:1–12.

[11] Kibena E., *et al*. Semi-specific *Microbacterium phyllosphaerae*-based microbial sensor for biochemical oxygen demand measurements in dairy wastewater. *Environmental Science and Pollution Research* 2012:1–7. https://doi.org/10.1007/s11356-012-1166-8

[12] Liu J., Mattiasson B. Microbial BOD sensors for wastewater analysis. *Water Research* 2002:36(15):3786–3802. https://doi.org/10.1016/s0043-1354(02)00101-x

[13] Bourgeois W., Burgess J. E., Stuetz R. M. Review On-line monitoring of wastewater quality: a review. *Journal of Chemical Technology and Biotechnology* 2001:76:337–348.

[14] Morris K., *et al*. Ferricyanide mediated biochemical oxygen demand – development of a rapid biochemical oxygen demand assay. *Analytica Chimica Acta* 2001:442:129–139.

[15] Liu C., *et al*. Immobilized multi-species based biosensor for rapid biochemical oxygen demand measurement. *Biosensors and Bioelectronics.* 2011:26(5):2074–2079. https://doi.org/10.1016/j.bios.2010.09.004

[16] Lin L., *et al*. Novel BOD optical fiber biosensor based on co-immobilized microorganisms in ormosils matrix. *Biosensors and Bioelectronics.* 2006:21(9):1703–1709. https://doi.org/10.1016/j.bios.2005.08.007

[17] Liu J., Björnsson L., Mattiasson B. Immobilised activated sludge based biosensor for biochemical oxygen demand measurement. *Biosensors and Bioelectronics.* 2000:14(12):883–893. https://doi.org/10.1016/s0956-5663(99)00064-0

[18] Webber J. B, *et al*. Appraising bacterial strains for rapid BOD sensing – an empirical test to identify bacterial strains capable of reliably predicting real effluent BODs. *Applied Microbiological Biotechnology* 2011:89:179–188. https://doi.org/10.1007/s00253-010-2889-4

[19] APHA, Standard methods for examination of water and wastewater. American Public Health Association: Washington 1985:525–531.

[20] Strade E., Kalnina D. Cost Effective Method for Toxicity Screening of Pharmaceutical Wastewater Containing Inorganic Salts and Harmful Organic Compounds. *Environmental and Climate Technologies* 2019:23(1):52–63. https://doi.org/10.2478/rtuect-2019-0004

[21] Chan C., *et al*. Designing an amperometric thick-film microbial BOD sensor. *Biosensors and Bioelectronics* 2000:15:343–353. https://doi.org/10.1016/s0956-5663(00)00090-7

[22] Wang J., *et al*. Ultramicroelectrode array modified with magnetically labelled Bacillus subtilis, palladium nanoparticles and reduced carboxy graphene for amperometric determination of biochemical oxygen demand. *Microchim Acta* 2017:184:763–771.

[23] Raud M., *et al*. Utilization potential of urban greening waste: Tartu case-study. *Urban Forestry and Urban Greening* 2017:21:96−101. https://doi.org/10.1016/j.ufug.2016.11.014

[24] Raud M., Olt J., Kikas T. N_2 explosive decompression pretreatment of biomass for lignocellulosic ethanol production. *Biomass & Bioenergy* 2016:90:1−6. https://doi.org/10.1016/j.biombioe.2016.03.034

[25] Lei H., Yi L. A novel BOD sensor immobilized active sludge bacteria for rapid determination of biochemical oxygen demand in industrial wastewater. *International Conference on Energy and Environment Technology* 2009. https://doi.org/10.1109/ICEET.2009.331

[26] Tan T. C., Wu C. BOD sensors using multi-species living or thermally killed cells of a BODSEED microbial culture. *Sensors and Actuators B: Chemical* 1999:54(3):252–260.

CURRICULUM VITAE

Personal data

Name:	Kätlin Pitman
Date of birth:	02.10.1986
Citizenship:	Estonian
Address:	Institute of Forestry and Engineering, Estonian University of Life Sciences, Fr.R.Kreutzwaldi 56/1, Tartu 51006,Estonia
Telephone:	+372 7313 315
E-mail:	katlin.pitman@student.emu.ee

Education

2014-...	Estonian University of Life Sciences, PhD
2009-2011	University of Tartu, M.Sc.
2005-2009	University of Tartu, B.Sc.
2002-2005	Tartu Tamme Gymnasium
1993-2002	Tartu Veeriku School

Professional employment

11/2011-06/2013	Estonian Veterinary and Food Laboratory (VFL), chief specialist

Involvement in research projects

2010-2011	The Study of Individual and Cooperative Effects of Antibiotics on Enzymatic Activity with Biosensor Systems
2014-2015	Bioelectronic nose for qualitative and quantitative analysis of organic pollution

Main scientific publications

ETIS 1.1: **Pitman, K.**; Raud, M.; Kikas, T. (2015) Biochemical oxygen demand sensor arrays. *Agronomy Research*, 13 (2), 382-395.

ETIS 1.1: **Pitman, K.**; Raud, M.; Scotti, G.; Jokinen, V. P.; Franssila, S.; Nerut, J.; Lust, E.; Kikas, T. (2017) Electrochemical Characterization of the Microfabricated Electrochemical Sensor-Array System. *Electroanalysis*, 29, 249-258. 10.1002/elan.201600559.

ETIS 1.1: **Pitman, K.**; Nerut, J.; Lust, E.; Franssila, S.; Raud, M.; Kikas, T. (2017) Electrooxidation of Hexacyanoferrate(II) Anions and Electroreduction of Oxygen in the Microfabricated Electrochemical Sensor-Array System. *ECS Transactions*, 77 (11), 1771-1782. 10.1149/07711.1771ecst.

ETIS 1.1: **Pitman, K.**; Nerut, J.; Raud, M.; Kikas, T. (2020) Characterisation of Electrochemical Sensor-Array for Utilisation in Construction of BOD Bioelectronic Tongue. *Environmental and Climate Technologies* 24 (3), 39-54. 10.2478/rtuect-2020-0084

Oral presentation

6th International Conference on Biosystems engineering, 07-08.05.2015, Tartu, Biochemical oxygen demand sensor arrays. **Pitman, K.**; Raud, M.; Kikas, T.

Poster presentations

Taastuvate energiaallikate uurimine ja kasutamine, TEUK XVII, 12.11.2015, Tartu, Biokeemilise hapnikutarbe sensor-rivid. **Pitman, K.**; Raud, M.; Kikas, T.

231st ECS (The Electrochemical Society) meeting, 28.05-01.06, 2017, New Orleans, Electrooxidation of Hexacyanoferrate(II) Anions in the Microfabricated Electrochemical Sensor-Array System. **Pitman, K.**; Nerut, J.; Lust, E.; Franssila, S.; Raud, M.; Kikas, T.

9th International Conference Biosystems Engineering, 9-11.05, 2018, Tartu, Measuring oxygen with different electrochemical arrays. **Pitman, K**.; Nerut, J.; Lust, E.; Raud, M.; Kikas, T.

CONECT 2020 Conference of Environmental and Climate Technologies, 13-15.05, 2020, Characterisation of electrochemical sensor-array for utilisation in construction of BOD bioelectronic tongue. **Pitman, K.**; Nerut, J.; Raud, M.; Kikas, T.

ELULOOKIRJELDUS

Isikuandmed

Nimi:	Kätlin Pitman
Sünniaeg:	02.10.1986
Kodakondsus:	Eesti
Aadress:	Metsanduse ja inseneeria instituut, Eesti Maaülikool, Fr.R.Kreutzwaldi 56/1, Tartu 51006, Eesti
Telefon:	+372 7313 315
E-post:	katlin.pitman@student.emu.ee

Haridus

2014-...	Eesti Maaülikool, PhD tehnikateadus
2009-2011	Tartu Ülikool, M.Sc. keskkonnatehnoloogia
2005-2009	Tartu Ülikool, B.Sc. keemia
2002-2005	Tartu Tamme Gümnaasium
1993-2002	Tartu Veeriku Kool

Teenistuskäik

11/2011-06/2013	Veterinaar- ja Toidulaboratoorium (VTL), peaspetsialist

Osalemine projektides

2010-2011	Antibiootikumide toime ja koostoime uurimine ensüümide katalüütilistele omadustele optiliste biosensorsüsteemidega
2014-2015	Bionina orgaanilise reostuse kvalitatiivseks ja kvantitatiivseks analüüsiks

Peamised teaduspublikatsioonid

ETIS 1.1: **Pitman, K.**; Raud, M.; Kikas, T. (2015) Biochemical oxygen demand sensor arrays. *Agronomy Research*, 13 (2), 382-395.

ETIS 1.1: **Pitman, K.**; Raud, M.; Scotti, G.; Jokinen, V. P.; Franssila, S.; Nerut, J.; Lust, E.; Kikas, T. (2017) Electrochemical Characterization of the Microfabricated Electrochemical Sensor-Array System. Electroanalysis, 29, 249-258. 10.1002/elan.201600559.

ETIS 1.1: **Pitman, K.**; Nerut, J.; Lust, E.; Franssila, S.; Raud, M.; Kikas, T. (2017) Electrooxidation of Hexacyanoferrate(II) Anions and Electroreduction of Oxygen in the Microfabricated Electrochemical Sensor-Array System. *ECS Transactions*, 77 (11), 1771-1782. 10.1149/07711.1771ecst.

ETIS 1.1: **Pitman, K.**; Nerut, J.; Raud, M.; Kikas, T. (2020) Characterisation of Electrochemical Sensor-Array for Utilisation in Construction of BOD Bioelectronic Tongue. *Environmental and Climate Technologies* 24 (3), 39-54. 10.2478/rtuect-2020-0084

Suuline ettekanne

6th International Conference on Biosystems engineering, 07-08.05.2015, Tartu, Biochemical oxygen demand sensor arrays. **Pitman, K.**; Raud, M.; Kikas, T.

Stendiettekanded

Taastuvate energiaallikate uurimine ja kasutamine, TEUK XVII, 12.11.2015, Tartu, Biokeemilise hapnikutarbe sensor-rivid. **Pitman, K.**; Raud, M.; Kikas, T.

231st ECS (The Electrochemical Society) meeting, 28.05-01.06, 2017, New Orleans, Electrooxidation of Hexacyanoferrate(II) Anions in the Microfabricated Electrochemical Sensor-Array System. **Pitman, K.**; Nerut, J.; Lust, E.; Franssila, S.; Raud, M.; Kikas, T.

9th International Conference Biosystems Engineering, 9-11.05, 2018, Tartu, Measuring oxygen with different electrochemical arrays. **Pitman, K.**; Nerut, J.; Lust, E.; Raud, M.; Kikas, T.

CONECT 2020 Conference of Environmental and Climate Technologies, 13-15.05, 2020, Characterisation of electrochemical sensor-array for utilisation in construction of BOD bioelectronic tongue. **Pitman, K.**; Nerut, J.; Raud, M.; Kikas, T.

VIIS VIIMAST KAITSMIST

FARIBA BAHRINI
PATTERN OF URBAN PARK USE,SPATIAL ACCESSIBILITY AND PREFERANCES OF URBAN PARK USERS IN TEHRAN, IRAN
LINNAPARKIDE KASUTUSMUSTRID, RUUMILINE LIGIPÄÄSETAVUS JA KASUTAJAEELISTUSED IRAANI PEALINNAS TEHERANIS
Professor Simon Bell
10. juuni 2022

ASSAR LUHA
OCCUPATIONAL NOISE EXPOSURE AND HEARING PROBLEMS AMONG ACTIVE MILITARY SERVICE PERSONNEL IN ESTONIA
MILITAARMÜRA EKSPOSITSIOON JA KUULMISPROBLEEMID EESTI TEGEVVÄELASTEL
Professor Eda Merisalu, kaasprofessor Hans Orru
17. juuni 2022

HENRI JÄRV
THE IMPACT OF PROTECTED AREAS GOVERNANCE AND MANAGEMENT PRACTICES ON HUMAN WELL-BEING AND LOCAL SOCIOECONOMIC CONDITIONS
KAITSEALADE HALDUSSÜSTEEMI JA KAITSEKORRALDUSLIKE MEETMETE MÕJU INIMESTE HEAOLULE NING KOHALIKELE SOTSIAALMAJANDUSLIKELE OLUDELE
Professor Kalev Sepp, lektor Raymond David Ward
21. juuni 2022

JORDI ESCUER GATIUS
MITIGATION OF NITROUS OXIDE EMISSIONS FROM ARABLE SOILS
PÕLLUMULLAST ERALDUVA DILÄMMASTIKOKSIIDI VÄHENDAMINE
Kaasprofessor Merrit Shanskiy, kaasprofessor Kaido Soosaar, professor Alar Astover
30. juuni 2022

MARTA MARIA ALOS ORTI
URBAN ECOLOGY: NOVEL ECOSYSTEMS, NOVEL CHALLENGES
LINNAÖKOLOOGIA VÄLJAKUTSED: UUED ÖKOSÜSTEEMID, UUED LAHENDUSED
Professor Lauri Laanisto
29. august 2022

ISSN 2382-7076
ISBN 978-9916-669-34-1 (trükis)
ISBN 978-9916-669-35-8 (pdf)